Neoclassical Polarization

by

Yong Xiao

B.S., Peking University (1999)

Submitted to the Department of Nuclear Science and Engineering
in partial fulfillment of the requirements for the degree of

Doctor of Philosophy in Applied Plasma Physics

at the

MASSACHUSETTS INSTITUTE OF TECHNOLOGY

June 2006

Signature of Author .....
Department of Nuclear Science and Engineering
15 May 2006

Certified by .....
Peter J. Catto
Head of Fusion Theory and Computational Group, PSFC
Thesis Supervisor

Certified by .....
Kim Molvig
Associate Professor of Nuclear Science and Engineering
Thesis Supervisor

Accepted by .....
Jeffrey A. Coderre
Chairperson, Department Committee on Graduate Students

Neoclassical Polarization

by

Yong Xiao

Submitted to the Department of Nuclear Science and Engineering
on 15 May 2006, in partial fulfillment of the
requirements for the degree of
Doctor of Philosophy in Applied Plasma Physics

Abstract

Sheared zonal flow is known to be the predominant saturation mechanism of plasma turbulence. Rosenbluth and Hinton(R-H) have shown that the zonal flow level is inversely proportional to the plasma radial polarizability due to magnetic drift departure from a flux surface. In another calculation, Hinton and Rosenbluth (H-R) considered the weakly collisional case in the banana regime and calculated the neoclassical polarization and associated zonal flow damping in the high frequency and low frequency limits. The work presented here extends R-H's calculation in several aspects. We calculate the neoclassical polarization for arbitrary radial wavelength zonal flows so that finite ion banana width and ion gyroradius are retained. We also add plasma shape effects into the R-H collisionless calculation and find the influence of elongation and triangularity on neoclassical polarization and zonal flow damping. In addition, we extend the H-R collisional calculation using an exact eigenfunction expansion of the collision operator to calculate neoclassical polarization for the entire range of frequencies. A semi-analytical fit of the exact results is obtained that gives the polarization to within 15% and allows the collisional zonal flow damping rate to be evaluated for arbitrary collisionality.

Thesis Supervisor: Peter J. Catto
Title: Head of Fusion Theory and Computational Group, PSFC

Thesis Supervisor: Kim Molvig
Title: Associate Professor of Nuclear Science and Engineering

Acknowledgement

I own my thanks to many people who made this thesis possible.

First of all, I thank my thesis advisors Peter J. Catto and Kim Molvig, without whom this thesis could never be finished.

Peter's knowledge, insight, initiative and diligence have been a reliable resource throughout this thesis. It was a great privilege to work with the main founder of gyrokinetics. Peter kindly shared his research experience and results with me and helped me learn the importance of mathematical rigor in plasma theory and finish this thesis smoothly.

Kim taught me how to tackle a physics problem and patiently trained me to develop physics understanding. He introduced me this important field and shared his wonderful insights generously with me. Kim's optimism, patience, generosity and encouragement taught me the joy of doing research and helped me develop a positive attitude in times of difficulty.

Both of them are very caring advisors and indispensable source of learning. It is my great pleasure to work with them. One would feel lucky if one of them could serve as his/her advisor. I feel very fortunate to have both of them as advisors.

I thank Darin Ernst for numerous helpful physics discussions, guidance and computational advice in great detail. His expertise, enthusiasm and patience should make him an excellent thesis advisor in the future. I also thank Jesus Ramos for helping me on MHD, John Wright for helping me on programming and Abhay Ram for helping me on some numerics.

Many other professors at MIT have also helped and inspired me, particularly, Jeffrey Freidberg, Ron Parker, Sidney Yip, Ian Hutchinson, Miklos Porkolab, William Dorland (UMD) and Fred L. Hinton (GA). I own my thanks to them.

Ted Baker, Leslie West, Macia Tench-Mora, Doris Carty, Thomas Hrycaj, Elizabeth Parmelee and other staff members at PSFC should also receive my thanks.

I thank my friends who made my MIT life a pleasant and unforgettable experience.

Among them are Shizhong Mei, Tiangang Shang, Weiren (Eric) Chen, Liang Lin, Yun liu, Ruopeng Wang, Jinhong Chen, Zhe Sun, Shaomin Wang, Ping Wang, Jing Wang, Chunyun Wang, Hongyu Jiang, Hang Qi, Yile Li, and my officemates James Dorris, Joe Wleklinski, William Fox and Paul Nerenberg. My hosts Alberta and Roger Lipson deserve special thanks. Due to the limit of space, I can only list a few of them and hope the rest could forgive my neglect.

In addition, I'm very grateful to my beloved wife Youling Bin. Without her companionship and love, staying at MIT could not have been so enjoyable. I also thank my parents for their enormous love, trust, and patience. Last but not least, I thank my late grandfather. In heaven he must be proud to see my thesis finished.

Contents

List of Figures

List of Tables

Chapter 1

Introduction

It has been observed in tokamak experiments [45] that radial particle and heat transport are much larger than neoclassical theory predicts [26][41]. Neoclassical theory based on a collisional diffusion model only sets up a minimal transport level for fusion plasmas. The majority of the radial transport is believed to be from small spatial scale (compared to the tokamak size), low frequency (compared to the ion gyrofrequency) microinstabilities [29][35][6][39]. These drift wave type instabilities include the ion temperature gradient (ITG) [4][33][11] mode, the electron temperature gradient (ETG) [31] mode, the trapped ion mode [42][43] and the trapped electron mode (TEM) [19][8][37][32]. The ITG mode and TEM mode have recently been observed in experiments [40][20] and identified as the main instabilities that lead to anomalous transport [31].

A focus of the last several decades of fusion research has been identifying new microinstabilities, investigating the physics behind these microinstabilities, and searching for possible approaches to avoid or suppress the microturbulence associated with these microinstabilities. These microinstabilities can lead to an axisymmetric flow called zonal flows that can impact the fluctuation levels. The zonal flow produced by the sheared radial electric field is found to be an effective way to reduce tokamak turbulent transport [13][47] once it is excited by the microturbulence. Gyrokinetic simulations find that the threshold of ITG turbulence is shifted upwards by the excitation of the zonal flow[14].

The discovery of this *Dimits Shift* has been important evidence of the regulation effect of the zonal flow. Therefore the damping of the zonal flow and the asymptotic residual zonal flow level becomes an important issue in setting the turbulence saturation amplitude.

Different simulation models have provided different predictions on the zonal flow damping. Gyrokinetic simulations [36][15][34] found a much larger residual zonal flow level than the gyrofluid models [35][2][17]. In an analytical gyrokinetic calculation[44], *Rosenbluth* and *Hinton* (*R-H*) showed that an axisymmetric zonal flow can't be damped by linear collisionless kinetic effects. Therefore, the severe damping term embedded in gyrofluid codes is not appropriate for describing the zonal flow evolution and gyrofluid modeling has been largely replaced by gyrokinetic models in the last few years. The *R-H* calculation also showed that the residual zonal flow level is inversely proportional to the radial plasma polarization. This radial polarization is associated with departure of charge from a flux surface due to the magnetic drifts or even gyromotion. In the collisionless regime, the plasma polarization is dominated by the ion neoclassical polarization, which originates from the trapped and passing ion departure from flux surfaces in a tokamak.

In a later calculation[27], *Hinton* and *Rosenbluth* (*H-R*) calculated the neoclassical polarization and associated zonal flow damping in the presence of collisions for the following two asymptotic limits: the high frequency limit where the driving frequency is much larger than the ion-ion collision frequency, and the low frequency limit, where the driving frequency is much smaller than the ion-ion collision frequency. They did not give explicit results for the intermediate driving frequencies, but found the zonal flow to be strongly damped at high collisionality.

In this thesis, several advances have been made to understanding neoclassical polarization and the associated residual zonal flow following *H-R*'s approach [27][44]. These advances include the following calculations:

- the neoclassical polarization and residual zonal flow level for arbitrary perpendicular wavelengths;
- the neoclassical polarization and residual zonal flow level for shaped plasma with

finite elongation and triangularity;

- the collisional neoclassical polarization for the entire range of driving frequencies or arbitrary collisional frequencies below the transit frequency.

To set the stage for these calculations, we review the basic *R-H* zonal flow physics, and show that the residual zonal flow is closely related to the polarization of the plasma in Chapter 2. Then in Chapter 3, we first develop the formalism to calculate the neoclassical polarization following *H-R* [27]. We review the calculation of the neoclassical polarization in the collisionless limit and show the importance of the distribution function's structure in pitch angle space. We also calculate the classical polarization for a screw pinch model. In addition, we calculate the poloidal and toroidal rotation with the collisionless *R-H* distribution and find that zonal flow not only has a poloidal component, but also has a comparable toroidal component.

In Chapter 4, we calculate the neoclassical polarization and the associated zonal flow analytically for short wavelengths (wavelengths of the order of the ion poloidal gyroradius) in the collisionless limit, since short wavelength zonal flow plays a different role in regulating turbulence [9]. We find that for a given initial density perturbation the residual zonal flow level is much smaller for short wavelengths in the core. The short wavelength zonal flow is expected to be of interest in the pedestal edge plasma region as well. We then calculate the neoclassical polarization and the residual zonal flow level for arbitrary wavelengths numerically so that both finite ion banana width and ion gyroradius effects are retained. We find the zonal flow can become totally undamped in this case. Since magnetic geometry is pertinent to the residual zonal flow level [22], we then calculate the neoclassical polarization for shaped plasma cross sections with nontrivial elongation and triangularity, and find that the residual zonal flow level increases with elongation, while decreasing with triangularity.

The next chapter, Chapter 5, reviews the *H-R* collisional calculation in two asymptotic limits: the high driving frequency limit and the low driving frequency limit. We then proceed to develop a semi-analytical method, based on an eigenfunction expansion of

the collision operator [30][12], to calculate the collisional neoclassical polarization for the entire driving frequency range or arbitrary collisionalities in Chapter 6. For collision frequencies comparable to the driving wave frequency the damping of the zonal flow increases slightly as the inverse aspect ratio increases, and of course, the zonal flow is strongly damped at high collisionality.

The last chapter summarizes and discusses what we have discovered in the previous chapters.

Chapter 2

Background

Heat and particle transport in experiments is observed to be much larger than neoclassical theory[26][3] or collisional diffusion predicts. It is widely believed that this anomalous transport is caused by small spatial scale, low frequency fluctuations. These fluctuations, namely turbulence, stem from microinstabilities, such as the ion temperature gradient (ITG) mode[4][14][16][11] and trapped electron mode (TEM)[19][8][37][10][43][32]. A focus of fusion plasma research has been the physical mechanism of these micro instabilities and how to reduce the associated turbulence level [44][9][13].

An important tool to study turbulence is the gyrokinetic equation[5][1][7][21]. The gyrokinetic equation is the gyro phase averaged kinetic equation holding the guiding center fixed. For a strongly magnetized plasma, the gyromotion is the fastest motion of interest. Based on this fact, the gyrokinetic approach eliminates the gyro phase dependence of the distribution function when it is written as a function of guiding center. This gyrokinetic approach is believed to contain all the relevant physics of turbulence. Although it is greatly simplified, the gyrokinetic equation is still quite difficult to solve, even numerically. Additional simplifications are normally required. For example, in the case of drift wave turbulence, some of the neoclassical drives are usually ignored.

Another useful approach to deal with turbulence is through reduced fluid models, which essentially take the moments of the kinetic equation and then close the moment

hierarchy by approximate kinetic models. One of these fluid models is the gyrofluid model [35], which includes magnetic drift and finite Larmor radius(FLR) effects in the moment equations.

Numerical simulations show that the low frequency poloidal (and toroidal) rotation, or zonal flow, plays an important role in regulating turbulence. Specifically, in the presence of sheared zonal flows, the turbulence can be strongly reduced. Hence, the damping of these poloidal flows became an important issue. Both gyrokinetic and gyrofluid simulation can predict zonal flow damping, but gyrofluid codes [35][2] observed a much larger damping than gyrokinetic codes [36].

Rosenbluth and Hinton (R-H) performed an analytic check[44][27]. Their kinetic calculation demonstrated that the axisymmetric fluctuations can't be damped by linear collisionless kinetic effects; consistent with gyrokinetic simulations. R-H found that the linear damping term implemented in gyrofluid models is not appropriate for axisymmetric poloidal flows. Their calculation also shows that the residual zonal flow level is inversely proportional to the polarization constant of the plasma. Therefore the plasma polarization plays a crucial role in regulating zonal flow damping. In tokamaks, the majority of the polarization comes from the bounce motion of the particle trajectories, rather than the gyromotion of the particle trajectories. In fact, neoclassical polarization is bigger than classical polarization by a factor of B_T^2/B_p^2, where B_T and B_p are the toroidal and poloidal components of the magnetic field. As a result, neoclassical polarization will be the main focus of our investigations. The classical polarization is usually easy to identify.

To set the stage for our work, we briefly review the R-H model[44][27] in the remainder of this section. To determine the neoclassical part of the polarization, they start with the gyrokinetic equation and ignore the FLR effect to obtain the drift kinetic equation[23][26].

$$\frac{\partial f_1}{\partial t} + (v_{\shortparallel}\mathbf{b} + \mathbf{v}_B)\cdot\nabla f_1 - C_{ii}\{f_1\} = -\frac{e}{T}F_0\,(v_{\shortparallel}\mathbf{b} + \mathbf{v}_d)\cdot\nabla\phi + S_n, \qquad (2.1)$$

where e is the charge of the particles, including sign. For simplicity, here we assume only hydrogenic ions in the plasma. Note that f_1 is the first order or linearized distribution

function, F_0 is the lowest order distribution function, assumed to be a *Maxwellian*, and ϕ is the perturbed electrostatic potential. In addition, ∇ is the spatial gradient holding the kinetic energy $E = v^2/2$ and magnetic moment $\mu = v_\perp^2/2B$ fixed; $\mathbf{b} = \mathbf{B}/B$, is the unit vector along magnetic field; $\Omega = eB/mc$ is the gyro frequency; $\mathbf{v}_d = \mathbf{v}_B - \frac{c}{B}\mathbf{b} \times \nabla\phi$, is the total drift velocity with

$$\mathbf{v}_B = \frac{\mathbf{b}}{\Omega} \times (\mu \nabla B + v_\parallel^2 \mathbf{b} \cdot \nabla \mathbf{b}) \tag{2.2}$$

the magnetic drift; and C_{ii} is the linearized ion-ion collision operator. The source term S_n in Eq.(2.1) is the gyro average of the nonlinear term in the drift kinetic equation,

$$S_n = \frac{c}{B} \nabla\phi \times \mathbf{b} \cdot \nabla f_1 \tag{2.3}$$

The R-H's approach is to divide the electrostatic fluctuations into two groups: non-axisymmetric fluctuations and axisymmetric fluctuations. The non-axisymmetric fluctuations include unstable modes that are coupled together in the source term. On the other hand, the axisymmetric fluctuations are driven by this first group through mode coupling and then act to regulate the first group. Although solving the whole nonlinear problem consistently is desirable, it is generally too complicated and more convenient to use the R-H's approach to gain some physical insight. In R-H's approach, the axisymmetric fluctuations are treated in detail, while the effect of the non-axisymmetric fluctuations are modelled as an axisymmetric noise source with known properties.

From Eq.(2.1), the first order distribution f_1 is composed of two parts,

$$f_1 = f_1^L + f_1^{NL}, \tag{2.4}$$

where the linear part f_1^L is driven by the axisymmetric source $\frac{e}{T} F_0 \left(v_\parallel \mathbf{b} + \mathbf{v}_d\right) \cdot \nabla\phi$, and the nonlinear part f_1^{NL} is driven by the axisymmetric noise source S_n. It is convenient

to introduce the notation

$$f_1^{NL} = \int dt S_n,$$

then

$$f_1 = f_1^L + \int dt S_n, \tag{2.5}$$

and f_1^L satisfies the following equation,

$$\frac{\partial f_1^L}{\partial t} + (v_{\shortparallel}\mathbf{b} + \mathbf{v}_B) \cdot \nabla f_1^L - C_{ii}\left\{f_1^L\right\} = -\frac{e}{T} F_0 \left(v_{\shortparallel}\mathbf{b} + \mathbf{v}_d\right) \cdot \nabla \phi. \tag{2.6}$$

A Fourier representation in the direction perpendicular to the magnetic field can be applied to the preceding equation by defining,

$$\phi(\mathbf{r}, t) = \sum_k \phi_k(t)\, e^{iS}, \tag{2.7}$$

$$f_1^L(\mathbf{r}, t) = \sum_k f_k(t)\, e^{iS}, \tag{2.8}$$

with $\mathbf{k}_\perp = \nabla S$. Then in Fourier space, Eq.(2.6) becomes

$$\frac{\partial f_k}{\partial t} + \left(v_{\shortparallel}\mathbf{b} \cdot \nabla + \mathbf{v}_B \cdot i\mathbf{k}_\perp\right) f_k - C_{ii}\left\{f_k\right\} = -\frac{e}{T} F_0 \left(v_{\shortparallel}\mathbf{b} \cdot \nabla + \mathbf{v}_B \cdot i\mathbf{k}_\perp\right) \phi_k. \tag{2.9}$$

We can solve the preceding equation for f_k in terms of ϕ_k by Laplace transforming to frequency domain, by utilizing the transform pair

$$\phi_k(p) = \int_0^\infty dt e^{-pt} \phi_k(t), \tag{2.10}$$

$$\phi_k(t) = \frac{1}{2\pi i} \int dp e^{pt} \phi_k(p), \tag{2.11}$$

where $p = i\omega$, is the frequency-like variable in the Laplace transform.

We may define a polarization $\varepsilon_k^{pol}(p)$ in Fourier and frequency domain by

$$\varepsilon_k^{pol}(p)\left\langle k_\perp^2\right\rangle \phi_k(p) \equiv -4\pi\left\langle \rho_k^{pol}(p)\right\rangle, \tag{2.12}$$

where $\langle\ \ \rangle$ is the flux surface average and $\rho_k^{pol}(p)$ is polarization charge density. This definition for polarization retains only the linear portion of f_1 and may be rewritten as

$$\varepsilon_k^{pol}(p)\left\langle k_\perp^2\right\rangle \phi_k(p) = -4\pi e\left\langle \int d^3v\left(f_k^i(p) - f_k^e(p)\right)\right\rangle. \tag{2.13}$$

In the case of interest to be considered here, the ion and electron response will cancel the adiabatic response and leaving only the polarization effect. The ion polarization is larger than the electron polarization by the mass ratio, m_i/m_e, so the electron polarization is generally ignored in calculation, and we only need to consider

$$\varepsilon_k^{pol}(p)\left\langle k_\perp^2\right\rangle \phi_k(p) = -4\pi e\left\langle \int d^3v f_k^i(p)\right\rangle. \tag{2.14}$$

This expression will be used to calculate the polarization constant, $\varepsilon_k^{pol}(p)$.

The axisymmetric potential ϕ_k is determined by quasineutrality within a flux surface with both the linear and nonlinear portion of f_1 retained,

$$\left\langle \int d^3v f_1^e\right\rangle = \left\langle \int d^3v f_1^i\right\rangle. \tag{2.15}$$

In addition, we may define a noise source combining both electron and ion contributions

$$s \equiv \left\langle \int d^3v \int dt\,(S_e - S_i)\right\rangle.$$

Inserting Eq.(2.5) in Eq.(2.15) and introducing $s_k(p)$, the frequency and Fourier spectrum of the noise source s, and then combining with Eqs.(2.13,2.15), we find

$$\varepsilon_k^{pol}(p)\left\langle k_\perp^2\right\rangle \phi_k(p) = -4\pi e s_k(p). \tag{2.16}$$

For a known noise source s (one whose spectrum in Fourier and frequency domain is known), we see from Eq.(2.16) that the axisymmetric electrostatic potential $\phi_k(p)$, which drives the zonal flow, is inversely proportional to the polarizability of the plasma, $\varepsilon_k^{pol}(p)$. Moreover, we assume an initial charge $e\delta n_k(t=0)$ is established by the nonlinear noise source, during a time larger than the gyroperiod, but much smaller than a bounce time. The nonlinear source is assumed to be of the form

$$\int d^3v\,(S_{ek} - S_{ik}) = -\delta n_k(0)\,\delta(t)\,.$$

It is convenient to relate $e\delta n_k(t=0)$ to the initial electrostatic potential $\phi_k(t=0)$ by employing the following relation,

$$4\pi e\delta n_k(0) = \varepsilon_{k,cl}^{pol}\left\langle k_\perp^2\right\rangle \phi_k(t=0)\,, \tag{2.17}$$

with the classical polarization defined as

$$\varepsilon_{k,cl}^{pol} = \frac{\omega_{pi}^2}{\omega_{ci}^2}, \tag{2.18}$$

where ω_{pi} defines the ion plasma frequency, and $\omega_{ci} = eB_0/m_ic$, is the ion gyrofrequency at the magnetic axis. The preceding source gives the following noise spectrum,

$$s_k(p) = \frac{\varepsilon_{k,cl}^{pol} k_\perp^2 \phi_k(t=0)}{4\pi ep}. \tag{2.19}$$

As a result, the axisymmetric electrostatic potential $\phi_k(p)$ calculated from Eq.(2.16) is given by

$$\frac{\phi_k(p)}{\phi_k(t=0)} = \frac{\varepsilon_{k,cl}^{pol}}{p\varepsilon_k^{pol}(p)}. \tag{2.20}$$

The polarization, $\varepsilon_k^{pol}(p)$, usually contains two parts:

$$\varepsilon_k^{pol}(p) = \varepsilon_{k,cl}^{pol} + \varepsilon_{k,nc}^{pol}(p)\,. \tag{2.21}$$

The classical part $\varepsilon_{k,cl}^{pol}$ is due to the gyromotion of particles, while the neoclassical part comes from the particle's drift departure from flux surface. They are decoupled in a tokamak for large wavelength perturbations. Inverting the transform, we find that

$$\phi_k(t) = \phi_k(t=0) K_k(t), \tag{2.22}$$

where the response kernel for an initial charge perturbation, $K_k(t)$, is defined as

$$K_k(t) = \frac{\varepsilon_{k,cl}^{pol}}{2\pi i} \int \frac{dp e^{pt}}{p \varepsilon_k^{pol}(p)}, \tag{2.23}$$

with the path of the p integration from $-\infty i$ to $+\infty i$, and to the right of all the singularities of the integrand. From the preceding equation, the long time asymptotic behavior of zonal flows depends on the zero frequency polarization response, i.e.,

$$\frac{\phi_k(t=\infty)}{\phi_k(t=0)} = \frac{\varepsilon_{k,cl}^{pol}}{\varepsilon_{k,cl}^{pol} + \varepsilon_{k,nc}^{pol}(0)} \tag{2.24}$$

R-H found that in the collisionless case, the polarization doesn't depend on frequency p [44]. Therefore this collisionless polarization determines the residual zonal flow level. In R-H's paper, the dielectric susceptibility $\widetilde{\chi}_k(p)$ is used instead of the polarization constant $\varepsilon_k^{pol}(p)$. They differ from each other by a constant,

$$\widetilde{\chi}_k(p) = \frac{k_\perp^2 \rho_i^2}{\omega_{pi}^2/\omega_{ci}^2} \varepsilon_k^{pol}(p). \tag{2.25}$$

where $\rho_i = \sqrt{T_i/m_i}/\omega_{ci}$, is the gyroradius at the magnetic axis.

From the preceding expression, we conclude that for a fixed source, the smaller the polarization $\varepsilon_k^{pol}(p)$, the larger the axisymmetric electrostatic potential $\phi_k(p)$, and therefore, the larger the zonal flow which acts to reduce the turbulence level.

The polarization can also be derived by introducing a polarization current. According

to Maxwell's equation

$$\nabla \times B = \frac{4\pi}{c}\mathbf{J} + \frac{4\pi}{c}\mathbf{J}^{pol} + \frac{1}{c}\frac{\partial \mathbf{E}}{\partial t}, \tag{2.26}$$

where the current $\mathbf{J}$ refers to all the other currents except the linear polarization current $\mathbf{J}^{pol}$ and the vacuum displacement current $\partial \mathbf{E}/\partial t$. We can define the polarization through the linear polarization current $\mathbf{J}^{pol}$,

$$\varepsilon^{pol}\frac{\partial \mathbf{E}}{\partial t} = 4\pi \mathbf{J}^{pol}, \tag{2.27}$$

or in the Fourier space

$$-i\mathbf{k}_\perp \varepsilon_k^{pol}\frac{\partial \phi_k}{\partial t} = 4\pi \mathbf{J}_k^{pol}(t). \tag{2.28}$$

The polarization current $\mathbf{J}_k^{pol}$ itself should satisfy the continuity equation on a flux surface,

$$\frac{\partial}{\partial t}\left\langle \rho_k^{pol}(t)\right\rangle + \left\langle i\mathbf{k}_\perp \cdot \mathbf{J}_k^{pol}(t)\right\rangle = 0. \tag{2.29}$$

Combining the preceding two equations, we find

$$\varepsilon_k^{pol}\left\langle k_\perp^2\right\rangle \phi_k \equiv 4\pi \left\langle \rho_k^{pol}\right\rangle, \tag{2.30}$$

consistent with the previous definition for ε_k^{pol} in Eq.(2.12).

Chapter 3

Neoclassical Polarization

The previous chapter has demonstrated that the magnitude of zonal flow is inversely proportional to the neoclassical polarization for a given source. This chapter will demonstrate the calculation of neoclassical polarization and evaluate it for a circular tokamak in the collisionless limit[27]. We also calculate the classical polarization and compare it to the neoclassical polarization. Finally, we will discuss some features of the zonal flow.

3.1 Neoclassical Polarization

For a known axisymmetric potential source, the linear portion of the density fluctuations can be calculated by solving the linearized drift kinetic equation for ions ($Z_i = 1$) in $E = v^2/2$ and $\mu = v_\perp^2/2B$ variables:

$$\frac{\partial f_1^L}{\partial t} + (v_\parallel \mathbf{b} + \mathbf{v}_B) \cdot \nabla f_1^L - C_{ii}\left\{f_1^L\right\} = -\frac{e}{T} F_0 \left(v_\parallel \mathbf{b} + \mathbf{v}_B\right) \cdot \nabla \phi. \tag{3.1}$$

The linearized or perturbed distribution f_1^L is driven by the perturbed axisymmetric potential ϕ. The parallel drift $v_\parallel \mathbf{b}$ and magnetic drift $\mathbf{v}_d$, defined in Eq.(2.2), must be retained for this analysis. The lowest order distribution F_0 is assumed to be a local

Maxwellian,

$$F_0 = n_0 \left(\frac{m_i}{2\pi T_i} \right) \exp \left(-\frac{m_i v^2}{2T_i} \right). \tag{3.2}$$

In a tokamak, the potential fluctuations vary rapidly across the magnetic field, but vary smoothly along the magnetic field. This existence of disparate length scales facilitate the use of eikonal analysis. For neoclassical polarization calculations we may assume

$$\phi(\mathbf{r}, t) = \sum_k \phi_k e^{iS},$$

where ϕ_k is taken to be independent of the position along a field line. The eikonal S is assumed to be a function of flux surface, $S = S(\psi)$. The perpendicular wave vector $\mathbf{k}_\perp$ is then defined by

$$\mathbf{k}_\perp = \nabla S = S'(\psi) \nabla \psi. \tag{3.3}$$

The perturbed distribution f_1^L takes a similar form

$$f_1^L(\mathbf{r}, t) = \sum_k f_k e^{iS},$$

but f_k is allowed to vary along a field line. Therefore, in Fourier space, the drift kinetic equation in Eq.(3.1) becomes

$$\frac{\partial f_k}{\partial t} + (v_\parallel \mathbf{b} \cdot \nabla + i\omega_d) f_k - C_{ii}\{f_k\} = -\frac{e}{T} F_0 (v_\parallel \mathbf{b} \cdot \nabla + i\omega_D) \phi_k, \tag{3.4}$$

where the magnetic drift frequency ω_d is defined as,

$$\omega_d = \mathbf{k}_\perp \cdot \mathbf{v}_B.$$

The magnetic drift from Eq.(2.2) gives $\mathbf{v}_B \cdot \nabla \psi = v_\parallel \mathbf{b} \cdot \nabla \left(\frac{I v_\parallel}{\Omega} \right)$. Inserting the perpendicular wave vector $\mathbf{k}_\perp$ of Eq.(3.3) in the preceding equation, the magnetic drift frequency

ω_d can be conveniently written as

$$\omega_d = v_{\shortparallel}\mathbf{b}\cdot\nabla Q, \tag{3.5}$$

with Q defined as

$$Q = \frac{IS'v_{\shortparallel}}{\Omega}, \tag{3.6}$$

and $Q \sim k_\perp\rho_p \sim \rho_p/L_\perp$, where $\rho_p = \rho_i q/\varepsilon$ is the poloidal gyroradius, and $L_\perp$ is the perpendicular scale length. For zonal flows, the perpendicular scale length is generally much larger than the poloidal gyroradius. So $Q \ll 1$ is a reasonable assumption for the ions. For electrons, $Q \to 0$ is assumed.

Based on the preceding discussion, Eq.(3.4) can be further simplified to

$$\frac{\partial f_k}{\partial t} + \left(v_{\shortparallel}\mathbf{b}\cdot\nabla + iv_{\shortparallel}\mathbf{b}\cdot\nabla Q\right) f_k - C_{ii}\left\{f_k\right\} = -\frac{e\phi_k}{T}F_0 iv_{\shortparallel}\mathbf{b}\cdot\nabla Q. \tag{3.7}$$

To solve this equation, we may define

$$f_k \equiv -\frac{e}{T_i}\phi_k F_0 + H_k e^{-iQ}. \tag{3.8}$$

Then, the new distribution to be determined, H_k, satisfies the following equation,

$$\frac{\partial H_k}{\partial t} + v_{\shortparallel}\mathbf{b}\cdot\nabla H_k - e^{iQ}C_{ii}\left\{H_k e^{-iQ}\right\} = e^{iQ}\frac{e}{T_i}F_0\frac{\partial\phi_k}{\partial t}. \tag{3.9}$$

We may solve the preceding equation by a perturbation method for small Q. For $Q \ll 1$, we may expand H_k

$$H_k = H_k^{(0)} + H_k^{(1)} + H_k^{(2)} + ...,$$

where $H_k^{(j+1)} = H_k^{(j)} \mathcal{O}(Q)$. The leading order kinetic equation in this expansion becomes

$$\frac{\partial H_k^{(0)}}{\partial t} + v_{\shortparallel} \mathbf{b} \cdot \nabla H_k^{(0)} - C_{ii}\left\{H_k^{(0)}\right\} = \frac{e}{T_i} F_0 \frac{\partial \phi_k}{\partial t}. \tag{3.10}$$

By inspection, we find that the leading order solution is simply,

$$H_k^{(0)} = \frac{e}{T_i} F_0 \phi_k, \tag{3.11}$$

since $\mathbf{b} \cdot \nabla H_k^{(0)} = C_{ii}\left\{H_k^{(0)}\right\} = 0$. The next order kinetic equation in the preceding expansion gives

$$\frac{\partial H_k^{(1)}}{\partial t} + v_{\shortparallel} \mathbf{b} \cdot \nabla H_k^{(1)} - C_{ii}\left\{H_k^{(1)}\right\} = iQ \frac{e}{T_i} F_0 \frac{\partial \phi_k}{\partial t}, \tag{3.12}$$

since $C_{ii}\left\{H_k^{(0)} Q\right\} = 0$ as well. In addition, the second order kinetic equation in the preceding expansion becomes

$$\frac{\partial H_k^{(2)}}{\partial t} + v_{\shortparallel} \mathbf{b} \cdot \nabla H_k^{(2)} - C_{ii}\left\{H_k^{(2)}\right\} - iQC_{ii}\left\{H_k^{(1)}\right\} + C_{ii}\left\{iQH_k^{(1)}\right\} = -\frac{1}{2} Q^2 \frac{e}{T_i} F_0 \frac{\partial \phi_k}{\partial t}. \tag{3.13}$$

In terms of the $H_k^{(j)}$, the perturbed density function f_k to the requisite accuracy can be written as,

$$\begin{aligned} f_k &= e^{-iQ}\left(H_k - e^{iQ}\frac{e}{T_i}F_0\phi_k\right) \\ &\cong e^{-iQ}\left(\frac{e}{T_i}F_0\phi_k\left(1 - e^{iQ}\right) + H_k^{(1)} + H_k^{(2)}\right) \\ &= \left(-\frac{e}{T_i}F_0\phi_k iQ + H_k^{(1)}\right)(1 - iQ) + \frac{e}{T_i}F_0\phi_k\frac{1}{2}Q^2 + H_k^{(2)} \end{aligned} \tag{3.14}$$

Fortunately, it is not necessary to solve Eq.(3.12) and (3.13) for $H_k^{(1)}$ and $H_k^{(2)}$. Instead, to calculate the polarization constant, it is convenient to make a detour and first calculate the time change of flux-surface averaged polarization density, $\left\langle n_k^{pol} \right\rangle = \left\langle \int d^3v f_k \right\rangle$, to

obtain

$$\frac{\partial}{\partial t}\left\langle n_k^{pol}\right\rangle = \frac{\partial}{\partial t}\left\langle \int d^3v f_k \right\rangle = \left\langle \int d^3v \frac{\partial}{\partial t} f_k \right\rangle \tag{3.15}$$
$$= \left\langle \int d^3v \left[\left(-\frac{ieQF_0}{T_i}\frac{\partial \phi_k}{\partial t} + \frac{\partial H_k^{(1)}}{\partial t} \right)(1-iQ) + \frac{eQ^2F_0}{2T_i}\frac{\partial \phi_k}{\partial t} + \frac{\partial H_k^{(2)}}{\partial t} \right] \right\rangle$$

Inserting Eqs.(3.12) and (3.13) for $\frac{\partial H_k^{(1)}}{\partial t}$ and $\frac{\partial H_k^{(2)}}{\partial t}$ in the preceding equation and utilizing the properties of linear ion-ion collisional operator C_{ii}, we find

$$\frac{\partial}{\partial t}\left\langle n_k^{pol}\right\rangle = \left\langle \int d^3v \left(-\frac{e}{T_i}F_0 iQ \frac{\partial \phi_k}{\partial t} + \frac{\partial H_k^{(1)}}{\partial t} \right)(-iQ) \right\rangle .$$

Thus, we obtain

$$\left\langle n_k^{pol}\right\rangle = -\left\langle \int d^3v \left(iQh_k + \frac{e}{T_i}\phi_k F_0 Q^2 \right) \right\rangle , \tag{3.16}$$

where we let $h_k \equiv H_k^{(1)}$. This expression for the polarization density is accurate to second order in Q^2, yet we need only solve the first order equation, Eq.(3.12), for the first order distribution $H_k^{(1)} = h_k$:

$$\frac{\partial h_k}{\partial t} + v_{\shortparallel}\mathbf{b}\cdot\nabla h_k - C_{ii}\left\{h_k\right\} = iQ\frac{e}{T_i}F_0\frac{\partial \phi_k}{\partial t}. \tag{3.17}$$

At this stage, a further simplification can be made to the polarization density in Eq.(3.16) for a large aspect ratio circular tokamak model. Define the pitch angle variable $\lambda = v_\perp^2 B_0/v^2 B$, with B_0 the on axis value of magnetic field and $B_0/B = R/R_0 = 1+\varepsilon\cos\theta$, then the velocity volume element d^3v can be written as

$$d^3v = \frac{4\pi BE dE d\lambda}{B_0\left|v_{\shortparallel}\right|} \tag{3.18}$$

Inserting the definition of Q in Eq.(3.6), and carrying out the energy E integration, we

find a form convenient for our purposes:

$$\left\langle n_k^{pol} \right\rangle = n_0 \frac{e\phi_k}{T_i} k_\perp^2 \rho_i^2 \frac{B_0^2}{B_p^2} \frac{3}{2} \int d\lambda \left(\left\langle \frac{\Omega_0 T_i}{i\sigma I S' v e \phi_k F_0} \oint \frac{d\theta h}{2\pi} h_k \right\rangle_E - \oint \frac{d\theta h^2}{2\pi} \xi \right), \quad (3.19)$$

where $\xi = |v_\parallel| / v$, is the dimensionless parallel speed, $h \equiv \frac{B_0}{B} = 1 + \varepsilon \cos\theta$ for a large aspect ratio circular tokamak, and the energy average is defined as

$$\langle A \rangle_E = \frac{\int_0^\infty dE E^{3/2} e^{-mE/T} A}{\int_0^\infty dE E^{3/2} e^{-mE/T}}. \quad (3.20)$$

The preceding equation can be used in Eq.(2.14) to obtain the neoclassical polarization constant in the form,

$$\varepsilon_{k,nc}^{pol}(p) = \frac{\omega_{pi}^2}{\omega_{ci}^2} \frac{q^2}{\varepsilon^2} \frac{3}{2} \int d\lambda \left(- \left\langle \frac{\Omega_0 T_i}{i\sigma I S' v e \phi_k F_0} \oint \frac{d\theta h}{2\pi} h_k \right\rangle_E + \oint \frac{d\theta h^2}{2\pi} \xi \right) \quad (3.21)$$

where $\varepsilon = r/R_0$ is the inverse aspect ratio for a tokamak. This form of the expression for $\varepsilon_{k,nc}^{pol}(p)$ is convenient to display the λ space structure of total perturbed distribution and determine the contributions from trapped particles and passing particles separately, even though the second term in the preceding equation can easily be integrated by using

$$\int d^3 v v_\parallel^2 F_0 = \frac{n_0 T_i}{m_i}$$

to obtain the neoclassical polarization constant in the form,

$$\varepsilon_{k,nc}^{pol}(p) = \frac{\omega_{pi}^2}{\omega_{ci}^2} \frac{q^2}{\varepsilon^2} \left(- \int d\lambda \left\langle \frac{3\Omega_0 T_i}{2i\sigma I S' v e \phi_k F_0} \oint \frac{d\theta h}{2\pi} h_k \right\rangle_E + 1 \right). \quad (3.22)$$

The remaining task is to solve the kinetic equation, Eq.(3.17), for the distribution h_k.

Compared to the original drift kinetic equation Eq.(3.1), Eq.(3.17) is greatly simplified, but it is still difficult to solve directly. However, we can solve it in some interesting limits. In particular, when the drive frequency of zonal flows is much smaller than the ion bounce frequency, $\omega \ll \omega_b$, we may perform transit average to annihilate the streaming

term in Eq.(3.17).

3.2 Transit Average Kinetic Equation

Following H-R's approach [27], we solve Eq.(3.17) perturbatively by expanding in $\omega/\omega_b \ll 1$, by writing

$$h_k = h_k^{(1)} + h_k^{(2)} + ...$$

Then, the leading order equation reads

$$v_{\shortparallel}\mathbf{b}\cdot\nabla h_k^{(1)} = 0, \tag{3.23}$$

which gives that $h_k^{(1)}$ is independent of poloidal angle θ, i.e.,

$$h_k^{(1)} = h_k^{(1)}(\psi, \lambda, E) \tag{3.24}$$

The next order equation becomes,

$$\frac{\partial h_k^{(1)}}{\partial t} + v_{\shortparallel}\mathbf{b}\cdot\nabla h_k^{(2)} - C_{ii}\left\{h_k^{(1)}\right\} = iQ\frac{e}{T_i}F_0\frac{\partial\phi_k}{\partial t}. \tag{3.25}$$

A transit average of the preceding equation gives

$$\frac{\partial h_k^{(1)}}{\partial t} - \overline{C_{ii}\left\{h_k^{(1)}\right\}} = i\overline{Q}\frac{e}{T_i}F_0\frac{\partial\phi_k}{\partial t}, \tag{3.26}$$

where the transit average is defined as,

$$\overline{A} = \frac{\oint d\tau A}{\oint d\tau} \tag{3.27}$$

with $d\tau = d\theta/\left(v_{\shortparallel}\mathbf{b}\cdot\nabla\theta\right)$. For trapped particles, this average is over a full bounce; while for passing particles, it is over one complete poloidal circuit. Specifically, for a large aspect

ratio circular cross section tokamak, a convenient approximation is $d\tau \cong qR_0 d\theta/v_{\shortparallel}$, where q is the safety factor. In this case the transit average is thus written as

$$\overline{A} = \frac{\oint \frac{d\theta}{v_{\shortparallel}} A}{\oint \frac{d\theta}{v_{\shortparallel}}}, \tag{3.28}$$

The preceding transit averaged equation (3.26) is what Hinton and Rosenbluth(*H-R*) solve to obtain their collisional polarization [27].

3.3 Collisionless Polarization

It is difficult to find a general analytic solution to the transit average kinetic equation Eq.(3.26) in the presence of collisions. However, following R-H we can solve it in the collisionless limit, where it becomes

$$\frac{\partial h_k^{(1)}}{\partial t} = i\overline{Q}\frac{e}{T_i}F_0\frac{\partial \phi_k}{\partial t}. \tag{3.29}$$

This equation is easily integrated to obtain

$$h_k^{(1)} = i\overline{Q}\frac{e\phi_k}{T_i}F_0, \tag{3.30}$$

giving the perturbed distribution

$$f_k = i\left(\overline{Q} - Q\right)\frac{e\phi_k}{T_i}F_0 + \mathcal{O}\left(Q^2\right). \tag{3.31}$$

Note that $h_k^{(1)}$ vanishes for trapped particles, since $\overline{Q} = 0$ for trapped particles. Inserting this solution in Eq.(3.21), we obtain the expression for the collisionless polarization,

$$\varepsilon_{k,nc}^{pol}(p) = \frac{\omega_{pi}^2}{\omega_{ci}^2}\frac{q^2}{\varepsilon^2}\frac{3}{2}\int d\lambda\left(-\frac{2\pi}{\oint \frac{d\theta}{\xi}} + \frac{1}{2\pi}\oint d\theta\xi\right). \tag{3.32}$$

where $\sigma = 1$ for passing particles and $\sigma = 0$ for trapped particles. We may rewrite the preceding equation as

$$\varepsilon_{k,nc}^{pol}(p) = \frac{\omega_{pi}^2}{\omega_{ci}^2}\frac{q^2}{\varepsilon^2}(S_2 - P_1), \tag{3.33}$$

where

$$P_1 = \frac{3}{2}\int_0^{\lambda_c} d\lambda T_1(\lambda), \text{ with } T_1(\lambda) = \frac{2\pi}{\oint \frac{d\theta}{\xi}}, \tag{3.34}$$

$$S_2 = \frac{3}{2}\int_0^{\lambda_m} d\lambda T_2(\lambda), \text{ with } T_2(\lambda) = \frac{1}{2\pi}\oint d\theta \xi. \tag{3.35}$$

The detailed calculations that follow are performed for a circular tokamak in the large aspect ratio limit, $\varepsilon \ll 1$, since in this limit, analytic solutions are possible. In the preceding equations, λ_c is the pitch angle of the trapped-passing boundary. For a circular tokamak, $\lambda_c = 1 - \varepsilon$. We denote the maximum value of pitch angle by λ_m; for a circular tokamak, $\lambda_m = 1 + \varepsilon$.

The function $T_1(\lambda)$ and $T_2(\lambda)$ can be evaluated explicitly using elliptic integrals in the large aspect ratio limit. For passing particles, $\lambda \leq \lambda_c$, we find

$$T_1^p(\lambda) = \frac{\pi}{2}\frac{\sqrt{1-\lambda+\varepsilon}}{K\left(\frac{2\varepsilon}{1+\varepsilon-\lambda}\right)}, \tag{3.36}$$

$$T_2^p(\lambda) = \frac{2}{\pi}\sqrt{1-\lambda+\varepsilon}E\left(\frac{2\varepsilon}{1+\varepsilon-\lambda}\right). \tag{3.37}$$

For trapped particles, $\lambda_c \leq \lambda \leq \lambda_m$, we find

$$T_2^t(\lambda) = \frac{2}{\pi}\sqrt{2\varepsilon}\left(E\left(\frac{1+\varepsilon-\lambda}{2\varepsilon}\right) + \left(\frac{1+\varepsilon-\lambda}{2\varepsilon} - 1\right)K\left(\frac{2\varepsilon}{1+\varepsilon-\lambda}\right)\right). \tag{3.38}$$

With these expressions, the integrals of P_1 and S_2 in Eqs.(3.34) and (3.35) can be eval-

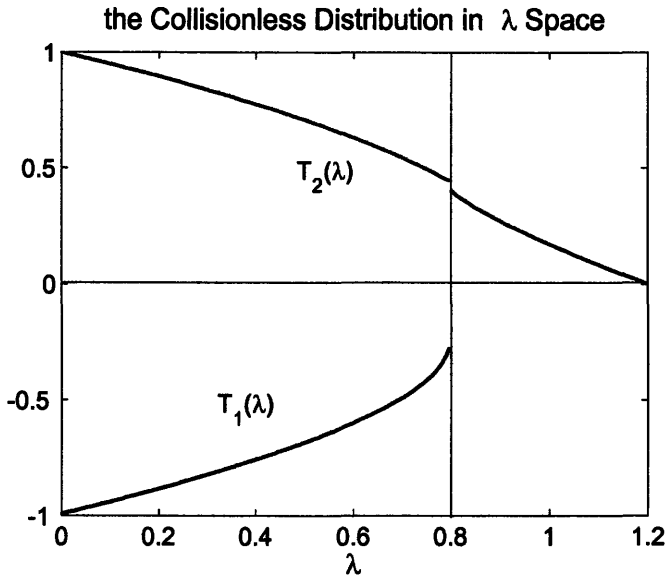

Figure 3-1: The collisionless distribution in λ space for $\varepsilon = 0.2$.

uated to $\mathcal{O}\left(\varepsilon^{3/2}\right)$ accuracy to find:

$$P_1 = 1 - 1.635\varepsilon^{3/2}, \tag{3.39}$$

$$S_2^p = 1 - \frac{4}{3\pi}(2\varepsilon)^{3/2}, \tag{3.40}$$

$$S_2^t = \frac{4}{3\pi}(2\varepsilon)^{3/2}, \tag{3.41}$$

and $S_2 = S_2^t + S_2^p$. From these calculations, we see that the passing particle's polarization cancels the trapped particle's polarization to the leading order, $\mathcal{O}(1)$, and a small residue, of order $\mathcal{O}\left(\varepsilon^{3/2}\right)$, remains. Hence, the final value for the collisionless neoclassical polarization is

$$\varepsilon_{k,nc}^{pol}(p) = 1.6\frac{q^2}{\sqrt{\varepsilon}}\frac{\omega_{pi}^2}{\omega_{ci}^2}. \tag{3.42}$$

Adding in the classical polarization discussed next, the total polarization in the collision-

less limit for $k_\perp^2 \rho_i^2 \ll 1$, is

$$\varepsilon_k^{pol}(p) = \frac{\omega_{pi}^2}{\omega_{ci}^2}\left(1 + 1.6\frac{q^2}{\sqrt{\varepsilon}}\right). \tag{3.43}$$

This result is the well known *Rosenbluth-Hinton* collisionless polarization.

3.4 Classical Polarization

The classical polarization can be obtained by considering a screw pinch model, where no neoclassical effects like drift departures from flux surfaces are involved. To calculate the classical polarization, we need to consider the gyrokinetic equation [7][21], instead of the drift kinetic equation employed earlier. As a result, we consider

$$\frac{\partial}{\partial t} g_k + \left(v_\parallel \mathbf{b}\cdot\nabla + i\omega_D\right) g_k = \frac{e}{T_i} F_0 J_0 \frac{\partial \phi_k}{\partial t}, \tag{3.44}$$

where g_k is the Fourier transform of the nonadiabatic part of the perturbed distribution and the total distribution is given by

$$f = F_0 - \frac{e\phi}{T_i} + g. \tag{3.45}$$

The function $J_0 = J_0\left(\frac{k_\perp v_\perp}{\Omega}\right)$, is the zeroth order Bessel function, and comes from gyroaveraging the potential ϕ holding the guiding center fixed instead of the particle location. For simplicity, we also assume no collisions in this calculation.

For a screw pinch model, the magnetic field is helical and given by

$$B = B_0 \widehat{z} + B_\theta(r)\,\widehat{\theta}. \tag{3.46}$$

Therefore, the magnetic drift is

$$\mathbf{v}_B = \frac{1}{\Omega}\mathbf{b} \times \widehat{r}\left(\frac{\mu B_\theta' B_\theta}{\sqrt{B_0^2 + B_\theta^2}} - \frac{B_\theta^2}{B_0^2 + B_\theta^2}\frac{v_\parallel^2}{r}\right) \tag{3.47}$$

where the factor $B_0 = const.$ Since this drift has no component in the radial direction, the drift frequency $\omega_d = 0$. If we assume no θ dependence for the potential ϕ_k, as we did in the neoclassical case, the distribution g_k will be independent of θ due to axisymmetry, giving $v_\parallel \mathbf{b} \cdot \nabla g_k = 0$. Then, the gyrokinetic equation becomes simply

$$\frac{\partial}{\partial t} g_k = \frac{e}{T_i} F_0 J_0 \frac{\partial \phi_k}{\partial t}, \tag{3.48}$$

and has the solution

$$g_k = \frac{e\phi_k}{T_i} F_0 J_0. \tag{3.49}$$

Using this result along with Eqs.(3.45) and (2.14), we find

$$\varepsilon_{k,cl}^{pol}(p) = \frac{4\pi n_0 e^2}{\langle k_\perp^2 \rangle T_i}\left(1 - \frac{1}{n_0}\left\langle \int d^3 v F_0 J_0^2 \right\rangle\right). \tag{3.50}$$

The integral can be carried out to obtain

$$\varepsilon_{k,cl}^{pol}(p) = \frac{\omega_{pi}^2}{\omega_{ci}^2}\frac{1}{\langle k_\perp^2 \rangle \rho_i^2}\left(1 - \left\langle \Gamma_0\left(k_\perp^2 \rho_i^2 \frac{B_0^2}{B^2}\right)\right\rangle\right), \tag{3.51}$$

where the function $\Gamma_0(b) \equiv I_0(b) e^{-b}$, with I_0 a modified *Bessel* function of the first kind. When $k_\perp \rho_i \ll 1$, $\Gamma_0(k_\perp^2 \rho_i^2) = 1 - k_\perp^2 \rho_i^2 \frac{B_0^2}{B^2} + O\left(k_\perp^4 \rho_i^4 \frac{B_0^4}{B^4}\right)$, giving

$$\varepsilon_{k,cl}^{pol}(p) \cong \varepsilon_{k,cl}^{pol} = \frac{\omega_{pi}^2}{\omega_{ci}^2}. \tag{3.52}$$

This classical polarization is purely due to the gyromotion of the particles. When the gyromotion and bounce motion are on disparate time scales, such as in a tokamak, the classical polarization and neoclassical polarization are decoupled from each other and

become additive in the long wavelength limit. Usually neoclassical polarization is much larger than classical polarization, as we have shown, due to neoclassical enhancement q^2/ε^2.

3.5 Poloidal and Toroidal Rotation

It is widely accepted that the zonal flow only includes poloidal rotation of plasmas. In truth the zonal flow also includes a toroidal rotation as demonstrated by the following calculation.

The complete solution to the linearized kinetic equation includes both gyrophase independent $\overline{f}$ and gyrophase dependent $\widetilde{f}$ contributions: $f = \overline{f} + \widetilde{f}$. The gyrophase independent part $\overline{f}$ produces a parallel flow, which can be calculated to accuracy of $\mathcal{O}(Q^2)$ in the collisionless limit using $\overline{f} = F_0 + f_1^L$. Here f_1^L is the linearized distribution, satisfying Eq.(3.1), so includes neoclassical and polarization effects. For the demonstration here, only the polarization part is of interest. It has been calculated and is given by Eq.(3.14) in Fourier space to $\mathcal{O}(Q^2)$ accuracy. Therefore, the parallel flow is

$$u_{\|} = \frac{1}{n_0}\int d^3v v_{\shortparallel}\overline{f} = \frac{1}{n_0}\int d^3v v_{\shortparallel} f_1^L. \tag{3.53}$$

The Q^2 terms in Eq.(3.14) contribute nothing to the preceding integral due to the odd parity of the integrand. Recalling Eqs.(3.30) and (3.8), and $H_k \cong h_k^{(1)}$, to $\mathcal{O}(Q^2)$ accuracy, we only need to insert $f_1^L = \sum_{\mathbf{k}} \frac{e\phi_k}{T_i} i\left(\overline{Q} - Q\right) F_0$ to obtain

$$u_{\|} = \frac{eI}{n_0 T_i}\frac{\partial\phi}{\partial\psi}\int d^3v F_0 v_{\shortparallel}\left(\overline{\left(\frac{v_{\shortparallel}}{\Omega}\right)} - \frac{v_{\shortparallel}}{\Omega}\right). \tag{3.54}$$

Carrying out the integration for the second term in the preceding equation, we find

$$u_{\|} = BF(\psi) - \frac{\partial\phi}{\partial\psi}\frac{cI}{B}, \tag{3.55}$$

with the flux function $F(\psi)$ defined as

$$F(\psi) = \frac{eI}{n_0 T_i}\frac{\partial \phi}{\partial \psi}\int d^3v F_0 \frac{v_{\shortparallel}}{B}\overline{\left(\frac{v_{\shortparallel}}{\Omega}\right)}. \tag{3.56}$$

The perpendicular flow is given by the gyrophase dependent part $\widetilde{f}$, which is simply the diamagnetic term

$$\widetilde{f} = \frac{1}{\Omega}\mathbf{v}\times\mathbf{b}\cdot\nabla|_{\epsilon}F_0, \tag{3.57}$$

with gradient taken holding the total energy $\epsilon \equiv v^2/2 + \frac{e}{m_i}\phi$ fixed. Therefore, taking the gradient holding E fixed gives

$$\widetilde{f} = \frac{1}{\Omega}\mathbf{v}\times\mathbf{b}\cdot\left(\nabla|_E F_0 + \frac{e}{T_i}F_0\nabla\phi\right). \tag{3.58}$$

The first term in the preceding equation gives the diamagnetic flow, which combines with the parallel neoclassical flow to give a divergence free flow. This piece is ignored as small when evaluating the zonal flow. The second term in the preceding equation gives the poloidal zonal flow that is of interest, namely

$$\begin{aligned}\mathbf{u}_{\perp} &= \frac{1}{n_0}\int d^3v \mathbf{v}_{\perp}\widetilde{f} \\ &= \frac{e}{n_0 T_i \Omega}\mathbf{b}\times\nabla\phi\cdot\int d^3v \mathbf{v}_{\perp}\mathbf{v}_{\perp}F_0,\end{aligned} \tag{3.59}$$

which not surprisingly simply turns out to be

$$\mathbf{u}_{\perp} = \frac{c}{B}\mathbf{b}\times\nabla\phi. \tag{3.60}$$

Combining the parallel flow in Eq.(3.55) and perpendicular flow from the preceding equation, we find the divergence free flow

$$\mathbf{u} = -c\frac{\partial\phi}{\partial\psi}R\widehat{\zeta} + \mathbf{B}F(\psi), \tag{3.61}$$

with $\widehat{\zeta} = R\nabla\zeta$, the unit vector in the toroidal direction. From the preceding equation, we see that the zonal flow not only contains poloidal rotation, but also toroidal rotation. In the collisionless limit, the function $F(\psi)$ can be evaluated for a circular tokamak in the same way we calculate the collisionless polarization in the previous section to find

$$F(\psi) = \frac{\partial\phi}{\partial\psi}\frac{cI}{B_0^2}(1 - 1.6\varepsilon^{3/2}), \tag{3.62}$$

where $B_0 = I/R_0$. Therefore, the total flow becomes

$$\mathbf{u} = -cR\frac{\partial\phi}{\partial\psi}\widehat{\zeta} + \frac{cR_0}{B_0}\frac{\partial\phi}{\partial\psi}(1 - 1.6\varepsilon^{3/2})\mathbf{B}, \tag{3.63}$$

which gives the toroidal velocity

$$u_\zeta = -R_0 c\frac{\partial\phi}{\partial\psi}\left(2\varepsilon\cos\theta + 1.6\varepsilon^{3/2}\right) \tag{3.64}$$

and

$$u_{pol} = R_0 c\frac{\partial\phi}{\partial\psi}\frac{\varepsilon}{q}(1 - 1.6\varepsilon^{3/2}). \tag{3.65}$$

Hence, toroidal rotation and poloidal rotation both exist for zonal flows and are of similar magnitude, $O\left(\varepsilon c R_0 \frac{\partial\phi}{\partial\psi}\right)$, with the toroidal flow larger on the outboard side than on the inboard side.

Chapter 4

Several Collisionless Issues

In the preceding chapter, we have discussed the collisionless neoclassical polarization to some detail. But there are still several interesting issues worth exploring in the collisionless limit, e.g., when Q in Eq.(3.6) is large enough that the $Q \ll 1$ expansion is no longer accurate; and when the shape of plasma is not circular so that the elongation and triangularity effects need to be considered. In this chapter we will explore these interesting issues to see how the neoclassical polarization and residual zonal flow level are influenced.

4.1 Large Q Case

When we calculate the collisionless neoclassical polarization, we assume that the Q factor in Eq.(3.6) is much smaller than one and expand the distribution f_k for $Q \ll 1$. Actually, in the collisionless limit, there exists a general solution to the distribution f_k[44], valid for all orders of Q.

To start the calculation we return to Eq.(3.9). The transit average is performed to annihilate the streaming term to obtain

$$H_k = \frac{e\phi_k}{T_i} F_0 \overline{e^{iQ}}. \tag{4.1}$$

With this expression, the perturbed distribution f_k in Eq.(3.8) becomes

$$f_k = \frac{e\phi_k}{T_i} F_0 \left(-1 + e^{-iQ}\overline{e^{iQ}}\right). \tag{4.2}$$

Inserting this expression in Eq.(2.14) we obtain the neoclassical polarization

$$\varepsilon_{k,nc}^{pol} = \frac{\omega_{pi}^2/\omega_{ci}^2}{k_\perp^2 \rho_i^2} \left(1 - \frac{1}{n_0} \left\langle \int d^3v F_0 e^{-iQ}\overline{e^{iQ}} \right\rangle\right), \tag{4.3}$$

where $Q \sim k_\perp \rho_p \sim k_\perp \rho_i q/\varepsilon$. In the preceding chapter, we assume $Q \ll 1$ and calculate the polarization accurate to $\mathcal{O}(Q^2)$. The assumption $Q \ll 1$ is usually adequate for the core plasma. However, in the edge plasma or for large $k_\perp$, the factor Q becomes of order unity or even larger so the small Q assumption is no longer valid. Therefore, polarization in the range of $k_\perp \rho_p \sim 1$, but $k_\perp \rho_i \ll 1$ is of practical interest.

4.1.1 Analytical Calculation

It is not possible to integrate Eq.(4.3) analytically for arbitrary Q. Therefore, we first study the case where $Q^2 \ll 1$ by extending the expansion to order Q^4. In this case, we may expand Eq.(4.3) to obtain an approximate analytical result for a large aspect ratio circular tokamak:

$$\begin{aligned}
\frac{1}{n_0}\left\langle \int d^3v F_0 e^{-iQ}\overline{e^{iQ}} \right\rangle &= \frac{1}{n_0}\left\langle \int d^3v F_0 \overline{e^{-iQ}}\ \overline{e^{iQ}} \right\rangle \\
&= \frac{1}{2\pi^{3/2}} \int_0^{+\infty} dy e^{-y}\sqrt{y} \int d\lambda \oint \frac{d\theta}{\xi} \overline{e^{-iQ}}\ \overline{e^{iQ}} \qquad (4.4) \\
&= \frac{1}{2\pi^{3/2}} \int_0^{+\infty} dy e^{-y}\sqrt{y} \int d\lambda \oint \frac{d\theta}{\xi} (1 + \overline{Q}^2 - \overline{Q^2} \\
&\quad + \frac{1}{12}\overline{Q^4} + \frac{1}{4}\overline{Q^2}^2 - \frac{1}{3}\overline{QQ^3}), \qquad (4.5)
\end{aligned}$$

where $y = m_i E/T_i$ and $Q = IS'\xi h/\Omega_0$, with $h = 1 + \varepsilon\cos\theta$. Inserting the preceding equation in Eq.(4.3), we obtain

$$\varepsilon^{pol}_{k,nc} = -\frac{\omega^2_{pi}/\omega^2_{ci}}{k^2_\perp \rho^2_i}\frac{1}{2\pi^{3/2}}\int_0^{+\infty} dy e^{-y}\sqrt{y}\int d\lambda \oint \frac{d\theta}{\xi}\left(\overline{Q}^2 - \overline{Q^2} + \frac{1}{12}\overline{Q^4} + \frac{1}{4}\overline{Q^2}^2 - \frac{1}{3}\overline{Q}\;\overline{Q^3}\right). \tag{4.6}$$

We can evaluate the preceding expression term by term for $\varepsilon \ll 1$, accurate to $\mathcal{O}(\varepsilon^4)$. The full details of the calculation are given in Appendix B.

Recalling that $\overline{Q} = 0$ for the trapped particles, there are two terms that only contains contributions from the passing particles, $\overline{Q}^2$ and $-\frac{1}{3}\overline{Q}\;\overline{Q^3}$. They are computed first to obtain

$$\begin{aligned}\int_0^{1-\varepsilon} d\lambda \oint \frac{d\theta}{\xi}\overline{Q}^2 &= \frac{8\pi m_i E}{3T}(1 - 1.6\varepsilon^{3/2} + \varepsilon^2 - 0.36\varepsilon^{5/2} \\ &\quad -0.03\varepsilon^{7/2} + \frac{1}{10}\varepsilon^4)k^2_\perp \rho^2_p, \qquad (4.7)\\ \int_0^{1-\varepsilon} d\lambda \oint \frac{d\theta}{\xi}\overline{Q}\;\overline{Q^3} &= \frac{16\pi}{5}\left(\frac{m_i E}{T}\right)^2(1 - \frac{1}{6}\varepsilon^2 - 0.23\varepsilon^{5/2} \\ &\quad +3.9\varepsilon^{7/2} - \frac{55}{12}\varepsilon^4)k^4_\perp \rho^4_p. \qquad (4.8)\end{aligned}$$

where the details are left to Appendix B and $k_\perp \rho_p$ is defined as

$$k_\perp \rho_p = \frac{IS'}{\Omega_0}\sqrt{\frac{T_i}{m_i}}. \tag{4.9}$$

The remaining three terms contain contributions from both trapped and passing particles. However, two of them can be computed exactly,

$$\begin{aligned}\int d^3v v^2_\parallel F_0 &= n_0\frac{T_i}{m_i}, \qquad (4.10)\\ \int d^3v v^4_\parallel F_0 &= 3n_0\left(\frac{T_i}{m_i}\right)^2, \qquad (4.11)\end{aligned}$$

Using these results, we find

$$\int d\lambda \oint \frac{d\theta}{\xi} \overline{Q^2} = \frac{2}{3}\frac{m_i E}{T}\left(1+\frac{3}{2}\varepsilon^2\right) k_\perp^2 \rho_p^2, \tag{4.12}$$

$$\int d\lambda \oint \frac{d\theta}{\xi} \overline{Q^4} = \frac{16\pi}{5}\left(\frac{m_i E}{T}\right)^2 \left(1+5\varepsilon^2+\frac{15}{8}\varepsilon^4\right) k_\perp^4 \rho_p^4. \tag{4.13}$$

The last term involves the most effort to compute accurately. The full details are provided in Appendix B and lead to the result

$$\int d\lambda \oint \frac{d\theta}{\xi} \overline{Q^2}^2 = \frac{16\pi}{5}\left(\frac{m_i E}{T}\right)^2 \left(1+\frac{1}{3}\varepsilon^2+1.46\varepsilon^{5/2}-0.4\varepsilon^{7/2}+\frac{7}{4}\varepsilon^4\right) k_\perp^4 \rho_p^4. \tag{4.14}$$

Combining with the preceding results, the polarization in Eq.(4.6) is found to be

$$\begin{aligned} \varepsilon_{k,nc}^{pol} &= \frac{\omega_{pi}^2}{\omega_{ci}^2}\frac{q^2}{\varepsilon^2}[(1.6\varepsilon^{3/2}+\frac{1}{2}\varepsilon^2+0.36\varepsilon^{5/2}+0.03\varepsilon^{7/2}-\frac{1}{10}\varepsilon^4) \\ &\quad -k_\perp^2\rho_p^2(\frac{5}{3}\varepsilon^2+1.3\varepsilon^{5/2}-4.2\varepsilon^{7/2}+\frac{611}{96}\varepsilon^4)]. \end{aligned} \tag{4.15}$$

This analytical expression allows $k_\perp \rho_p$ to be closer to one, but still requires $k_\perp^4 \rho_p^4$ to be much smaller than one. It also provides a benchmark to check the $Q \sim 1$ numerical calculation of ε_k^{pol} considered next.

4.1.2 Numerical Calculation

A numerical calculation is necessary when $k_\perp^4 \rho_p^4$ is no longer small. First, we notice

$$\oint \frac{d\theta}{\xi} e^{-iQ}\overline{e^{iQ}} = \left(\oint \frac{d\theta}{\xi}\right)^{-1}\left[\left(\oint \frac{d\theta}{\xi}\cos Q\right)^2+\left(\oint \frac{d\theta}{\xi}\sin Q\right)^2\right]. \tag{4.16}$$

However, this form is not very convenient for numerical integration because the function $\cos Q$ contains a unity factor that cancels in Eq.(4.3), after which we expect to observe very small variations, of $\mathcal{O}\left(\varepsilon^{3/2}\right)$. Hence, it is useful to transform the preceding equation

to the following form,

$$\oint \frac{d\theta}{\xi} e^{-iQ\overline{e^{iQ}}} = \oint \frac{d\theta}{\xi} + K(Q), \tag{4.17}$$

with the function $K(Q)$ defined as

$$\begin{aligned} K(Q) &= 2\oint \frac{d\theta}{\xi}(\cos Q - 1) + \left(\oint \frac{d\theta}{\xi}\right)^{-1} \\ &\quad \left\{\left[\oint \frac{d\theta}{\xi}(\cos Q - 1)\right]^2 + \left(\oint \frac{d\theta}{\xi}\sin Q\right)^2\right\}. \end{aligned} \tag{4.18}$$

As a result, the polarization becomes

$$\varepsilon_{k,nc}^{pol} = -\frac{\omega_{pi}^2/\omega_{ci}^2}{k_\perp^2\rho_i^2}\frac{1}{2\pi^{3/2}}\int_0^{+\infty} dy e^{-y}\sqrt{y}\int d\lambda K(Q). \tag{4.19}$$

Notice that for $Q \ll 1$ we may expand to obtain

$$\overline{\cos Q - 1} = -\frac{1}{2}\overline{Q^2} + \frac{1}{24}\overline{Q^4} + \mathcal{O}\left(Q^6\right), \tag{4.20}$$

$$\overline{\cos Q - 1}^2 = \frac{1}{4}\overline{Q^2}^2 + \mathcal{O}\left(Q^6\right), \tag{4.21}$$

$$\overline{\sin Q}^2 = \overline{Q}^2 - \frac{1}{3}\overline{QQ^3} + \mathcal{O}\left(Q^6\right). \tag{4.22}$$

Inserting these expressions in Eq.(4.18), we find

$$\begin{aligned} K(Q) &= \oint \frac{d\theta}{\xi}\left(2\overline{\cos Q - 1} + \overline{\cos Q - 1}^2 + \overline{\sin Q}^2\right) \\ &= \oint \frac{d\theta}{\xi}\left(\overline{Q}^2 - \overline{Q^2} + \frac{1}{12}\overline{Q^4} + \frac{1}{4}\overline{Q^2}^2 - \frac{1}{3}\overline{Q}\ \overline{Q^3}\right), \end{aligned} \tag{4.23}$$

which recovers the result in Eq.(4.5). Therefore, the analytical solution from these small

Q expansions can be utilized to benchmark the numerical calculation, specifically

$$\int d\lambda \oint \frac{d\theta}{\xi} \overline{2\cos Q - 1} = \frac{8\pi}{3}(1+\frac{3}{2}\varepsilon^2)\left(k_\perp \rho_p\right)^2 \frac{m_i E}{T_i} + \frac{4\pi}{15}(1+5\varepsilon^2+\frac{15}{8}\varepsilon^4)\left(k_\perp\rho_p\right)^4 \left(\frac{m_i E}{T_i}\right)^2, \quad (4.24)$$

$$\int d\lambda \oint \frac{d\theta}{\xi} \overline{\cos Q - 1}^2 = \frac{4\pi}{5}(1+\frac{1}{3}\varepsilon^2+1.46\varepsilon^{5/2} - 0.4\varepsilon^{7/2}+\frac{7}{4}\varepsilon^4)\left(k_\perp\rho_p\right)^4 \left(\frac{m_i E}{T_i}\right)^2, \quad (4.25)$$

$$\int d\lambda \oint \frac{d\theta}{\xi} \overline{\sin Q}^2 = \frac{8\pi}{3}(-1.6\varepsilon^{3/2}-\frac{1}{2}\varepsilon^2-0.36\varepsilon^{5/2}-0.03\varepsilon^{7/2} + \frac{1}{10}\varepsilon^4)\left(k_\perp\rho_p\right)^2 \frac{E}{T_i} + (\frac{16\pi}{9}\varepsilon^2+4.44\varepsilon^{5/2} - 14.07\varepsilon^{7/2}+\frac{611\pi}{90}\varepsilon^4)\left(k_\perp\rho_p\right)^4 \left(\frac{m_i E}{T_i}\right)^2. \quad (4.26)$$

Next we carry out the integration in Eq.(4.19), noting that the $\sin Q$ integration in Eq.(4.18) vanishes for trapped particles due to the odd parity of the integrand. The transit average of an arbitrary function $F(\theta,\lambda,y)$ can be evaluated using

$$\oint \frac{d\theta}{\xi} F(\theta,\lambda,y) = \left\{ \begin{array}{c} 2\int_0^\pi d\theta \sqrt{\frac{1+\varepsilon\cos\theta}{1+\varepsilon\cos\theta-\lambda}} F(\theta,\lambda,y), \text{ for } \lambda < 1-\varepsilon \\ 2\int_0^{\theta_b} d\theta \sqrt{\frac{1+\varepsilon\cos\theta}{1+\varepsilon\cos\theta-\lambda}} F(\theta,\lambda,y), \text{ for } 1-\varepsilon<\lambda<1+\varepsilon \end{array} \right\}, \quad (4.27)$$

with $\theta_b = \arccos\left((\lambda-1)/\varepsilon\right)$ the turning point angle. The function $F(\theta,\lambda)$ is either 1, $\sin Q$ or $\cos Q - 1$, for the different integrals in Eq.(4.18). The θ and λ integrals are carried out by adaptive Lobatto quadrature in Matlab, accurate to 10^{-8}. For the energy integral, a Gaussian quadrature is applied with 20 Gauss points in the integration range of $[0,12]$. The energy integral is accurate until perpendicular wave number $k_\perp\rho_p$ is up to ten. When the number $k_\perp\rho_p$ gets even larger, an oscillating feature appears in the low energy part and more Gauss points are required for accurate numerical integration.

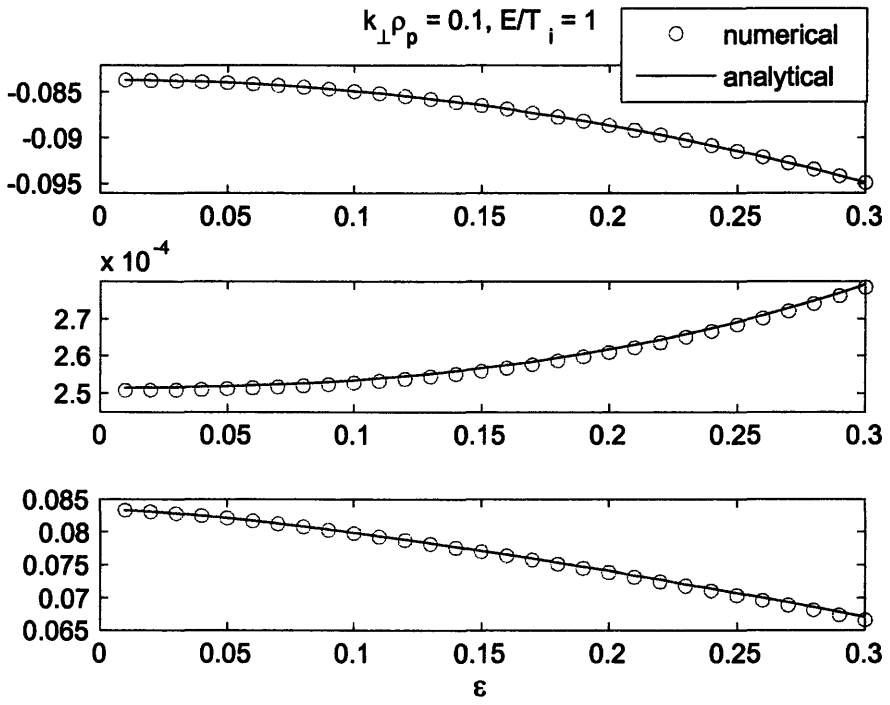

Figure 4-1: Comparison of the integrations: (a)$\int d\lambda \oint \frac{d\theta}{\xi} 2\overline{\cos Q - 1}$, (b)$\int d\lambda \oint \frac{d\theta}{\xi} \overline{\cos Q - 1}^2$ and (c)$\int d\lambda \oint \frac{d\theta}{\xi} \overline{\sin Q}^2$ evaluated numerically and analytically. The comparison shows good agreement between these two methods for small perpendicular wave vector $k_\perp \rho_p$.

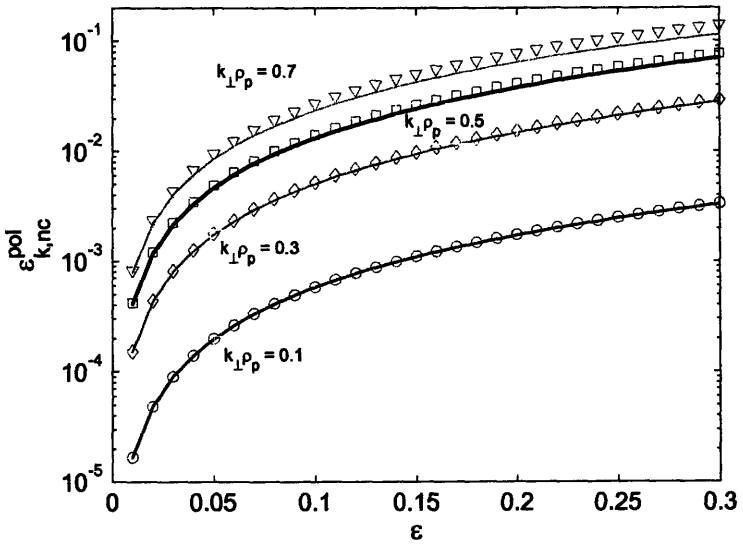

Figure 4-2: The neoclassical polarization $\varepsilon^{pol}_{k,nc}$ in unit of $\frac{\omega^2_{pi}/\omega^2_{ci}}{k^2_\perp \rho^2_i}$, as a function of the inverse aspect ratio ε for various perpendicular wavenumbers $k_\perp \rho_p$. The solid curves represent the analytical results from Eq.(4.15), and the discrete shapes represent the numerical results. The polarization increases with $k_\perp \rho_p$.

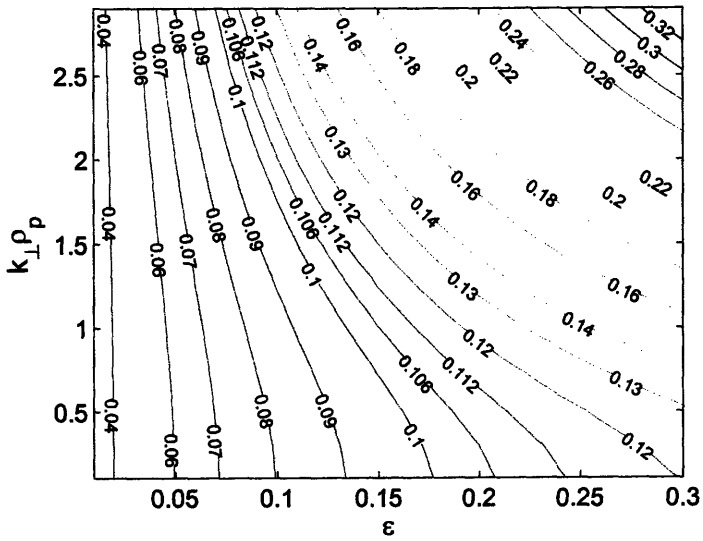

Figure 4-3: A contour plot of the residual factor γ, for $q = 1.4$. For small inverse aspect ratio ε, the factor γ changes slowly with the wavelength.

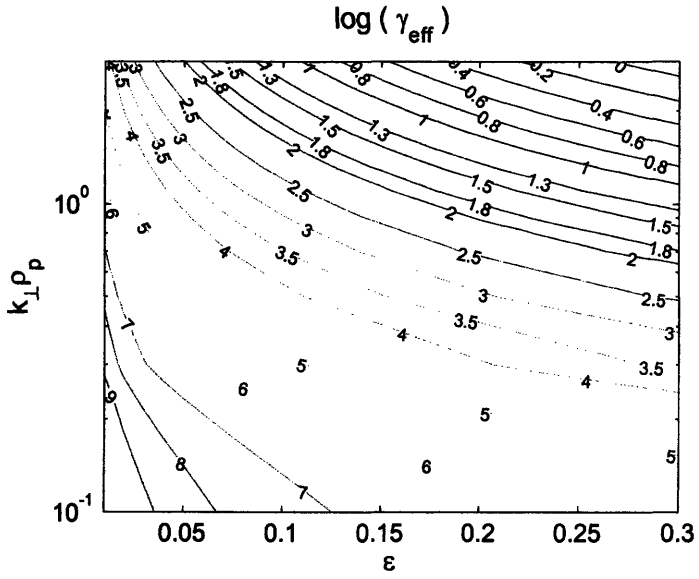

Figure 4-4: A contour plot of the logarithm of the effective residual factor γ_{eff}, which include the source's strength. The factor γ_{eff} decreases with $k_\perp \rho_p$ rapidly.

Recall that the zonal flow residual factor was given by Eq.(2.24) to be

$$\gamma = \frac{\phi_k(\infty)}{\phi_k(0)} = \frac{\varepsilon_{k,cl}^{pol}}{\varepsilon_k^{pol}(0)}. \tag{4.28}$$

For the case considered here, $k_\perp \rho_p \sim 1$ and $k_\perp^2 \rho_i^2 \ll 1$, the residual factor becomes

$$\gamma = \frac{1}{1 + \varepsilon_{k,nc}^{pol}(0)\,\omega_{ci}^2/\omega_{pi}^2}, \tag{4.29}$$

where $\varepsilon_{k,nc}^{pol}(0)$ is defined by Eq.(4.3). We may plot the residual factor γ as a function of $k_\perp \rho_p$ and inverse aspect ratio ε for a given safety factor $q = 1.4$, as show in Fig.(4-3). When $\varepsilon \ll 1$, the residual factor γ doesn't change much with the perpendicular wavenumber $k_\perp \rho_p$. Even when $\varepsilon \sim 0.3$, γ only changes by a factor of three between $k_\perp \rho_p \sim 0.1$ and $k_\perp \rho_p \sim 2$. However, according to Eq.(2.17), $\phi(0) \sim \delta n_k(0)/k_\perp^2$. Therefore, if the initial density fluctuation $\delta n_k(0)$ remains fixed, the initial zonal flow is much larger at long

wavelengths than short wavelengths [31]. Hence, it is convenient to define an effective residual factor γ_{eff} to include this source strength effect by introducing

$$\gamma_{eff} \equiv \frac{e\phi_k(\infty)\, n_0}{T_i \delta n_k(0)}. \tag{4.30}$$

Using Eqs.(2.24) and (4.29), the effective residual factor then can be rewritten as

$$\gamma_{eff} = \frac{1}{k_\perp^2 \rho_i^2 \left(1 + \varepsilon_{k,nc}^{pol}(0)\, \omega_{ci}^2/\omega_{pi}^2\right)}. \tag{4.31}$$

The Fig.(4-4) shows a contour plot of γ_{eff} for various ε and $k_\perp \rho_p$. When the source strength is included, the residual zonal flow increases rapidly with the wavelength. Hence, in the edge plasma where $k_\perp \rho_p \sim 1$, the residual zonal flow level is much smaller than that in the core plasma where $k_\perp \rho_p \ll 1$. This observation indicates that the turbulence is much more virulent in the edge due to lack of zonal flow regulation for a fixed source.

We may extend our discussion to the limit where the wavelength is the same size as ion gyroradius. In this limit, the total polarization can no longer be decoupled to neoclassical part and classical part and only numerical solution is available.

In the collisionless case, the gyrokinetic equation gives the following total polarization [44]

$$\varepsilon_k^{pol}(p) = \frac{\omega_{pi}^2/\omega_{ci}^2}{\langle k_\perp^2 \rangle \rho_i^2} \left(1 - \frac{1}{n_0} \left\langle \int d^3v F_0 J_0 e^{-iQ} \overline{J_0 e^{iQ}} \right\rangle \right). \tag{4.32}$$

Comparing this result to the collisionless neoclassical polarization in Eq.(4.3), we see that the preceding equation includes finite gyroradius effects through J_0. Therefore, the arbitrary $k_\perp$ residual factor is given by

$$\gamma = \frac{\varepsilon_{k,cl}^{pol}}{\varepsilon_k^{pol}(0)} = \frac{1 - \frac{1}{n_0} \left\langle \int d^3v F_0 J_0^2 \right\rangle}{1 - \frac{1}{n_0} \left\langle \int d^3v F_0 J_0 e^{-iQ} \overline{J_0 e^{iQ}} \right\rangle}. \tag{4.33}$$

Use of a *Schwarz inequality* gives

$$\overline{J_0 e^{-iQ}}\ \overline{J_0 e^{iQ}} \leq \overline{J_0^2}. \tag{4.34}$$

Therefore,

$$\left\langle \int d^3v F_0 J_0 e^{-iQ} \overline{J_0 e^{iQ}} \right\rangle \leq \left\langle \int d^3v F_0 J_0^2 \right\rangle. \tag{4.35}$$

We also have $J_0^2 \leq 1$. Hence, the residual factor

$$\gamma \leq 1. \tag{4.36}$$

When the polarization Q is large, the residual zonal flow level is low and γ is small. When the residual factor γ reaches unity, there is no effect due to polarization. Notice that $\frac{1}{n_0}\left\langle \int d^3v F_0 J_0^2 \right\rangle = \langle \Gamma_0 \rangle$, which decreases rapidly when $k_\perp \rho_i > 1$. Therefore, we expect to see γ approaching unity smoothly without the oscillations seen in Fig. 7. of Ref. [31]. In Ref.[31], the extra oscillations are due to the electron polarization effect which is ignored here.

It is straight forward to implement the numerical calculation for $\varepsilon_k^{pol}(p)$ using Eq.(4.32), or γ from Eq.(4.33). We need only change the factor $K(Q)$ in Eq.(4.18) to the following:

$$\begin{aligned} K(Q) \;=\; & 2\oint \frac{d\theta}{\xi} J_0 (\cos Q - 1) + \left(\oint \frac{d\theta}{\xi}\right)^{-1} \\ & \left\{ \left[\oint \frac{d\theta}{\xi} J_0 (\cos Q - 1)\right]^2 + \left(\oint \frac{d\theta}{\xi} J_0 \sin Q\right)^2 \right\}. \end{aligned} \tag{4.37}$$

We may then plot the residual factor γ as a function of the perpendicular wave number $k_\perp \rho_i$, as shown in Fig.(4-5). When $k_\perp \rho_i < 0.1$, the small residual flow is determined by the *R-H* polarization, which has no dependence on $k_\perp \rho_i$. When $0.1 < k_\perp \rho_i < 1$, there is transitional region where the residual zonal flow increases with $k_\perp \rho_i$. When $k_\perp \rho_i > 1$ the damping effect is effectively zero for the zonal flow.

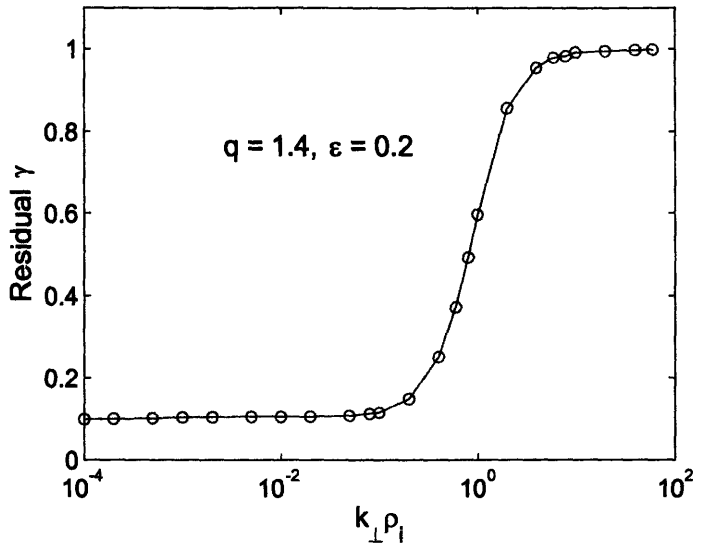

Figure 4-5: The residual zonal flow potential for a unit initial potential varies with the perpendicular wavelength $k_\perp \rho_i$.

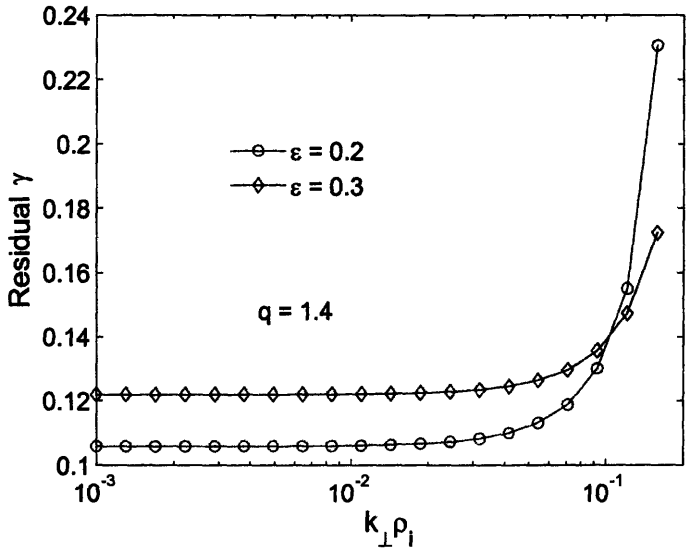

Figure 4-6: The residual zonal flow potential for a unit initial potential varies with the perpendicular wavelength $k_\perp \rho_i$ for $\varepsilon = 0.2$ and 0.3, which is sensitive to q/ε.

The transitional region for the residual is sensitive to q/ε, as shown in Fig.(4-6). When $k_\perp \rho_i \ll 1$ the residual zonal flow level remains at the *R-H* value, that is inversely proportional to the neoclassical polarization. Recall that the neoclassical polarization $\varepsilon_{k,nc}^{pol} \propto \sqrt{\varepsilon}/q^2$ in the collisionless long wavelength limit. Therefore, the plateau residual zonal flow level as $k_\perp \rho_i \to 0$ is proportional to $q^2/\sqrt{\varepsilon}$ and becomes larger at smaller inverse aspect ratio ε, as shown in Fig.(4-6), or at larger q. When $k_\perp \rho_i$ increases, the residual zonal flow enters the transitional region and increases with $k_\perp \rho_i$. This increase is due to the finite Q effect, e.g., the Q^4 terms in Eq.(4.6) can no longer be ignored. Note that $Q \sim k_\perp \rho_i q/\varepsilon$ so that for a constant $k_\perp \rho_i$, the smaller the ε/q, the larger the Q factor becomes. As a result, we expect a smaller ε/q residual zonal flow will enter the transitional region earlier than a larger ε/q one. This is confirmed by Fig.(4-6). As Q increases, eventually $k_\perp \rho_i \succeq 1$ effects enter to create a second plateau as shown in Fig.(4-5) for $k_\perp \rho_i \gg 1$. The width of this transitional region $\Delta\{k_\perp \rho_i\}$ between the two plateaus can be estimated by letting $\Delta\{k_\perp \rho_i\}\, q/\varepsilon \sim const.$ Therefore, the width $\Delta\{k_\perp \rho_i\}$ is proportional to ε/q, which indicates that smaller ε/q residual zonal flow has a narrower transitional region. This behavior is why in the transitional regime the $\varepsilon = 0.2$ residual zonal flow increases faster than the $\varepsilon = 0.3$ residual zonal flow, as shown in Fig.(4-6).

4.2 Plasma Shape Effect

Elongation and triangularity are used to help improve tokamak performance. In this section, we explore the effect of the plasma shape in regulating zonal flow. It is not possible to find an analytically tractable MHD equilibrium which contains all the important shape ingredients, such as elongation and triangularity. However, for constant $dp/d\psi$ and $IdI/d\psi$, there exists an MHD equilibrium that satisfies the *Grad-Shafranov* equation. Following Helander and Sigmar [25], the flux surfaces in this case may be written

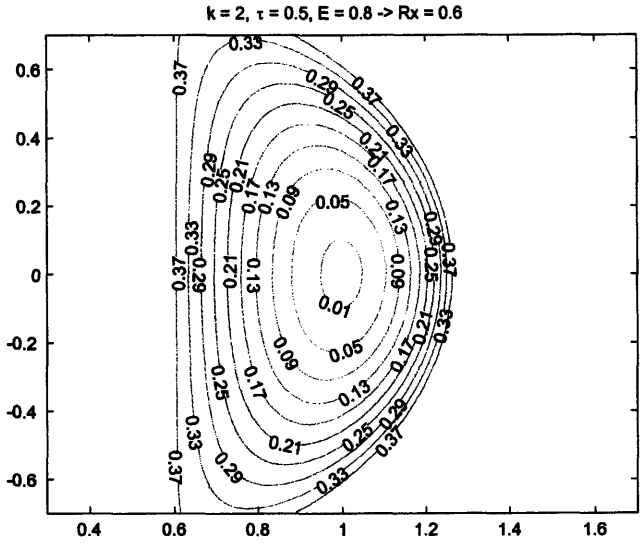

Figure 4-7: Flux surface of the solution (4.38) to the *Grad-Shafranov* equation for $\psi_0 = 1$

in the form

$$\begin{aligned}\psi(R,Z) &= \frac{\psi_0}{R_0^4}[(R^2-R_0^2)^2+\frac{Z^2}{E^2}(R^2-R_x^2) \\ &\quad -\tau R_0^2\left(R^2\ln\frac{R^2}{R_0^2}-(R^2-R_0^2)-\frac{(R^2-R_0^2)^2}{2R_0^2}\right)],\end{aligned} \tag{4.38}$$

where R_x, E, and τ are free parameters which determine the plasma shape, such as the X point location of the separatrix, elongation, and triangularity. The constant ψ_0 controls the magnitude of the magnetic flux ψ, the constant R_0 represent the radial location of magnetic axis where $\psi = 0$, and R_x is the radial X point location. A typical flux surface is shown in Fig.(4-7).

Near the magnetic axis the magnetic flux becomes an approximate ellipse satisfying

$$\frac{\psi(x,z)}{\psi_0} = 4(x+\delta)^2+\frac{z^2}{E^2}\left(1-\frac{R_x^2}{R_0^2}\right), \tag{4.39}$$

where the *Shafranov* shift Δ is defined as

$$\Delta = \left(1 + \frac{\tau}{3}\right) \frac{x^2}{2} + \frac{z^2}{4E^2}, \tag{4.40}$$

and we have corrected the sign of τ and a factor of 2 in Ref. [25]. We introduce the new dimensionless variables x and z defined as

$$R = R_0 (1 + x), \tag{4.41}$$

$$Z = R_0 z. \tag{4.42}$$

We may change variables from (x, z) to (ε, θ) using

$$x = -\Delta + \varepsilon \cos\theta, \tag{4.43}$$

$$z = \kappa \varepsilon \sin\theta, \tag{4.44}$$

where ε is the inverse aspect ratio, θ is the poloidal angle, and the constant κ is the elongation of this ellipse,

$$\kappa \equiv \frac{2E}{\sqrt{1 - R_x^2/R_0^2}}. \tag{4.45}$$

Then in the new (ε, θ) coordinates the magnetic flux ψ becomes

$$\psi = 4\psi_0 \varepsilon^2, \tag{4.46}$$

making the inverse aspect ratio a flux label. Ignoring higher order terms of $\mathcal{O}(\varepsilon^3)$ and noting $\delta \sim \mathcal{O}(\varepsilon^2)$, we find the *Shafranov* shift to be

$$\Delta \cong \left(1 + \frac{\tau}{3}\right) \frac{\varepsilon^2}{2} \cos^2\theta + \frac{\kappa^2}{4E^2} \varepsilon^2 \sin^2\theta. \tag{4.47}$$

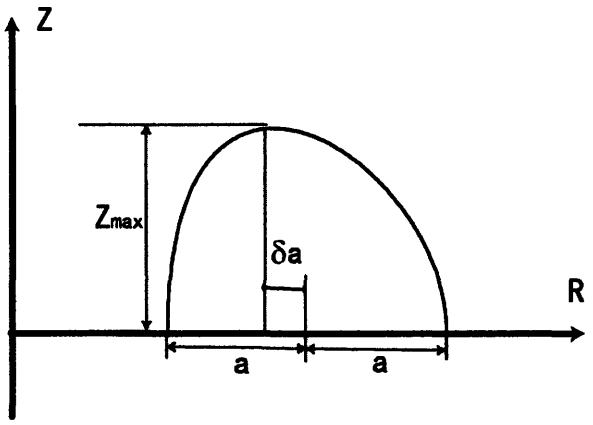

Figure 4-8: The triangularity δ of the plasma describes the deviation between the plasma center and the radial location of the maximum Z point.

This form suggests

$$x = \varepsilon\cos\theta - \left(1+\frac{\tau}{3}\right)\frac{\varepsilon^2}{2}\cos^2\theta - \frac{\kappa^2}{4E^2}\varepsilon^2\sin^2\theta, \tag{4.48}$$

$$z = \kappa\varepsilon\sin\theta. \tag{4.49}$$

The flux shape defined by the preceding equations contains both elongation and triangularity effects. We may define the triangularity δ in the conventional manner [38], as noted in Fig.(4-8), to find

$$\delta = \left[\frac{\kappa^2}{4E^2} - \frac{1}{2}\left(1+\frac{\tau}{3}\right)\right]\varepsilon. \tag{4.50}$$

Therefore, the triangularity is related to κ, τ and E. Notice, however, that for a given elongation κ and triangularity δ, the position of the separatrix R_x is determined by E.

To simplify the notation, it is convenient to use the following two variables instead of

τ and E,

$$\widetilde{A} \equiv \frac{1}{2}\left(1+\frac{\tau}{3}\right) = \frac{\kappa^2}{4E^2} - \frac{\delta}{\varepsilon}, \tag{4.51}$$

$$\widetilde{B} \equiv \frac{\kappa^2}{4E^2}. \tag{4.52}$$

Then the magnetic flux can be written in the following way:

$$\begin{aligned} R &= R_0\left(1+\varepsilon\cos\theta - \widetilde{A}\varepsilon^2\cos^2\theta - \widetilde{B}\varepsilon^2\sin^2\theta\right), \\ Z &= R_0\kappa\varepsilon\sin\theta, \end{aligned} \tag{4.53}$$

where ε is a flux function, as shown by Eq.(4.46).

The poloidal magnetic field is computed using the following relationship,

$$RB_p = |\nabla\psi|. \tag{4.54}$$

Combining with Eq.(4.46) we obtain

$$B_p = \frac{8\psi_0\varepsilon\,|\nabla\varepsilon|}{R}. \tag{4.55}$$

The gradient $|\nabla\varepsilon|$ can be calculated from Eq.(4.53),

$$|\nabla\varepsilon| = \frac{\eta}{\kappa R_0\left(1-2\widetilde{A}\varepsilon\cos\theta\right)}, \tag{4.56}$$

where the numerator η is defined as

$$\eta = \sqrt{\kappa^2\cos^2\theta + \sin^2\theta + 4\varepsilon\sin^2\theta\cos\theta\left(\widetilde{B}-\widetilde{A}\right) + 4\varepsilon^2\sin^2\theta\cos^2\theta\left(\widetilde{B}-\widetilde{A}\right)^2}. \tag{4.57}$$

With this expression for $|\nabla\varepsilon|$, we find

$$B_p = \frac{8\psi_0\varepsilon}{\kappa R_0^2}\frac{\eta}{\left(1-2\widetilde{A}\varepsilon\cos\theta\right)\left(1+\varepsilon\cos\theta-\widetilde{A}\varepsilon^2\cos^2\theta-\widetilde{B}\varepsilon^2\sin^2\theta\right)}. \tag{4.58}$$

The safety factor q is defined by

$$q(\psi) \equiv \frac{I(\psi)}{2\pi}\oint\frac{dl_p}{R^2B_p}, \tag{4.59}$$

where the poloidal field line length is

$$dl_p = \sqrt{dR^2+dZ^2}. \tag{4.60}$$

Using Eq.(4.53) we find

$$dl_p = \eta R_0\varepsilon d\theta. \tag{4.61}$$

Inserting dl_p into the preceding equation, and B_p from Eq.(4.58) into Eq.(4.59), we obtain

$$q = \frac{\kappa R_0 I}{8\psi_0}\oint\frac{d\theta}{2\pi}\frac{\left(1-2\widetilde{A}\varepsilon\cos\theta\right)}{\left(1+\varepsilon\cos\theta-\widetilde{A}\varepsilon^2\cos^2\theta-\widetilde{B}\varepsilon^2\sin^2\theta\right)}. \tag{4.62}$$

In the large aspect ratio limit we may first expand ε and then integrate to obtain

$$q = \frac{kR_0I}{8\psi_0}\left[1+\frac{1}{2}\left(1+3\widetilde{A}+\widetilde{B}\right)\varepsilon^2+\mathcal{O}\left(\varepsilon^4\right)\right]. \tag{4.63}$$

Then we can write the poloidal field B_p in terms of this safety factor instead of constant ψ_0 to obtain

$$B_p = \frac{I}{R_0}\frac{\varepsilon}{q}\sqrt{\kappa^2\cos^2\theta+\sin^2\theta}\left(1+\mathcal{O}(\varepsilon)\right), \tag{4.64}$$

and

$$\frac{dl_p}{B_p} = \frac{q}{I}R_0^2 d\theta \left(1 - 2\widetilde{A}\varepsilon\cos\theta\right)\left(1 + \varepsilon\cos\theta - \widetilde{A}\varepsilon^2\cos^2\theta - \widetilde{B}\varepsilon^2\sin^2\theta\right) \left[1 - \frac{1}{2}\left(1 + 3\widetilde{A} + \widetilde{B}\right)\varepsilon^2 + \mathcal{O}\left(\varepsilon^4\right)\right]. \tag{4.65}$$

Fortunately, in the polarization calculation we need only evaluate flux surface averages,

$$\langle A \rangle = \frac{\oint \frac{dl_p}{B_p} A}{\oint \frac{dl_p}{B_p}}, \tag{4.66}$$

where the factor dl_p/B_p appears in both the numerator and denominator so we may simply use the replacement

$$\frac{dl_p}{B_p} \to d\theta \left(1 - 2\widetilde{A}\varepsilon\cos\theta\right)\left(1 + \varepsilon\cos\theta - \widetilde{A}\varepsilon^2\cos^2\theta - \widetilde{B}\varepsilon^2\sin^2\theta\right). \tag{4.67}$$

To evaluate the polarization and other flux surface averages, we will need an expression for B, the magnitude of magnetic field,

$$B = \sqrt{B_T^2 + B_p^2} = \sqrt{\frac{I^2}{R^2} + B_p^2}.$$

Therefore, accurate to the order of $\mathcal{O}\left(\varepsilon^2\right)$, we find the magnetic field to be

$$B = B_0\left\{1 - \varepsilon\cos\theta + \varepsilon^2\left[\left(\widetilde{A} + 1 + \frac{\kappa^2}{2q^2}\right)\cos^2\theta + \left(\widetilde{B} + \frac{1}{2q^2}\right)\sin^2\theta\right]\right\}, \tag{4.68}$$

and its inverse to be

$$\frac{1}{B} = \frac{1}{B_0}\left\{1 + \varepsilon\cos\theta - \varepsilon^2\left[\left(\widetilde{A} + \frac{\kappa^2}{2q^2}\right)\cos^2\theta + \left(\widetilde{B} + \frac{1}{2q^2}\right)\sin^2\theta\right]\right\}, \tag{4.69}$$

where B_0 is defined by

$$B_0 \equiv \frac{I}{R_0} = \frac{RB_T}{R_0}. \tag{4.70}$$

Notice that in $\xi = \sqrt{1-\lambda B/B_0}$ the magnetic well is altered by an amount $\left(\widetilde{A}+\frac{\kappa^2}{2q^2}\right)$: becoming deeper due to the elongation κ, and shallower due to the triangularity Δ, as can be seen from Eq.(4.51). In addition, the trapped passing boundary is given by

$$\lambda_c = 1-\varepsilon-\varepsilon^2\left(\widetilde{A}+\frac{\kappa^2}{2q^2}\right). \tag{4.71}$$

Therefore, we expect that shaping effects will enter at one order higher in the ε expansion than trapping effects. Recalling that the trapped particle contribution to polarization is of order $\mathcal{O}\left(\varepsilon^{3/2}\right)$, we expect the shaping effects to be of order $\mathcal{O}\left(\varepsilon^{5/2}\right)$.

The residual zonal flow is determined by both the neoclassical and classical polarization, as can be seen from Eq.(2.24). In a shaped plasma the classical polarization needs to be evaluated with more care, but the leading order classical polarization still turns out to be $\omega_{pi}^2/\omega_{ci}^2$. To see that this is the case, recall that the classical polarization of Eq.(3.51), in the large wavelengths limit simplifies to

$$\left\langle k_\perp^2\right\rangle \varepsilon_{k,cl}^{pol} = \frac{\omega_{pi}^2}{\omega_{ci}^2}\left\langle k_\perp^2\frac{B_0^2}{B^2}\right\rangle, \tag{4.72}$$

where B_0 is defined in Eq.(4.70), and $\omega_{ci} = eB_0/m_ic$. The perpendicular wave vector is now given by

$$k_\perp = S'\left|\nabla\psi\right| = S'8\psi_0\varepsilon\left|\nabla\varepsilon\right|, \tag{4.73}$$

when we use Eq.(4.46). Inserting $|\nabla\varepsilon|$ from Eq.(4.56) in the preceding equation, we obtain

$$k_\perp = \frac{\varepsilon}{q}\frac{IS'\eta}{\left(1-2\widetilde{A}\varepsilon\cos\theta\right)}\left[1+\frac{1}{2}\left(1+3\widetilde{A}+\widetilde{B}\right)\varepsilon^2+\mathcal{O}\left(\varepsilon^4\right)\right]. \tag{4.74}$$

Therefore, the flux surface averages in Eq.(4.72) become

$$\left\langle k_\perp^2\right\rangle = \left(IS'\frac{\varepsilon}{q}\right)^2\left[1+\frac{1}{2}\left(1+3\widetilde{A}+\widetilde{B}\right)\varepsilon^2\right]^2\frac{\oint\frac{dl_p}{B_p}\frac{\eta^2}{\left(1-2\widetilde{A}\varepsilon\cos\theta\right)^2}}{\oint\frac{dl_p}{B_p}}, \tag{4.75}$$

and

$$\left\langle k_\perp^2 \frac{B_0^2}{B^2} \right\rangle = \left(IS' \frac{\varepsilon}{q} \right)^2 \left[1 + \frac{1}{2} \left(1 + 3\widetilde{A} + \widetilde{B} \right) \varepsilon^2 \right]^2 \frac{\oint \frac{dl_p}{B_p} \frac{\eta^2}{\left(1 - 2\widetilde{A}\varepsilon \cos\theta\right)^2} \frac{B_0^2}{B^2}}{\oint \frac{dl_p}{B_p}}, \tag{4.76}$$

with dl_p/B_p given by Eq.(4.67). The integrals in the preceding equation can be evaluated by first expanding the integrand in powers of ε to accuracy $\mathcal{O}(\varepsilon^2)$, and then integrating over poloidal angle θ. The results of these integrations are

$$\begin{aligned} \oint \frac{dl_p}{B_p} \frac{\eta^2}{\left(1 - 2\widetilde{A}\varepsilon \cos\theta\right)^2} \;\rightarrow\; & \pi \{ \left(1 + \kappa^2\right) + \frac{\varepsilon^2}{4} \{ -3\widetilde{A} + \widetilde{B} + 4\widetilde{B}^2 \\ & + \left[3\widetilde{A} \left(1 + 4\widetilde{B} \right) - \widetilde{B} \right] \kappa^2 \} \}, \end{aligned} \tag{4.77}$$

and

$$\oint \frac{dl_p}{B_p} \rightarrow 2\pi \left[1 - \frac{\varepsilon^2}{2} \left(3\widetilde{A} + \widetilde{B} \right) \right], \tag{4.78}$$

where the use of an arrow indicates that Eq.(4.67) is employed. Similarly, using B_0/B in Eq.(4.69), we obtain

$$\begin{aligned} \oint \frac{dl_p}{B_p} \frac{\eta^2}{\left(1 - 2\widetilde{A}\varepsilon \cos\theta\right)^2} \frac{B_0^2}{B^2} \;\rightarrow\; & \pi \{ \left(1 + \kappa^2\right) + \frac{\varepsilon^2}{4q^2} [-3 - 3\kappa^4 + \left(3 - 9\widetilde{A} + \widetilde{B}(3 + 4\widetilde{B}) \right) q^2 \\ & + \kappa^2 \{ -2 + 3q^2 [3 + \widetilde{A}(3 + 4\widetilde{A}) - \widetilde{B}] \}] \}. \end{aligned} \tag{4.79}$$

With the preceding integrals, we find the classical polarization in Eq.(4.72) to be

$$\varepsilon_{k,cl}^{pol} = \frac{\omega_{pi}^2}{\omega_{ci}^2} \left[1 + \mathcal{O}\left(\varepsilon^2\right) \right]. \tag{4.80}$$

The geometrical effects $\widetilde{A}$, $\widetilde{B}$, and κ, only enter in the $\mathcal{O}(\varepsilon^2)$ terms. We also find

$$\left\langle k_\perp^2 \right\rangle = \left(IS' \frac{\varepsilon}{q} \right)^2 \frac{\pi \left(1 + \kappa^2\right)}{\oint \frac{dl_p}{B_p}} \left[1 + \mathcal{O}\left(\varepsilon^2\right) \right], \tag{4.81}$$

which is needed to calculate the neoclassical polarization.

Next we consider shaping effects on the neoclassical polarization. In the large perpendicular wavelength limit, inserting Eq.(4.2) in Eq.(2.12), we have the following expression for neoclassical polarization,

$$\left\langle k_\perp^2 \right\rangle \varepsilon_{k,nc}^{pol} = \frac{4\pi e^2}{T_i} \left\langle \int d^3v F_0 \left(\overline{Q^2} - \overline{Q}^2 \right) \right\rangle . \tag{4.82}$$

Using the expression for Q in Eq.(3.6), we obtain

$$\left\langle k_\perp^2 \right\rangle \varepsilon_{k,nc}^{pol} = \frac{\omega_{pi}^2}{\omega_{ci}^2} \frac{\left(Is'B_0\right)^2 m_i}{n_0 T_i} \left\langle \int d^3v F_0 \left[\overline{\left(\frac{v_\parallel^2}{B^2} \right)} - \overline{\left(\frac{v_\parallel}{B} \right)}^2 \right] \right\rangle , \tag{4.83}$$

where the first term can be evaluated as

$$\begin{aligned} \left\langle \int d^3v F_0 \overline{\left(\frac{v_\parallel^2}{B^2} \right)} \right\rangle &= \left\langle \int d^3v F_0 \frac{v_\parallel^2}{B^2} \right\rangle \\ &= \frac{n_0 T_i}{m_i B_0^2} \left\langle \frac{B_0^2}{B^2} \right\rangle \\ &= \frac{n_0 T_i}{m_i B_0^2} \frac{\oint \frac{dl_p}{B_p} \frac{B_0^2}{B^2}}{\oint \frac{dl_p}{B_p}} . \end{aligned} \tag{4.84}$$

Just as we have done for the classical polarization, the integral in the preceding equation can be evaluated in the small ε limit using Eq.(4.67) for dl_p/B_p,

$$\oint \frac{dl_p}{B_p} \frac{B_0^2}{B^2} \to 2\pi \left\{ 1 - \left[\frac{3}{2} (3\widetilde{A} + \widetilde{B} - 1) + \frac{1+\kappa^2}{2q^2} \right] \varepsilon^2 \right\} . \tag{4.85}$$

Therefore, the integral in Eq.(4.84) can be written as

$$\left\langle \int d^3v F_0 \overline{\left(\frac{v_\parallel^2}{B^2} \right)} \right\rangle = \frac{n_0 T_i}{m_i B_0^2} \frac{2\pi}{\oint \frac{dl_p}{B_p}} \left\{ 1 - \left[\frac{3}{2} (3\widetilde{A} + \widetilde{B} - 1) + \frac{1+\kappa^2}{2q^2} \right] \varepsilon^2 \right\} , \tag{4.86}$$

where $\oint dl_p/B_p$ is given by Eq.(4.78).

The evaluation of the second term in Eq.(4.83) is much more involved. Fortunately we only need to consider the passing particles' contribution. Then

$$\left\langle \int d^3v F_0 \overline{\left(\frac{v_\parallel}{B}\right)}^2 \right\rangle = \frac{3n_0T_i}{2m_iB_0^2} \frac{\left(\oint \frac{dl_p}{B_p}\right)^2}{\oint \frac{dl_p}{B_p}} \int_0^{\lambda_c} d\lambda \frac{1}{\oint \frac{dl_p}{B_p}\frac{B}{B_0\xi}}, \tag{4.87}$$

where the trapped-passing boundary λ_c is defined in Eq.(4.71), $\xi = \left|v_\parallel\right|/v$, and $\oint dl_p/B_p$ is given by Eq.(4.78). The integral $\oint \frac{dl_p}{B_p}\frac{B}{B_0\xi}$ can be written as

$$\oint \frac{dl_p}{B_p}\frac{B}{B_0\xi} = \oint \frac{dl_p}{B_p}\frac{\sqrt{B/B_0}}{\sqrt{B_0/B-\lambda}}, \tag{4.88}$$

where we already have expressions for B_0/B and B/B_0 in Eqs.(4.69) and (4.68). Using these expressions, we find

$$\frac{1}{\sqrt{B_0/B-\lambda}} = \frac{1}{\sqrt{1-\lambda+\varepsilon\cos\theta-\left[\left(\widetilde{A}+\frac{\kappa^2}{2q^2}\right)\cos^2\theta+\left(\widetilde{B}+\frac{1}{2q^2}\right)\sin^2\theta\right]\varepsilon^2}}, \tag{4.89}$$

and recalling Eq.(4.67) we have

$$\begin{aligned}\frac{dl_p}{B_p}\sqrt{B/B_0} \;\rightarrow\; & d\theta\{1+\varepsilon\left(\frac{1}{2}-2\widetilde{A}\right)\cos\theta+[(-\frac{1}{8}+\frac{3}{2}\widetilde{A} \\ & +\frac{\kappa^2}{4q^2})\cos^2\theta+(-\frac{1}{2}\widetilde{B}+\frac{1}{4q^2})\sin^2\theta]\varepsilon^2\}. \end{aligned}\tag{4.90}$$

We may let $x = 1-\lambda$, then $\varepsilon < x \leq 1$ for the passing particles. Then $1/\sqrt{B_0/B-\lambda}$ may be expanded in powers of ε to obtain

$$\begin{aligned}\frac{1}{\sqrt{B_0/B-\lambda}} \;=\; & \frac{1}{\sqrt{x}}(1-\frac{1}{2}\frac{\varepsilon\cos\theta}{x}+\frac{1}{2}\frac{\varepsilon^2}{x}(\left(\widetilde{A}+\frac{\kappa^2}{2q^2}\right)\cos^2\theta+ \\ & \left(\widetilde{B}+\frac{1}{2q^2}\right)\sin^2\theta)+\frac{3}{8}\frac{\varepsilon^2}{x^2}\cos^2\theta+....+\mathcal{O}\left(\varepsilon^{M+1}\right), \end{aligned}\tag{4.91}$$

where the expansion order M depends on the desired accuracy of the final integral in

Eq.(4.87). We first assume $M = 2$ to get an initial result for Eq.(4.87). Then we increase M to see how the result changes with M, and thereby determine the value of M required for the requisite accuracy. Inserting Eqs.(4.90) and (4.91) in Eq.(4.88), we find

$$\oint \frac{dl_p}{B_p} \frac{B}{B_0 \xi} \rightarrow \frac{1}{\sqrt{x}} \sum_{n=0}^{M} a_n \left(\frac{1}{x}\right) \varepsilon^n, \tag{4.92}$$

where $a_n\left(\frac{1}{x}\right)$ is a nth degree polynomial for $1/x$. We find $a_0\left(\frac{1}{x}\right) = 2\pi$,

$$\begin{aligned} a_2\left(\frac{1}{x}\right) &= \frac{3\pi}{8x^2} + \frac{\pi}{8q^2 x}\left[2\left(1+\kappa^2\right) + \left(-2 + 12\widetilde{A} + 4\widetilde{B}\right) q^2\right] \\ &\quad -\frac{\pi}{8q^2}\left[-2\left(1+\kappa^2\right) + \left(1 + 12\widetilde{A} + 4\widetilde{B}\right) q^2\right], \end{aligned} \tag{4.93}$$

and for $m = 0, 1, 2, 3...$, $a_{2m+1}\left(\frac{1}{x}\right) = 0$. Therefore,

$$\frac{1}{\oint \frac{dl_p}{B_p} \frac{B}{B_0 \xi}} \rightarrow \frac{\sqrt{x}}{\sum_{n=0}^{M} a_n \left(\frac{1}{x}\right) \varepsilon^n}. \tag{4.94}$$

We may then expand the preceding expression to $\mathcal{O}\left(\varepsilon^M\right)$ to find

$$\frac{1}{\oint \frac{dl_p}{B_p} \frac{B}{B_0 \xi}} \rightarrow \sqrt{x} \sum_{n=0}^{M} b_n \left(\frac{1}{x}\right) \varepsilon^n, \tag{4.95}$$

where $b_n\left(\frac{1}{x}\right)$ is a nth degree polynomial in $\frac{1}{x}$, with $b_0\left(\frac{1}{x}\right) = 1/2\pi$, $b_{2m+1}\left(\frac{1}{x}\right) = 0$, and

$$\begin{aligned} b_2\left(\frac{1}{x}\right) &= -\frac{3}{32\pi x^2} - \frac{1 + \kappa^2 + \left(6\widetilde{A} + 2\widetilde{B} - 1\right) q^2}{16\pi q^2 x} \\ &\quad + \frac{-2 - 2\kappa^2 + \left(12\widetilde{A} + 4\widetilde{B} + 1\right) q^2}{32\pi q^2}. \end{aligned} \tag{4.96}$$

Hence, we have

$$\int_0^{\lambda_c} d\lambda \frac{1}{\oint \frac{dl_p}{B_p}\frac{B}{B_0\xi}} \rightarrow \int_{\varepsilon+\left(\widetilde{A}+\frac{\kappa^2}{2q^2}\right)\varepsilon^2}^{1} dx\sqrt{x}\sum_{n=0}^{M} b_n\left(\frac{1}{x}\right)\varepsilon^n. \tag{4.97}$$

This integral can be carried out easily, and we may then expand the result in ε to $O(\varepsilon^2)$, as shown in Appendix C, to find

$$\begin{aligned}\int_0^{\lambda_c} d\lambda \frac{1}{\oint \frac{dl_p}{B_p}\frac{B}{B_0\xi}} \rightarrow\ & \frac{1}{3\pi} - \frac{25}{48\pi}\varepsilon^{3/2} - \frac{1+\kappa^2+\left(-2+3\widetilde{A}+\widetilde{B}\right)q^2}{6\pi q^2}\varepsilon^2 \\ & + \left(-\frac{1}{8\pi} + \frac{11}{32\pi}\widetilde{A} + \frac{1}{4\pi}\widetilde{B} + \frac{8-5\kappa^2}{64\pi q^2}\right)\varepsilon^{5/2}.\end{aligned} \tag{4.98}$$

As we increase the expansion order M in Eq.(4.91), only the coefficient of $\varepsilon^{3/2}$ and $\varepsilon^{5/2}$ in the preceding equation changes slightly, but they converge very rapidly to the exact values given by

$$\begin{aligned}\int_0^{\lambda_c} d\lambda \frac{1}{\oint \frac{dl_p}{B_p}\frac{B}{B_0\xi}} \rightarrow\ & \frac{1}{3\pi} - 0.173\varepsilon^{3/2} - \frac{1+\kappa^2+\left(-2+3\widetilde{A}+\widetilde{B}\right)q^2}{6\pi q^2}\varepsilon^2 + (-0.0383 \\ & +0.0797\widetilde{A} + 0.0765\widetilde{B} + \frac{0.0383}{q^2} - \frac{0.0367\kappa^2}{q^2})\varepsilon^{5/2}.\end{aligned} \tag{4.99}$$

Inserting the preceding equation and Eq.(4.78) in Eq.(4.87), we find

$$\begin{aligned}\left\langle \int d^3v F_0 \overline{\left(\frac{v_\parallel}{B}\right)}^2 \right\rangle =\ & \frac{n_0 T_i}{m_i B_0^2}\frac{2\pi}{\oint \frac{dl_p}{B_p}}\{1 - 1.635\varepsilon^{3/2} - [\frac{1+\kappa^2}{2q^2} \\ & +(\frac{3}{2}(3\widetilde{A}+\widetilde{B}) - 1)]\varepsilon^2 - \frac{1}{2}(-0.722 + 1.502\widetilde{A} \\ & +1.443\widetilde{B} + \frac{0.722 - 0.692\kappa^2}{q^2})\varepsilon^{5/2}\},\end{aligned} \tag{4.100}$$

where $\oint dl_p/B_p$ is given by Eq.(4.78). Therefore, combining the preceding equation and

Eq.(4.86) we obtain

$$\begin{aligned}
&\left\langle \int d^3v F_0 \overline{\left(\frac{v_\parallel}{B}\right)}^2 \right\rangle - \left\langle \int d^3v F_0 \overline{\left(\frac{v_\parallel^2}{B^2}\right)} \right\rangle \\
= \; & \frac{n_0 T_i}{m_i B_0^2} \frac{2\pi}{\oint \frac{dl_p}{B_p}} [1.635\varepsilon^{3/2} + \frac{1}{2}\varepsilon^2 - \frac{1}{2}(-0.722 \\
& + 1.502\widetilde{A} + 1.443\widetilde{B} + \frac{0.722 - 0.692\kappa^2}{q^2})\varepsilon^{5/2}], \qquad (4.101)
\end{aligned}$$

where $\oint dl_p/B_p$ is given by Eq.(4.78). We keep $\oint dl_p/B_p$ in the preceding equation because it will cancel the corresponding term in Eq.(4.81) when calculating neoclassical polarization. Using the preceding expression and Eq.(4.81), we can write the neoclassical polarization in Eq.(4.83) as

$$\begin{aligned}
\varepsilon_{k,nc}^{pol} &= \frac{\omega_{pi}^2}{\omega_{ci}^2} \frac{q^2}{\varepsilon^2} \frac{1}{1+\kappa^2} [3.27\varepsilon^{3/2} + \varepsilon^2 - (-0.722 \\
&\quad + 1.502\widetilde{A} + 1.443\widetilde{B} + \frac{0.722 - 0.692\kappa^2}{q^2})\varepsilon^{5/2}] \\
&= \frac{\omega_{pi}^2}{\omega_{ci}^2} \frac{q^2}{\varepsilon^2} \frac{1}{1+\kappa^2} [3.27\varepsilon^{3/2} + \varepsilon^2 - (-0.722 \\
&\quad + \frac{0.736\kappa^2}{E^2} - \frac{1.502\delta}{\varepsilon} + \frac{0.722 - 0.692\kappa^2}{q^2})\varepsilon^{5/2}], \qquad (4.102)
\end{aligned}$$

where we have used $\widetilde{A} = \frac{\kappa^2}{4E^2} - \frac{\delta}{\varepsilon} \sim 1$, $\widetilde{B} = \frac{\kappa^2}{4E^2} \sim 1$. If we take $\kappa = 1$, $\widetilde{A} = \widetilde{B} = 0$, then the plasma shape becomes circular and the neoclassical polarization returns to the previous tokamak result, $1.6\varepsilon^{3/2} + 0.5\varepsilon^2 + \mathcal{O}\left(\varepsilon^{5/2}\right)$. From Eq.(4.102), we can see that the neoclassical polarization depends on the shaping effects, such as the elongation κ and triangularity δ. However, to leading order $\mathcal{O}\left(\varepsilon^{3/2}\right)$, only the elongation κ is important. The larger the elongation, the smaller the neoclassical polarization, which for a fixed source, increases the residual zonal flow and reduces the turbulence. Triangularity only plays a role in next order, $\mathcal{O}\left(\varepsilon^{5/2}\right)$, where it tries to cancel some of the beneficial effect of the elongation, but this negative effect is ε smaller than the leading elongation effect. Using Eq.(4.80) and (4.102) we find with the shaping retained the residual zonal flow of

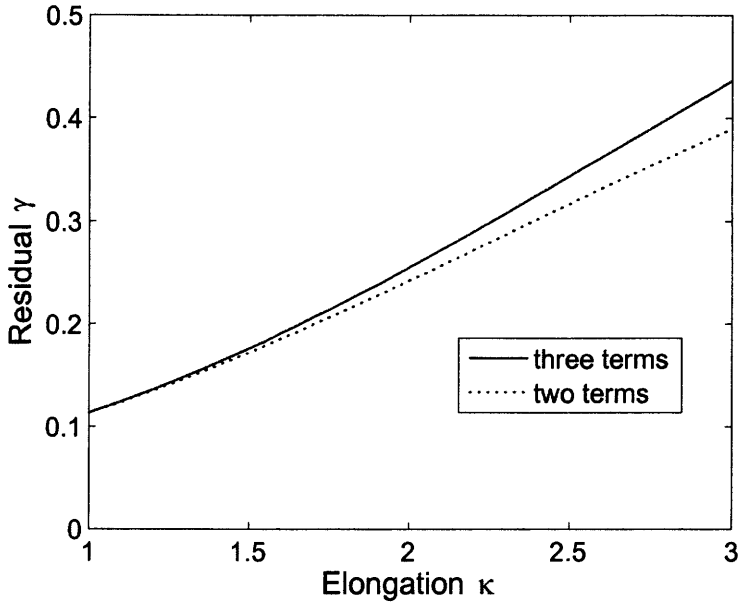

Figure 4-9: The residual zonal flow level for $q = 1.4$, $\varepsilon = 0.2$, $E = 1.0$, and $\delta = \varepsilon/4$. The dashed curve only uses the first two terms, namely $3.27 + \sqrt{\varepsilon}$, in Eq.(4.104), while the solid curve uses the whole expression. There is a significant increase of the zonal flow for large elongation.

Eq.(4.29) becomes

$$\gamma = \frac{1}{1 + N_s}, \tag{4.103}$$

where the function N_s is defined as

$$\begin{aligned} N_s &= \frac{q^2}{\sqrt{\varepsilon}} \frac{1}{1+\kappa^2} \{3.27 + \sqrt{\varepsilon} + [\frac{1.502\delta}{\varepsilon} \\ &\quad +0.722 \left(1 - \frac{1}{q^2}\right) + \left(\frac{0.692}{q^2} - \frac{0.736}{E^2}\right) \kappa^2] \varepsilon\}. \end{aligned} \tag{4.104}$$

Plots of the residual factor γ versus elongation and triangularity are given in Figs.(4-9) and (4-10), showing that the zonal flow increases with elongation and decreases with triangularity.

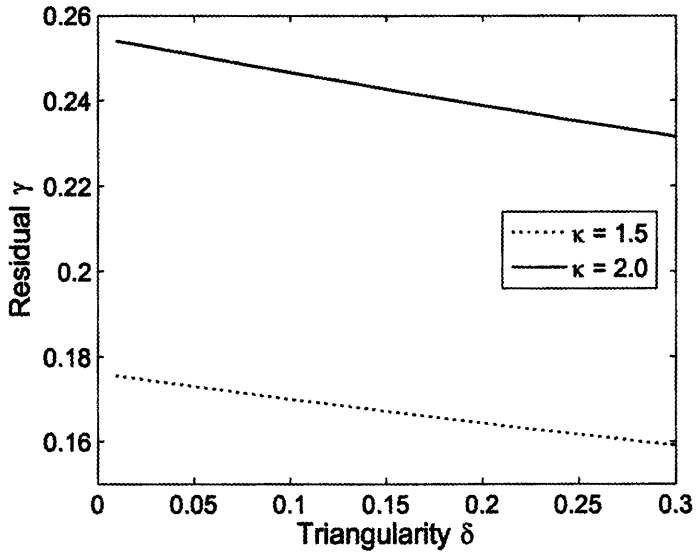

Figure 4-10: The residual zonal flow level for $q = 1.4$, $\varepsilon = 0.2$, and $E = 1.0$. The residual zonal flow decreases with triangularity δ.

Chapter 5

Collisional Neoclassical Polarization: Hinton & Rosenbluth Limits

In the preceding chapters, we have discussed neoclassical polarization and the associated zonal flow damping for a collisionless plasma. However, collisions always exist in a plasma. Even in a high temperature plasma where the collisions are weak, they can still make a significant change to the neoclassical polarization in the long time limit. For this collisional study, we only consider long wavelength zonal flows, since long wavelengths dominate the zonal flow spectrum for the core plasma. In this and the following chapter, we investigate how collisions can affect the neoclassical polarization. In this chapter, we will review *Hinton-Rosenbluth*'s approach [27] to treating collisional neoclassical polarization and then review the weak and strong collisionality limits.

The task here is to solve the transit averaged kinetic equation Eq.(3.26) for the passing particle distribution $h_k^{(1)}$, which is required to calculate neoclassical polarization in Eq.(3.22). Since the distribution $h_k^{(1)}$ is the leading order approximation to h_k and it is not necessary to evaluate higher order terms, we need not make distinction between $h_k^{(1)}$ and h_k. The trapped contribution remains $h_k^{(1)} = 0$, since it also satisfies Eq.(3.26) but the drive $\overline{Q}$ vanishes. *Laplace* transforming Eq.(3.26), the transit averaged kinetic

equation can be written as

$$h_k(p) - \frac{1}{p}\overline{C_{ii}\{h_k(p)\}} = i\bar{Q}\frac{e\phi_k(p)}{T_i}F_0, \tag{5.1}$$

where the distribution $h_k(p)$ is independent of the poloidal angle θ. Since all the analysis that follows is done in the frequency domain, $h_k(p)$ is abbreviated to h_k without causing any confusion. It is known that pitch angle scattering is the dominant collisional process in a large aspect ratio tokamak plasma [26][28]. We therefore approximate the ion-ion collisional operator by a model *Lorentz* operator by using the simplifying replacement

$$C_{ii}\{h_k\} = 2\left(\frac{T_i}{m_i E}\right)^{3/2}\nu_{ii}\frac{B_0}{B}\xi\frac{\partial}{\partial\lambda}\lambda\xi\frac{\partial h_k}{\partial\lambda}, \tag{5.2}$$

with

$$\nu_{ii} = \frac{4\pi e^4 n_i \ln\Lambda}{m_i^{1/2}T_i^{3/2}} \tag{5.3}$$

For a large aspect ratio circular tokamak, the preceding equation can be written as

$$h_k - 2\frac{\nu_{ii}}{p}\left(\frac{T_i}{m_i E}\right)^{3/2}\frac{1}{L(\lambda)}\frac{\partial}{\partial\lambda}D(\lambda)\frac{\partial}{\partial\lambda}h_k = i\frac{2\pi\sigma e\phi_k}{T_i L(\lambda)}\frac{IS'v}{\Omega}F_0, \tag{5.4}$$

where the functions $L(\lambda)$ and $D(\lambda)$ are defined by

$$\begin{aligned} L(\lambda) &= \oint \frac{d\theta}{\sqrt{1+\varepsilon\cos\theta-\lambda}} && (5.5)\\ &= 4\sqrt{\frac{k}{2\varepsilon}}K(k), && (5.6)\\ D(\lambda) &= \oint d\theta\lambda\sqrt{1+\varepsilon\cos\theta-\lambda} && (5.7)\\ &= 4\lambda\sqrt{\frac{2\varepsilon}{k}}E(k), && (5.8) \end{aligned}$$

with k defined as

$$k \equiv \frac{2\varepsilon}{1-\lambda+\varepsilon}. \tag{5.9}$$

Note that $L(\lambda)$ is essentially the bounce time. If we define a new distribution G_k through

$$G_k = \frac{\Omega_0 T_i}{i\sigma e\phi_k IS'vF_0} h_k, \tag{5.10}$$

then G_k satisfies

$$G_k - 2\frac{\nu_{ii}}{p}\left(\frac{T_i}{m_i E}\right)^{3/2} \frac{1}{L(\lambda)}\frac{\partial}{\partial\lambda} D(\lambda)\frac{\partial}{\partial\lambda} G_k = \frac{2\pi}{L(\lambda)}. \tag{5.11}$$

Therefore, the neoclassical polarization in Eq.(3.22) can be written as

$$\varepsilon^{pol}_{k,nc}(p) = \frac{\omega_{pi}^2}{\omega_{ci}^2}\frac{q^2}{\varepsilon^2}\left(-\frac{3}{2}\int_0^{1-\varepsilon} d\lambda \langle G_k\rangle_E + 1\right), \tag{5.12}$$

when the energy average defined by Eq.(3.20) is employed. *Hinton-Rosenbluth(H-R)* solved Eq.(5.11) analytically for two asymptotic limits: the high frequency, early time (low collisionality) limit where $p\tau_{ii} \gg 1$, and the low frequency, long time (collisional) limit where $p\tau_{ii} \ll 1$.

5.1 High Frequency Limit

Rather than repeating *H-R*'s variational approach to solving Eq.(5.11) for the normalized particle distribution G_k, we employ a direct approach [42]. In the high frequency limit, we expect only a small modification to the collisionless polarization, since the driving frequency is so fast that collisions don't have enough time to change the distribution significantly during a driving period. In fact, in this limit collisions can only make a significant modification to distribution function shape close to the trapping boundary. Therefore, the functions $L(\lambda)$ in Eqs.(5.6) and $D(\lambda)$ in Eq.(5.8) can both be further simplified by approximating them by their values close to trapping boundary, namely

$$L(\lambda) \cong \frac{2\sqrt{k}}{\sqrt{2\varepsilon}} \ln\frac{16}{1-k}, \tag{5.13}$$

which still keeps the singular behavior of $L(\lambda)$ near the trapping boundary ($k = 1$), and

$$D(\lambda) \cong 4\sqrt{2\varepsilon}. \tag{5.14}$$

Notice that $D(\lambda)$ varies smoothly near the trapping boundary so we take it approximately as a constant. Then the kinetic equation, Eq.(5.11), can be rewritten as

$$G_k - \frac{1}{p\tau_{ii}} \frac{8\varepsilon}{\ln \frac{16}{1-k}} \frac{\partial^2}{\partial \lambda^2} G_k = \frac{\pi}{2} \sqrt{\frac{2\varepsilon}{k}} \frac{1}{K(k)}, \tag{5.15}$$

where $\tau_{ii} = 1/\nu_{ii}$ is the ion collisional time. To further simplify the discussion, we have ignored the energy dependence of the collision operator in the preceding equation by letting $E = T_i/m_i$. Essentially, we treat all particles as if they are thermal particles. *H-R* used the same approximation. However, their treatment is variational so we anticipate an order unity error in our treatment. Moreover, recall that since their pitch angle scattering collision operator, like ours, does not retain the full E dependence, this replacement is similar in spirit to the replacement of C_{ii} by a model *Lorentz* operator.

When $p\tau_{ii} \to \infty$, the collisional term in the preceding equation can be ignored and the leading order solution to this equation will be the collisionless distribution, which we have calculated to evaluate the collisionless polarization. As shown in Fig.(3-1), the collisionless distribution $T_1(\lambda)$ is smooth for most of the passing space, particularly, the region away from the trapping boundary. Indeed in this freely passing region, the collisional term can be ignored and the collisionless distribution is a good approximation for this high frequency case $p\tau_{ii} \gg 1$. However, close to the trapping boundary, the collisionless distribution becomes singular and the collisional term in Eq.(5.15), $\partial^2 G_k/\partial\lambda^2$, becomes so large that we have to take ion-ion collisions into account. From another perspective, there exists a boundary layer close to trapping boundary, within which the weak collisions can no longer be ignored. Assume the width of this boundary is $\Delta\lambda$, then the collision frequency is magnified to an effective collision frequency, $\nu_{eff} \sim \nu_{ii}/\Delta\lambda^2$. When the effective frequency becomes as large as the driving frequency p, the collisional

term in Eq.(5.15) becomes about the same size as G_k.

Next we will estimate the size of this boundary layer. We change our variable from λ to x by using

$$\lambda = 1 - \varepsilon - x\Delta\lambda, \tag{5.16}$$

with $x \sim \mathcal{O}(1)$ for the boundary layer particles. The boundary layer $\Delta\lambda$ is assumed small here, $\Delta\lambda \ll 1$. Then Eq.(5.15) becomes

$$G_k - \frac{1}{p\tau_{ii}} \frac{8\varepsilon}{\ln \frac{16}{1-k}} \frac{1}{\Delta\lambda^2} \frac{\partial^2}{\partial x^2} G_k = \frac{\pi}{2} \sqrt{\frac{2\varepsilon}{k}} \frac{1}{K(k)}. \tag{5.17}$$

Making the two terms on the left hand side of the equation comparable by defining,

$$\frac{1}{p\tau_{ii}} \frac{8\varepsilon}{\ln \frac{16}{1-k}} \frac{1}{\Delta\lambda^2} = 1, \tag{5.18}$$

we obtain the size of the boundary layer as

$$\Delta\lambda = \sqrt{\frac{1}{p\tau_{ii}} \frac{8\varepsilon}{\ln \frac{16}{1-k}}}, \tag{5.19}$$

where k is evaluated at a point within the boundary layer. Noticing that

$$k = \frac{2\varepsilon}{2\varepsilon + x\Delta\lambda}, \tag{5.20}$$

and setting $x \cong 1$,

$$k \cong \frac{2\varepsilon}{2\varepsilon + \Delta\lambda},$$

gives,

$$\Delta\lambda \cong \sqrt{\frac{8\varepsilon}{p\tau_{ii}} \frac{1}{\ln \frac{32\varepsilon}{\Delta\lambda}}}, \tag{5.21}$$

where we assume the boundary layer width is small compared to the inverse aspect ratio, $\Delta\lambda \ll \varepsilon$. We apply an iterative method to solve the preceding equation. Taking the first

iteration as

$$\Delta\lambda^{(1)} = \sqrt{\frac{8\varepsilon}{p\tau_{ii}}},$$

then the second iteration becomes

$$\begin{aligned} \Delta\lambda \;\cong\; \Delta\lambda^{(2)} &= \sqrt{\frac{8\varepsilon}{p\tau_{ii}} \frac{1}{\ln \frac{32\varepsilon}{\Delta\lambda^{(1)}}}} \\ &= \frac{2\varepsilon}{\gamma}, \end{aligned} \tag{5.22}$$

where the constant γ is defined by

$$\gamma \equiv \sqrt{\frac{\varepsilon p\tau_{ii}}{2} \ln\left(16\sqrt{\frac{\varepsilon p\tau_{ii}}{2}}\right)}. \tag{5.23}$$

In the high frequency limit, $p\tau_{ii} \gg 1$, and $\Delta\lambda \ll \varepsilon$ then gives $\gamma \gg 1$.

Using the preceding boundary layer width from Eq.(5.19), Eq.(5.17) becomes

$$G_k - \frac{\partial^2}{\partial x^2} G_k = \frac{\pi}{2}\sqrt{\frac{2\varepsilon}{k}} \frac{1}{K(k)}. \tag{5.24}$$

We follow H-R by guessing a trial function for the preceding equation to be

$$G_k = \frac{\pi}{2}\sqrt{\frac{2\varepsilon}{k}} \frac{1}{K(k)} (1 - e^{-x}), \tag{5.25}$$

where k is defined in Eq.(5.9), and x is defined in Eq.(5.16) and related to k by

$$x = \frac{\gamma(1-k)}{k}. \tag{5.26}$$

This trial function satisfies the boundary condition $G_k(x=0) = 0$, thereby making the distribution continuous at the trapping boundary where the trapping particle distribution vanishes. Recall from Eq.(3.30) that $h_k \propto \overline{Q} \propto \overline{v_\parallel / B}$ and that at the trapping boundary,

$\oint d\tau \to \infty$ in Eq.(3.27) giving $\overline{Q} \to 0$. Away from the trapping boundary,

$$G_k = \frac{\pi}{2}\sqrt{\frac{2\varepsilon}{k}}\frac{1}{K(k)}, \tag{5.27}$$

which is the collisionless distribution given by $T_1^p(\lambda)$ in Eq.(3.36).

Next, we demonstrate that this trial function is a good approximation to the exact distribution that satisfies Eq.(5.24). We already know that the trial function is very good in the freely passing region. Therefore, we need only consider whether the trial function is a good approximation near the trapping boundary. Inserting the trial distribution from Eq.(5.25) into the left hand side of Eq.(5.24), we find

$$\begin{aligned} G_k - \frac{\partial^2}{\partial x^2}G_k &= \frac{\pi}{2}[\sqrt{\frac{2\varepsilon}{k}}\frac{1}{K(k)} + 2\frac{\partial}{\partial x}\left(\sqrt{\frac{2\varepsilon}{k}}\frac{1}{K(k)}\right)e^{-x} \\ &\quad + \frac{\partial^2}{\partial x^2}\left(\sqrt{\frac{2\varepsilon}{k}}\frac{1}{K(k)}\right)(1-e^{-x})]. \end{aligned} \tag{5.28}$$

The function $\sqrt{\frac{2\varepsilon}{k}}\frac{1}{K(k)}$ is singular near the trapping boundary. Therefore, derivatives of this function are very localized to the vicinity of the trapping boundary, or $k = 1$. As a result we can make the approximation

$$\frac{\partial}{\partial x}\left(\sqrt{\frac{2\varepsilon}{k}}\frac{1}{K(k)}\right) \cong \frac{\sqrt{2\varepsilon}}{2\left(\ln\frac{16}{1-k}\right)^2}\frac{\partial k}{\partial x}. \tag{5.29}$$

Inserting Eq.(5.22) in Eq.(5.20), we find

$$k = \frac{1}{1+x/\gamma} \equiv 1 - \frac{x}{\gamma}. \tag{5.30}$$

We also learned from Eq.(5.19) that in the boundary layer,

$$\ln\frac{16}{1-k} = \frac{2\varepsilon}{p\tau_{ii}}\frac{1}{\Delta\lambda^2}. \tag{5.31}$$

Inserting the boundary layer width from Eq.(5.22) in the preceding equation, we obtain

$$\ln \frac{16}{1-k} \cong \Lambda, \tag{5.32}$$

with Λ defined as

$$\Lambda = \ln\left(16\sqrt{\frac{\varepsilon p \tau_{ii}}{2}}\right). \tag{5.33}$$

Therefore, we can estimate

$$\frac{\partial}{\partial x}\left(\sqrt{\frac{2\varepsilon}{k}}\frac{1}{K(k)}\right) \cong \frac{\sqrt{2\varepsilon}}{2\gamma\Lambda^2}. \tag{5.34}$$

Similarly, we can find

$$\frac{\partial^2}{\partial x^2}\left(\sqrt{\frac{2\varepsilon}{k}}\frac{1}{K(k)}\right) \cong \frac{\sqrt{2\varepsilon}}{\gamma^2\Lambda^3}. \tag{5.35}$$

Hence, after inserting the trial function, the left hand side of Eq.(5.24) becomes

$$G_k - \frac{\partial^2}{\partial x^2}G_k = \frac{\pi}{2}\sqrt{\frac{2\varepsilon}{k}}\frac{1}{K(k)}\left[1+\frac{2}{\gamma\Lambda}e^{-x}+\frac{1}{\gamma^2\Lambda^2}\left(1-e^{-x}\right)\right]. \tag{5.36}$$

Therefore, as long as $\gamma\Lambda \gg 1$, the trial function is an adequate approximation to the full G_k that contains the weakly collisional effects.

Inserting the preceding trial function in Eq.(5.25) into Eq.(5.12), and noticing that $d\lambda = -2\varepsilon dk/k^2$ and that G_k doesn't depend on E, we obtain the neoclassical polarization

$$\begin{aligned}\varepsilon^{pol}_{k,nc}(p) &= \frac{\omega_{pi}^2}{\omega_{ci}^2}\frac{q^2}{\varepsilon^2}[1-\frac{3\pi(2\varepsilon)^{3/2}}{4}\int_{\frac{2\varepsilon}{1-\varepsilon}}^{1}\frac{dk}{k^{5/2}K(k)} \\ &\quad +\frac{3\pi(2\varepsilon)^{3/2}}{4}\int_{\frac{2\varepsilon}{1-\varepsilon}}^{1}\frac{dke^{-\gamma(1-k)/k}}{k^{5/2}K(k)}].\end{aligned} \tag{5.37}$$

Had we retained the energy factors in the Lorentz operator then $\gamma \to \gamma(E)$, but the last integral would have become an analytically intractable energy integral. The first two terms in the preceding equation come from purely collisionless effects, giving the $1.6\varepsilon^{3/2}$

R-H polarization we already calculated in Chapter 3. The third term is new and comes from the collisional effects. Note that

$$\int_{\frac{2\varepsilon}{1-\varepsilon}}^{1} \frac{dke^{-\gamma(1-k)/k}}{k^{5/2}K(k)} \cong \int_{2\varepsilon}^{1} \frac{dke^{-\gamma(1-k)}}{\ln\frac{4}{\sqrt{1-k}}}, \tag{5.38}$$

since the integrand is very localized at $k \sim 1$. Letting $t = \gamma(1-k)$, then the preceding integral becomes

$$\int_{\frac{2\varepsilon}{1-\varepsilon}}^{1} \frac{dke^{-\gamma(1-k)/k}}{k^{5/2}K(k)} \cong \frac{2}{\gamma\ln(16\gamma)} \int_0^{\infty} dte^{-t}\left(1 - \frac{\ln t}{\ln(16\gamma)} + ...\right) \tag{5.39}$$

$$\cong \frac{2}{\gamma\ln(16\gamma)}\left(1 + O\left(\frac{1}{\ln(16\gamma)}\right)\right). \tag{5.40}$$

Recall $\Lambda = \ln(16\gamma)$ and since $\ln(16\gamma) \gg 1$, we need only keep the leading term in the preceding equation. Therefore, the neoclassical polarization can be written as

$$\varepsilon_{k,nc}^{pol}(p) = \frac{\omega_{pi}^2}{\omega_{ci}^2}\frac{q^2}{\varepsilon^2}\left(1.6\varepsilon^{3/2} + \frac{3\sqrt{2}\pi}{\gamma\Lambda}\varepsilon^{3/2}\right)$$

$$= \frac{\omega_{pi}^2}{\omega_{ci}^2}\frac{q^2}{\sqrt{\varepsilon}}\left(1.6 + \frac{3\sqrt{2}\pi}{\gamma\Lambda}\right). \tag{5.41}$$

Since we assumed $\gamma\Lambda \gg 1$, this collisional correction is formally only a small modification to the collisionless result. However, the modification can be significant since $3\sqrt{2}\pi \sim 10$. This result is consistent with H-R's collisional result if we replace our collision frequency ν_{ii} with $\nu_{ii}/4$, or increase our collisional time τ_{ii} to $4\tau_{ii}$. Accordingly, the numerical factors γ and Λ need to be changed to,

$$\gamma \equiv \sqrt{2\varepsilon p\tau_{ii}\ln\left(16\sqrt{2\varepsilon p\tau_{ii}}\right)}, \tag{5.42}$$

$$\Lambda = \ln\left(16\sqrt{2\varepsilon p\tau_{ii}}\right). \tag{5.43}$$

This need to enhance collisional time occurs because we ignored the energy dependence

of the collision operator by simply setting $E = T_i/m_i$. In this $p\tau_{ii} \gg 1$ calculation we are essentially calculating the energy average of the collisional time, or $\langle 1/\gamma \rangle_E \propto \langle 1/\sqrt{p\tau_{ii}} \rangle_E$, where the energy weighting in the energy average is $E^{3/2}e^{-m_iE/T_i}$. In the high frequency limit, the polarization due to collisions decreases after considering the energy dependence of τ_{ii} because the energy integral changes from $\langle 1/\gamma \rangle_E$ to $\left\langle 1/\left(\sqrt{p\tau_{ii}}y^{3/4}\right)\right\rangle_E \sim 0.66/\sqrt{p\tau_{ii}}$. Since this polarization is inversely proportional to $\sqrt{p\tau_{ii}}$, the reduction of the polarization actually corresponds to an increase in the collision time. In the low frequency limit, we will see that the polarization due to collisions increases after considering the energy dependence of τ_{ii}. However, the polarization in this limit is proportional to $p\tau_{ii}$, so the enhancement of the polarization again corresponds to an increase in the collision time. We will confirm this point further in the low driving frequency case considered next.

5.2 Low Frequency Limit

In the low frequency limit $p\tau_{ii} \ll 1$ there is no singular layer to worry about. The problem becomes a regular perturbation problem. In Eq.(5.11), the collision term dominates the left hand side to give

$$-\frac{\partial}{\partial\lambda}D(\lambda)\frac{\partial}{\partial\lambda}G_k = \pi p\tau_{ii}\left(\frac{m_iE}{T_i}\right)^{3/2}, \tag{5.44}$$

where we have used $\tau_{ii} = 1/\nu_{ii}$ with ν_{ii} defined in Eq.(5.3). This equation can be integrated to get G_k without difficulty by noting that the particle flux should vanish at $\lambda = 0$, giving $D(\lambda)\frac{\partial}{\partial\lambda}G_k|_{\lambda=0} = 0$. The distribution G_k must vanish to be continuous with the trapped distribution. With these boundary conditions we find

$$G_k = \pi p\tau_{ii}\left(\frac{m_iE}{T_i}\right)^{3/2}\int_\lambda^{1-\varepsilon}\frac{d\lambda'}{4\sqrt{1+\varepsilon-\lambda'}E\left(\frac{2\varepsilon}{1+\varepsilon-\lambda'}\right)}, \tag{5.45}$$

with the diffusion coefficient $D(\lambda)$ inserted from Eq.(5.8). With this equation and Eq.(5.12), the neoclassical polarization is found to be

$$\varepsilon^{pol}_{k,nc}(p) = \frac{\omega^2_{pi}}{\omega^2_{ci}}\frac{q^2}{\varepsilon^2}\Big(1 - \frac{3\pi p\tau_{ii}}{2}\left\langle\left(\frac{m_iE}{T_i}\right)^{3/2}\right\rangle_E \int_0^{1-\varepsilon} d\lambda \int_\lambda^{1-\varepsilon} \frac{d\lambda'}{4\sqrt{1+\varepsilon-\lambda' E\left(\frac{2\varepsilon}{1+\varepsilon-\lambda'}\right)}}\Big). \tag{5.46}$$

Exchanging the integration order, we find

$$\begin{aligned}\int_0^{1-\varepsilon} d\lambda \int_\lambda^{1-\varepsilon} \frac{d\lambda'}{4\sqrt{1+\varepsilon-\lambda' E\left(\frac{2\varepsilon}{1+\varepsilon-\lambda'}\right)}} &= \int_0^{1-\varepsilon} d\lambda' \int_0^{\lambda'} \frac{d\lambda}{4\sqrt{1+\varepsilon-\lambda' E\left(\frac{2\varepsilon}{1+\varepsilon-\lambda'}\right)}} \\ &= \int_0^{1-\varepsilon} \frac{\lambda' d\lambda'}{4\sqrt{1+\varepsilon-\lambda' E\left(\frac{2\varepsilon}{1+\varepsilon-\lambda'}\right)}} \\ &= \frac{2}{3\pi} - 0.31\sqrt{\varepsilon} + \mathcal{O}\left(\varepsilon^{3/2}\right). \end{aligned} \tag{5.47}$$

Noting $\left\langle (m_iE/T_i)^{3/2}\right\rangle_E = 8/\sqrt{\pi}$, we see that in this case the higher energy ions are more important than the lower energy ones, and we then find

$$\varepsilon^{pol}_{k,nc}(p) = \frac{\omega^2_{pi}}{\omega^2_{ci}}\frac{q^2}{\varepsilon^2}\left(1 - \frac{8p\tau_{ii}}{\sqrt{\pi}}\left(1 - 1.461\sqrt{\varepsilon} + \mathcal{O}\left(\varepsilon^{3/2}\right)\right)\right). \tag{5.48}$$

This result tells that strong collisions can increase the neoclassical polarization from order $\varepsilon^{3/2}$ to order unity. This increase comes from the decrease of the distribution G_k. When the driving frequency is low $p\tau_{ii} \ll 1$, the distribution G_k has enough time to diffuse to form a constant shape in λ space independent of any boundary layer physics. Then, the magnitude of G_k is determined by the strength of the driving source, which is proportional to the driving frequency p.

In this case, due to its simplicity, we included the energy dependence of the collision operator. Had we ignored the energy dependence of the collision operator in the beginning, we would have needed to increase the collision time τ_{ii} to $(8/\sqrt{\pi})\,\tau_{ii} \cong 4.5\tau_{ii}$, to make the final result consistent with Eq.(5.48). This observation is interesting . Recall

that in the high frequency case we found a factor of 4 for the energy average magnification of τ_{ii}. Therefore, the average energy magnification for these two limits is close to the same. Consequently, we expect in the intermediate frequency case, the average energy magnification is between 4 and 4.5 over the $E = T_i/m_i$ value. As a result, in the next chapter, we will attempt one fit by ignoring the energy dependence of the collision operator at the beginning to simplify the calculation and then increasing the final collision time by 4 times once the calculation is finished. This approximation is justified by the preceding discussion showing that the thermal particles are a sufficient representation of the total particle population if we let $\nu_{ii} \rightarrow \nu_{ii}/4$ in Eq.(5.4).

Chapter 6

Collisional Neoclassical Polarization: Arbitrary Collisionality Eigenfunction Expansion

In the last chapter, we solved the transit averaged kinetic equation analytically for two asymptotic driving frequency limits: high frequency and low frequency [27]. A singular perturbation method is required for the high frequency limit, while regular perturbation theory is sufficient for the low. However, we still lack knowledge of the intermediate frequency range. It would be advantageous to find a general approach which leads to an solution suited for the entire frequency range. In this chapter we will explore such a general approach which is based on an eigenfunction expansion of the collision operator.

6.1 Eigenfunction Expansion and Shooting Method

The idea behind this general approach is straight forward. If the eigenfunctions and eigenvalues of the transit averaged collisional operator can be found, then the transit average kinetic equation of Eq.(5.1) essentially becomes an algebraic equation. To make the problem tractable, we continue to utilize a *Lorentz* operator as the ion-ion collisional

operator. A completely analytical method is desirable, but impractical even for this simple *Lorentz* operator. However, we can find the eigenfunctions and eigenvalues for this *Lorentz* operator [30] numerically and develop a semi-analytic approach. This semi-analytical method turns out to be useful to calculate the neoclassical polarization for the entire range of driving frequencies.

We continue to consider a large aspect ratio circular tokamak model, where the trapping boundary is $\lambda = 1 - \varepsilon$. To facilitate numerical implementation, we normalize the passing pitch angle space to $[0, 1]$ by setting $\lambda = (1 - \varepsilon) x$. Then the simplified transit average kinetic equation in Eq.(5.11) can be written in terms of the new x variable,

$$\frac{\partial}{\partial x}\tilde{D}(x)\frac{\partial}{\partial x}G_k - p\tilde{\tau}_{ii}\tilde{L}(x)G_k = -2\pi p\tilde{\tau}_{ii}, \tag{6.1}$$

where the collision time τ_{ii} includes the energy dependence implicitly,

$$\tilde{\tau}_{ii} \equiv \frac{1}{\nu_{ii}}\left(\frac{m_i E}{T_i}\right)^{3/2} = \tau_{ii}\left(\frac{m_i E}{T_i}\right)^{3/2}, \tag{6.2}$$

and the functions $\tilde{D}(x)$ and $\tilde{L}(x)$ are defined as

$$\tilde{D}(x) = \frac{2D(\lambda)}{(1-\varepsilon)^2} \tag{6.3}$$

$$= \frac{8x}{1-\varepsilon}\sqrt{1-x+\varepsilon+x\varepsilon}\,E\left(\frac{2\varepsilon}{1-x+\varepsilon+x\varepsilon}\right), \tag{6.4}$$

$$\tilde{L}(x) = L(\lambda) = \frac{4}{\sqrt{1-x+\varepsilon+x\varepsilon}}K\left(\frac{2\varepsilon}{1-x+\varepsilon+x\varepsilon}\right). \tag{6.5}$$

At the trapping boundary $x = 1$, the distribution function G_k must vanish to be continuous with the trapped particle distribution. At the other end $x = 0$, the velocity particle flux must vanish, $\tilde{D}(x)\frac{\partial}{\partial x}G_k|_{x=0} = 0$, to avoid a flux into a forbidden region. The boundary condition at this end is automatically satisfied since $\tilde{D}(x = 0) = 0$. In addition, the distribution function G_k is not allowed to diverge to infinity at either boundary.

In order to solve Eq.(6.1), we first find the eigenfunctions and eigenvalues of the colli-

sion operator $\frac{\partial}{\partial x}\tilde{D}(x)\frac{\partial}{\partial x}$ by considering the following eigenvalue problem and boundary condition [30][12]:

$$\frac{\partial}{\partial x}\tilde{D}(x)\frac{\partial}{\partial x}G = -\mu\tilde{L}(x)G, \tag{6.6}$$

$$G(x=0) = 1, G(x=1) = 0, \tag{6.7}$$

where μ is the eigenvalue and G the eigenfunction. We take $G(x=0)=1$ as a way to normalize the eigenfunctions. To facilitate numerical implementation, we write the preceding equation as follows:

$$\frac{\partial^2}{\partial x^2}G = -\tilde{M}(x)\frac{\partial}{\partial x}G - \mu\tilde{N}(x)G, \tag{6.8}$$

where the coefficients $\tilde{M}(x)$ and $\tilde{N}(x)$ are defined as

$$\begin{aligned}\tilde{M}(x) &= \frac{\partial\tilde{D}(x)/\partial x}{\tilde{D}(x)} \\ &= \frac{1}{x} - \frac{1-\varepsilon}{2(1-x+\varepsilon+x\varepsilon)}\frac{K\left(\frac{2\varepsilon}{1-x+\varepsilon+x\varepsilon}\right)}{E\left(\frac{2\varepsilon}{1-x+\varepsilon+x\varepsilon}\right)},\end{aligned} \tag{6.9}$$

$$\begin{aligned}\tilde{N}(x) &= \frac{\tilde{L}(x)}{\tilde{D}(x)} \\ &= \frac{1-\varepsilon}{2x(1-x+\varepsilon+x\varepsilon)}\frac{K\left(\frac{2\varepsilon}{1-x+\varepsilon+x\varepsilon}\right)}{E\left(\frac{2\varepsilon}{1-x+\varepsilon+x\varepsilon}\right)},\end{aligned} \tag{6.10}$$

and the boundary conditions remain as in Eq.(6.7).

We apply a shooting method to solve Eq.(6.6). With the prescribed initial parameter $G'(0)$ in the $(x, G(x))$ plane, we integrate Eq.(6.8) to shoot at the end point $(1,0)$ from the beginning point $(0,1)$. However, the point $x=0$ is a singular point for both $\tilde{M}(x)$ and $\tilde{N}(x)$. We can avoid this difficulty by determining the behavior of the function G

near $x = 0$. Notice that as $x \to 0$,

$$\tilde{D}(x) \to \frac{8x\sqrt{1+\varepsilon}}{1-\varepsilon} E\left(\frac{2\varepsilon}{1+\varepsilon}\right), \tag{6.11}$$

and

$$\tilde{L}(x) \to \frac{4}{\sqrt{1+\varepsilon}} K\left(\frac{2\varepsilon}{1+\varepsilon}\right). \tag{6.12}$$

Then the function G satisfies the following equation as $x \to 0$,

$$\frac{\partial}{\partial x} x \frac{\partial}{\partial x} G + \frac{\mu(1-\varepsilon) K\left(\frac{2\varepsilon}{1+\varepsilon}\right)}{2(1+\varepsilon) E\left(\frac{2\varepsilon}{1+\varepsilon}\right)} G = 0. \tag{6.13}$$

The solution to this equation turns out to be a *Bessel* function,

$$G = J_0\left(\sqrt{\frac{2\mu x(1-\varepsilon) K\left(\frac{2\varepsilon}{1+\varepsilon}\right)}{(1+\varepsilon) E\left(\frac{2\varepsilon}{1+\varepsilon}\right)}}\right) \tag{6.14}$$

$$\to 1 - \frac{\mu(1-\varepsilon) K\left(\frac{2\varepsilon}{1+\varepsilon}\right)}{2(1+\varepsilon) E\left(\frac{2\varepsilon}{1+\varepsilon}\right)} x + O\left(x^2\right), \text{ as } x \to 0. \tag{6.15}$$

This solution automatically satisfies the normalization condition $G(x = 0) = 1$. From Eq.(6.15) we also know that to leading order,

$$G'(x) = -\frac{\mu(1-\varepsilon) K\left(\frac{2\varepsilon}{1+\varepsilon}\right)}{2(1+\varepsilon) E\left(\frac{2\varepsilon}{1+\varepsilon}\right)}, \text{ as } x \to 0. \tag{6.16}$$

Therefore, we don't have to start shooting exactly at point $(1, 0)$. Instead, we can shoot a curve by starting at

$$\left(x_0, 1 - \frac{\mu(1-\varepsilon) K\left(\frac{2\varepsilon}{1+\varepsilon}\right)}{2(1+\varepsilon) E\left(\frac{2\varepsilon}{1+\varepsilon}\right)} x_0\right), \tag{6.17}$$

where $x_0 \ll 1$. The initial slope of curve is given by

$$G'(x_0) = -\frac{\mu(1-\varepsilon) K\left(\frac{2\varepsilon}{1+\varepsilon}\right)}{2(1+\varepsilon) E\left(\frac{2\varepsilon}{1+\varepsilon}\right)}, \tag{6.18}$$

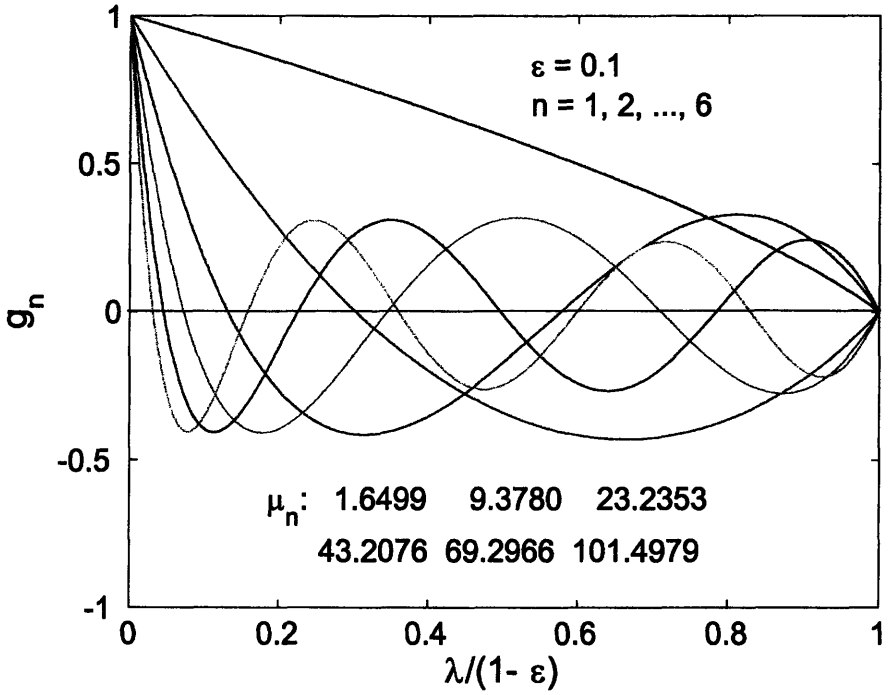

Figure 6-1: Eigenfunction G_n and eigenvalue μ_n in Eq.(6.19) for $n = 1 \rightarrow 6$, and $\varepsilon = 0.1$.

where the error of $G(x_0)$ is of order $O(x_0^2)$, while the error of $G'(x_0)$ is of order $O(x_0)$. When we shoot for some value of μ, only those curves which end at $(1,0)$ are eigenfunctions of Eq.(6.6). So only special values of μ are of interest. Increasing the value of μ gradually, we find a series of eigenfunctions $g_n(x)$ and corresponding eigenvalues μ_n, $n = 1, 2, ...$, as shown in Fig.(6-1).

The eigenfunctions $g_n(x)$ and the associated eigenvalues μ_n satisfy the following equation:

$$\frac{\partial}{\partial x}\tilde{D}(x)\frac{\partial}{\partial x}g_n(x) = -\mu_n \tilde{L}(x) g_n(x), \tag{6.19}$$

where $g_n(x)$ and μ_n depend on ε implicitly. The eigenfunctions are orthogonal to each other,

$$\int_0^1 dx g_m(x) g_n(x) \tilde{L}(x) = M_n \delta_{nm}, \tag{6.20}$$

where δ_{nm} is the *Kronecker delta*, and the constant M_n is defined as

$$M_n \equiv \int_0^1 dx g_n^2(x)\,\tilde{L}(x)\,. \tag{6.21}$$

The differential equation (6.19) is of the Sturm-Liouville form so that eigenfunctions are complete. We can therefore expand the solution of Eq.(6.1) as

$$G_k = \sum_{l=1}^{\infty} a_l g_l(x)\,. \tag{6.22}$$

Inserting this series into Eq.(6.1), we obtain

$$\sum_{l=1}^{\infty} a_l \frac{\partial}{\partial x}\tilde{D}(x)\frac{\partial}{\partial x}g_l(x) - \sum_{l=1}^{\infty} a_l p\tilde{\tau}_{ii}\tilde{L}(x)\,g_l(x) = -2\pi p\tilde{\tau}_{ii}\,. \tag{6.23}$$

Multiplying the preceding equation by $g_n(x)$ and integrating it from 0 to 1, we obtain an algebraic equation

$$a_n(\mu_n + \tilde{\gamma}_0)M_n = 2\pi\tilde{\gamma}_0\beta_n, \tag{6.24}$$

where the constants γ_0 and β_n are defined as

$$\tilde{\gamma}_0 \equiv p\tilde{\tau}_{ii}, \tag{6.25}$$

$$\beta_n \equiv \int_0^1 dx g_n(x)\,. \tag{6.26}$$

Note that γ_0 depends on energy implicitly and β_n depends on ε implicitly. From Eq.(6.24) we know that the eigenfunction expansion coefficient a_n is

$$a_n = \frac{2\pi\tilde{\gamma}_0\beta_n}{(\mu_n + \tilde{\gamma}_0)M_n}, \tag{6.27}$$

and the distribution function G_k becomes

$$G_k = \sum_{n=1}^{\infty} \frac{2\pi\tilde{\gamma}_0\beta_n}{(\mu_n + \tilde{\gamma}_0)M_n} g_n(x)\,. \tag{6.28}$$

Knowing the eigenfunctions g_n, we can then calculate β_n and M_n. These quantities, together with the eigenvalues μ_n and driving frequency $\tilde{\gamma}_0$, can be used to determine the distribution G_k and then the neoclassical polarization.

6.2 Properties of Eigenfunctions and Eigenvalues

Before going any further, we want to discuss some useful properties of the eigenfunctions $\{g_n\}$ and eigenvalues $\{\mu_n\}$. As shown in Fig.(6-1), the eigenfunctions show the usual *Sturm-Liouville* feature that the eigenfunction g_n has $n-1$ nodes in the interval $(0,1)$. This eigenvalue problem is a *Sturm-Liouville* problem since the bounce average *Lorentz* operator, $\frac{\partial}{\partial x}\tilde{D}(x)\frac{\partial}{\partial x}$, is self-ajoint. Therefore the eigenfunctions form an orthogonal function space.

We are particularly interested in the properties of the quantities β_n, M_n and μ_n, because these quantities are closely related to the passing particle distribution G_k, as we have shown in the preceding section. It is found that these quantities can expanded in the power series of inverse aspect ratio ε, [30]

$$\mu_n(\varepsilon) = \sum_{k=0}^{\infty} u(n,k)\,\varepsilon^{k/2}, \tag{6.29}$$

$$\beta_n(\varepsilon) = \sum_{k=0}^{\infty} B(n,k)\,\varepsilon^{k/2}, \tag{6.30}$$

$$M_n(\varepsilon) = \sum_{k=0}^{\infty} M(n,k)\,\varepsilon^{k/2}. \tag{6.31}$$

In order to obtain the leading order coefficients in the preceding expansions, we can let $\varepsilon \to 0$. Then the eigenequation, Eq.(6.6), becomes a *Legendre* equation with the variable $\xi = \sqrt{1-x}$,

$$\frac{\partial}{\partial \xi}\left(1-\xi^2\right)\frac{\partial}{\partial \xi}G = -2\mu G. \tag{6.32}$$

Therefore, we can easily determine the eigenvalues and eigenfunctions,

$$\mu_n(0) = 2n^2 - n, \tag{6.33}$$

and

$$g_n^{(0)}(x) = P_{2n-1}\left(\sqrt{1-x}\right). \tag{6.34}$$

With these eigenfunctions, we can evaluate $\beta_n(0)$ and $M_n(0)$ to find

$$\beta_n(0) = \int_0^1 dx P_{2n-1}\left(\sqrt{1-x}\right) = \frac{2}{3}\delta_{n1}, \tag{6.35}$$

$$M_n(0) = \int_0^1 dx P_{2n-1}^2\left(\sqrt{1-x}\right)\frac{2\pi}{\sqrt{1-x}} = \frac{4\pi}{4n-1}. \tag{6.36}$$

Therefore, we may write the leading term explicitly to obtain

$$\mu_n(\varepsilon) = 2n^2 - n + \sum_{k=1}^{\infty} u(n,k)\,\varepsilon^{k/2}, \tag{6.37}$$

$$\beta_n(\varepsilon) = \frac{2}{3}\delta_{n1} + \sum_{k=1}^{\infty} B(n,k)\,\varepsilon^{k/2}, \tag{6.38}$$

$$M_n(\varepsilon) = \frac{4\pi}{4n-1} + \sum_{k=1}^{\infty} M(n,k)\,\varepsilon^{k/2}. \tag{6.39}$$

We can compute the numerical values of $\mu_n(\varepsilon)$, $\beta_n(\varepsilon)$ and $M_n(\varepsilon)$ for various inverse aspect ratios ε and mode numbers n, as shown in Figs.(6-2). Then, for each mode number n, we can fit the numerical data for the first few power coefficients: $u(n,k)$, $B(n,k)$ and $M(n,k)$. More details about this fitting can be found in Appendix D.

In the next section, we will show that the coefficients $\beta_n(\varepsilon)$ and $M_n(\varepsilon)$ are related to the neoclassical polarization through a particular combination of the coefficients $\beta_n(\varepsilon)$ and $M_n(\varepsilon)$, namely $\beta_n^2(\varepsilon)/M_n(\varepsilon)$. If we define

$$\frac{\beta_n^2(\varepsilon)}{M_n(\varepsilon)} = \sum_{k=0}^{\infty} W(n,k)\,\varepsilon^{k/2}, \tag{6.40}$$

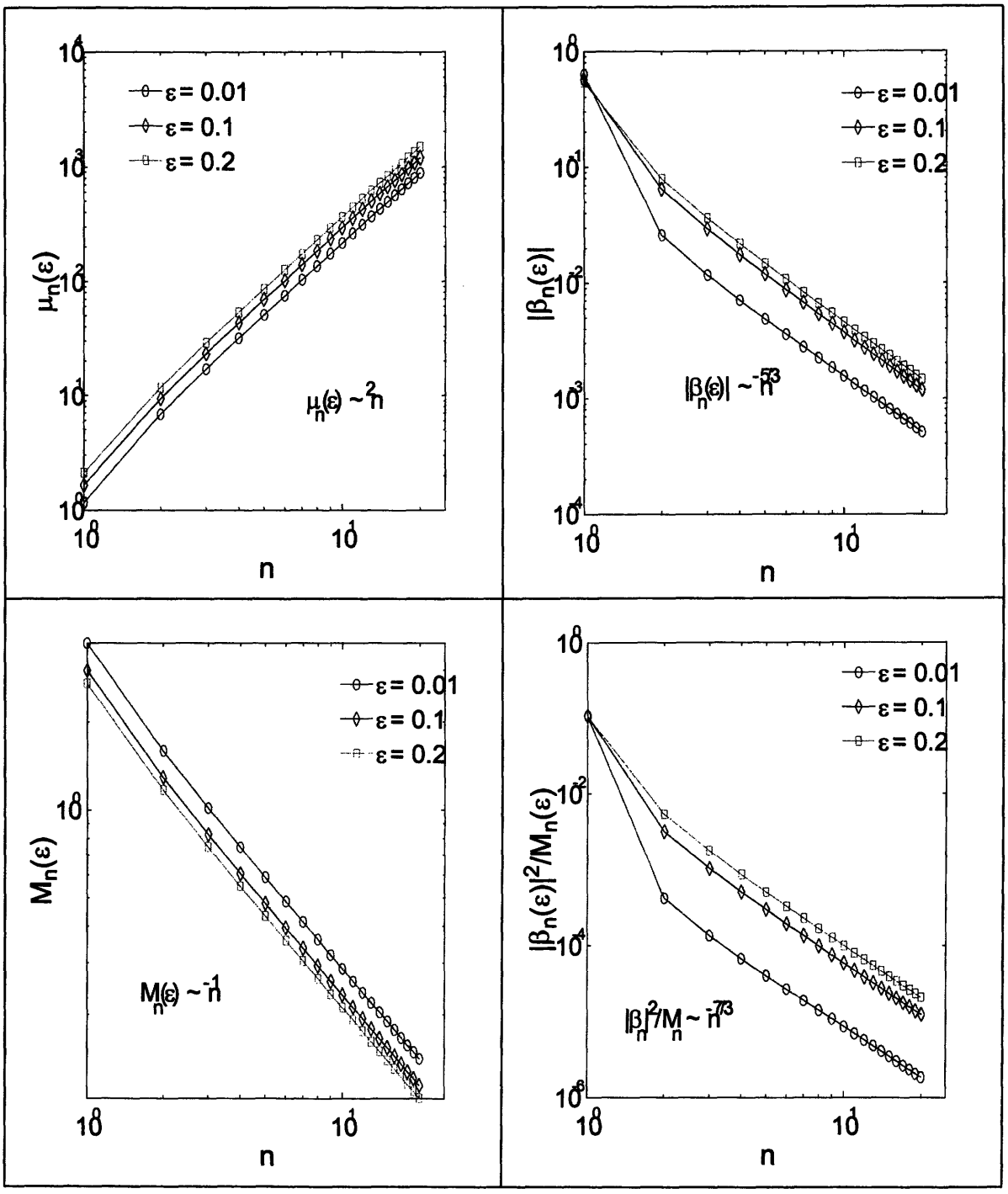

Figure 6-2: The quantities $\mu_n(\varepsilon)$, $|\beta_n(\varepsilon)|$, $M_n(\varepsilon)$ and $|\beta_n(\varepsilon)|^2/M_n(\varepsilon)$ versus mode number n in a log-log plot, for $\varepsilon = 0.01$, 0.1, 0.2. For large n, $\mu_n \propto n^2$, $|\beta_n(\varepsilon)| \propto n^{-5/3}$ and $M_n \propto n^{-1}$. Hence, $|\beta_n(\varepsilon)|^2/M_n(\varepsilon) \propto n^{-7/3}$.

$k \setminus n$	1	2	3	4	5	6
1	1.46	7.67	18.83	34.95	56.03	82.08
2	1.48	7.67	18.06	32.02	49.33	70.22
3	0.13	−0.36	−0.06	2.99	10.14	20.90

Table 6.1: The numerical power coefficients u(n,k)

$k \setminus n$	1	2	3	4	5	6
1	−0.41	−0.29	0.13	−0.08	0.056	−0.042
2	0.36	0.37	−0.15	0.10	−0.076	0.060
3	−0.24	−0.29	0.11	−0.086	0.072	−0.063

Table 6.2: The numerical power coefficients B(n,k)

then the leading order term can be obtained from Eqs.(6.38) and (6.39). This leads to the result

$$\frac{\beta_n^2(\varepsilon)}{M_n(\varepsilon)} = \frac{4n-1}{9\pi}\delta_{n1} + \sum_{k=1}^{\infty} W(n,k)\,\varepsilon^{k/2}. \tag{6.41}$$

The numerical coefficients $W(n,k)$ can be calculated from $B(n,k)$ and $M(n,k)$, which themselves are obtained from fitting the numerical data. These fitting results are tabulated in Tables (6.1), (6.2), (6.3) and (6.4).

.

6.3 Benchmark of Distribution Function

We can utilize the first few terms in Eq.(6.28) to approximate the exact distribution function. It is useful to check how many terms suffice to reproduce the exact distribution for various collisionalities and aspect ratios. Here we study several limiting cases in which

$k \setminus n$	1	2	3	4	5	6
1	−5.21	−2.24	−1.41	−1.04	−0.81	−0.67
2	5.48	2.64	1.71	1.27	0.98	0.79
3	−2.91	−2.22	−1.55	−1.21	−0.92	−0.74

Table 6.3: The numerical power coefficients M(n,k)

$k \backslash n$	1	2	3	4	5	6
1	0	0	0	0	0	0
2	0.017	0.048	0.015	0.0077	0.0047	0.0032
3	0.052	−0.060	−0.017	−0.010	−0.0072	−0.0054

Table 6.4: The numerical power coefficients W(n,k)

we have already found the analytical distributions in previous chapters.

First we study the collisionless limit. If no collisions exist, $\gamma_0 \to \infty$, then the numerical distribution G_k in Eq.(6.28) can be written as

$$G_k = \sum_{n=1}^{N} \frac{2\pi\beta_n}{M_n} g_n(x), \tag{6.42}$$

where N is the number of terms retained. The collisionless analytical distribution is known from Eq.(6.1) to be

$$G_k = \frac{2\pi}{\tilde{L}(x)}. \tag{6.43}$$

The comparison between the analytical distribution and the numerical distribution is shown in Fig.(6-3). We find that we need many eigenmodes to approach the exact analytical distribution. Even if we sum up to 20 terms there are still some small oscillations on the curve. To obtain a fairly smooth curve we would need many more terms because the coefficient of this eigenfunction expansion β_n/M_n decays rather slowly. We know from Fig.(6-2), $\beta_n \propto n^{-5/3}$ and $M_n \propto n^{-1}$. Therefore, the coefficient $\beta_n/M_n \propto n^{-2/3}$ doesn't converge. Fortunately, the integration of the nth term in Eq.(6.42) goes like $n^{-7/3}$ and converges. This feature occurs because the small oscillations seen in Fig.(6-3) tend to cancel.

If we add weak collisions the numerical distribution approaches to the analytical distribution much faster than the collisionless case. In the high frequency limit $p\tau_{ii} \gg 1$, only about ten terms are needed to make a smooth and consistent distribution, as shown in Fig.(6-4). This behavior indicates that the high eigenmode coefficients decay rather rapidly due to collisions. In this case, the numerical distribution is given by

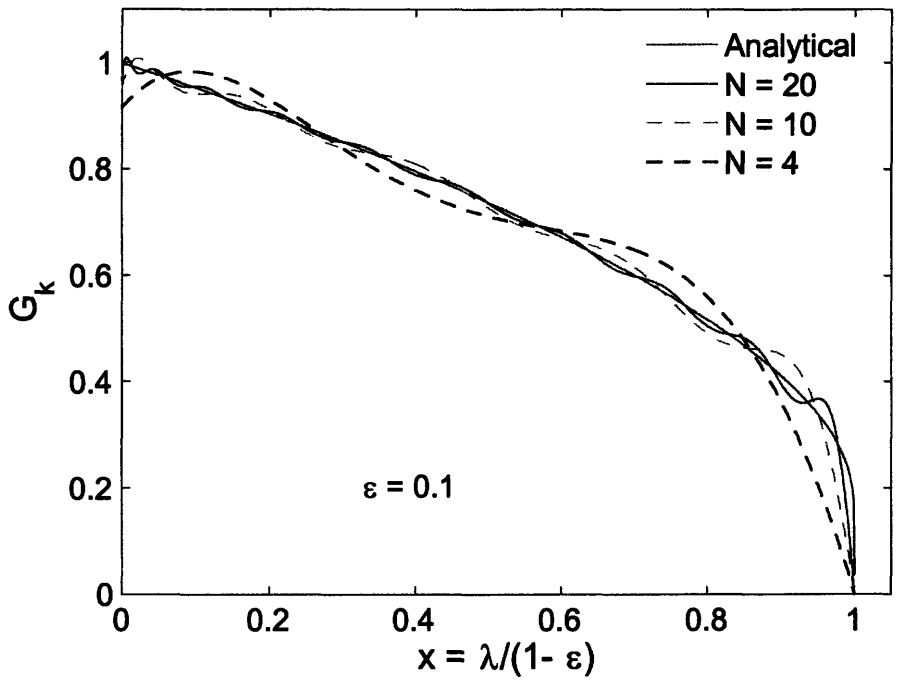

Figure 6-3: Comparison of collisionless distributions for $\varepsilon = 0.1$. The red solid line is the exact colisionless analytical distribution of Eq.(6.43). The other three curves are from the eigenfunction expansion in Eq.(6.42), keeping different numbers of terms N.

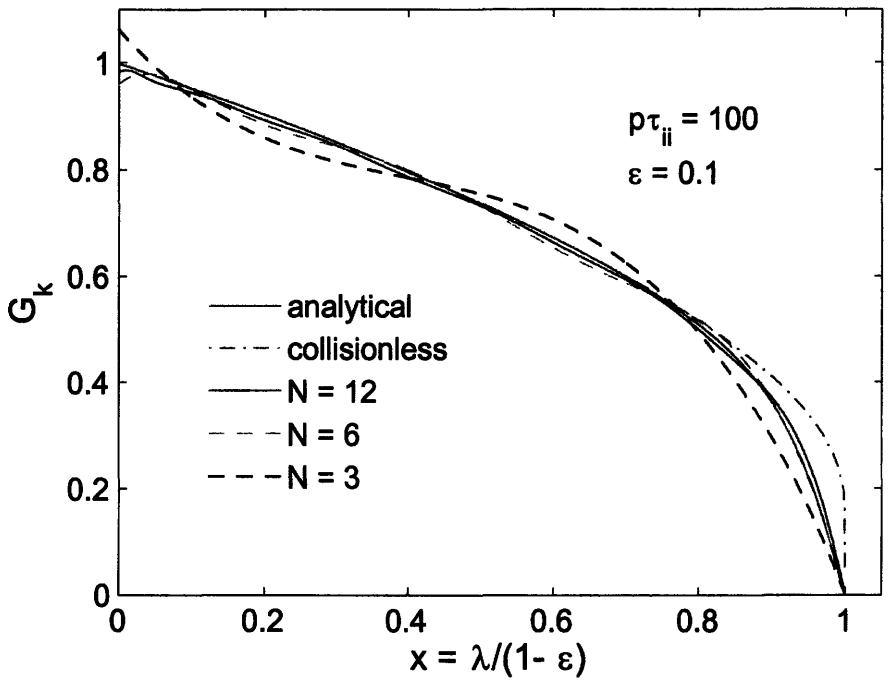

Figure 6-4: Comparison of the collisional distribution in the high frequency limit for $\varepsilon = 0.1$ and $p\tau_{ii} = 100$. Summing 12 terms in Eq.(6.44) suffices to approximate the exact distribution. The solid red curve is the H-R high frequency collisional response from Eq.(6.45).

$$G_k = \sum_{n=1}^{N} \frac{2\pi\tilde{\gamma}_0\beta_n}{(\mu_n + \tilde{\gamma}_0) M_n} g_n(x). \tag{6.44}$$

We now set $m_i E/T_i = 1$ to facilitate the numerical computation and comparison with the results from Chapter 5. For $p\tau_{ii} \gg 1$ and $m_i E/T_i = 1$, the analytical distribution is given by the trial function of Eq.(5.25),

$$G_k = \frac{2\pi}{\tilde{L}(x)} \left[1 - e^{-\gamma \frac{1-\varepsilon}{2\varepsilon}(1-x)}\right], \tag{6.45}$$

where γ is defined in Eq.(5.42), but in this equation we use $x = \lambda/(1-\varepsilon)$. From Eq.(6.44) we see that for a finite collision frequency $\tilde{\gamma}_0$, the eigenvalue μ_n will catch up with $\tilde{\gamma}_0$ very quickly since $\mu_n \propto n^2$. When $\mu_n \gg \tilde{\gamma}_0$, the total coefficient in Eq.(6.44) decays as $n^{-8/3}$. Therefore, the high eigenmodes will decay rapidly as $\mu_n \gg \tilde{\gamma}_0$, to make the distribution smooth.

In the low frequency limit, $p\tau_{ii} \ll 1$, the numerical distribution is still given by Eq.(6.44). From Fig.(6-5), we see that only two or three terms are required to obtain a good approximation. The analytical distribution in Fig.(6-5) is given by

$$G_k = \int_x^1 dx \frac{\pi\tilde{\gamma}_0(1-\varepsilon)}{4\sqrt{1-x+\varepsilon+x\varepsilon}E\left(\frac{2\varepsilon}{1-x+\varepsilon+x\varepsilon}\right)}, \tag{6.46}$$

which comes from Eq.(5.45). Recall that this expression is from the first order expansion of $p\tau_{ii}$. To be consistent with this distribution, we need to take the numerical distribution as follows

$$G_k = \sum_{n=1}^{N} \frac{2\pi\tilde{\gamma}_0\beta_n}{\mu_n M_n} g_n(x). \tag{6.47}$$

The numerical series converges much faster than the high frequency case, so only two terms are needed to approach the analytical distribution.

The consistency between the numerical series and analytical distribution confirms the usefulness of the eigenfunction expansion method for solving the collisional neoclassical polarization problem.

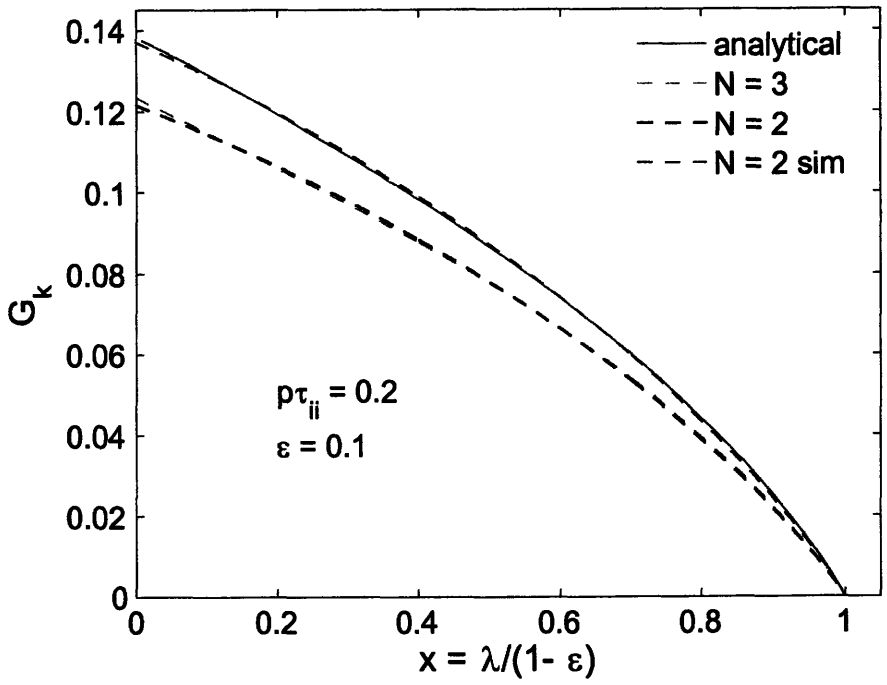

Figure 6-5: Comparison of the collisional distribution in the low frequency limit. The green dashed line and the black dashed line, calculated from Eq.(6.44), almost overlap. Hence, for $p\tau_{ii} \ll 1$, two terms suffice to approximate the exact distribution. The red solid line is from the H-R low frequency response in Eq.(6.46). The blue dashed line is from Eq.(6.47).

6.4 Collisional Neoclassical Polarization

We proceed to construct the neoclassical polarization from these eigenfunctions. According to Eq.(5.12), the neoclassical polarization can be written in terms of the distribution function G_k. To be consistent with the notation of Eq.(3.33) in Chapter 3, we let

$$P_1 = \frac{3}{2}\int_0^{1-\epsilon} d\lambda \langle G_k \rangle_E . \tag{6.48}$$

For the polarization we will use the form from Eq.(3.22) rather than the equivalent form from Eq.(3.21). Using the preceding, we have

$$\varepsilon_{k,nc}^{pol}(p) = \frac{\omega_{pi}^2}{\omega_{ci}^2}\frac{q^2}{\varepsilon^2}(1 - P_1) . \tag{6.49}$$

Once we know the term P_1, we effectively know the whole neoclassical polarization. Therefore, we focus on studying the term P_1. We insert the expression for G_k in Eq.(6.28) into the preceding equation to obtain

$$P_1 = 3\pi(1-\varepsilon)\sum_{n=1}^{\infty}\frac{\beta_n^2}{M_n}\left\langle \frac{\tilde{\gamma}_0}{\mu_n + \tilde{\gamma}_0}\right\rangle_E , \tag{6.50}$$

where the energy average is defined in Eq.(3.20). Letting $y = m_i E/T_i$, the preceding equation can be explicitly written as

$$P_1 = 4\sqrt{\pi}(1-\varepsilon)\sum_{n=1}^{\infty}\frac{\beta_n^2}{M_n}\int_0^{\infty}\frac{dyy^3e^{-y}}{\mu_n/\gamma_0 + y^{3/2}}, \tag{6.51}$$

where the frequency $\gamma_0 = p\tau_{ii}$ doesn't contain the energy dependence since $\tilde{\gamma}_0 = p\tau_{ii}y^{3/2}$.

Employing the preceding equation and Eq.(6.49) we can calculate the neoclassical polarization for various driving frequencies or collisionalities $p\tau_{ii}$, and inverse aspect ratios ε, as shown in Fig.(6-6). Recall that the residual zonal flow is inversely proportional to the neoclassical polarization so that the zonal flow is strongly damped for $p\tau_{ii} \to 0$. The damping of the zonal flow increases slightly as the inverse aspect ratio ε increases

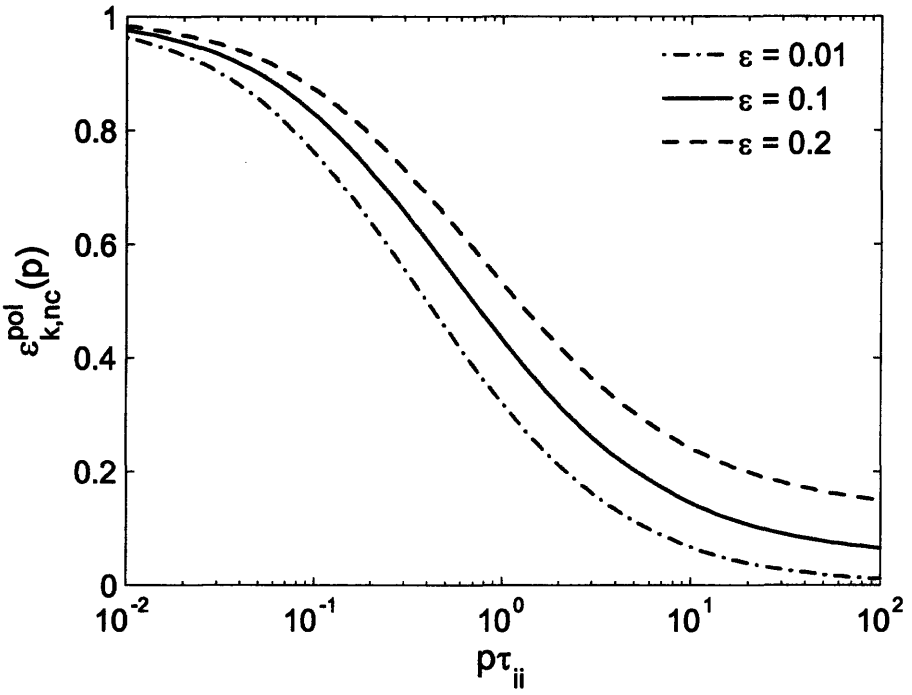

Figure 6-6: The neoclassical polarization in unit of $\frac{\omega_{pi}^2}{\omega_{ci}^2}\frac{q^2}{\epsilon^2}$, calculated by Eq.(6.49) by computing the coefficients μ_n, β_n, and M_n numerically and then adding total 20 terms to approach the exact value.

when the collision frequency is comparable to the driving wave frequency. Of course, the zonal flow is strongly damped at the high collisionalities and weakly damped at low collisionalities, as found by H-R, but their low collisionality or high driving frequency limit is only valid for $\sqrt{\varepsilon p \tau_{ii}} \gg 1$. From Fig.(6-6) we also see that, for high driving frequencies or low collisionalities, the neoclassical polarization is small, so it is sensitive to inverse aspect ratio ε. However, for low driving frequencies or high collisionalities, the neoclassical polarization becomes large and ignoring the ε dependence is not as critical to the final answer.

Since we need to calculate each point numerically in Fig.(6-6), it is sometimes more convenient to apply a more analytical, but approximate method. We can employ the fitting procedure described in Appendix D to obtain a ε power series for the coefficients μ_n and β_n^2/M_n in Eq.(6.51), as shown in Eq.(6.37) and (6.41). The coefficients $m(n,k)$ and $W(n,k)$ are listed in Table I (6.1) and IV. Since we have obtained analytical expressions for the coefficients μ_n and β_n^2/M_n, we only need to compute the integral in Eq.(6.51) numerically to obtain the neoclassical polarization in Eq.(6.49). This method can be regarded as a semi-analytical approach.

6.4.1 Approximate Methods for Neoclassical Polarization

The preceding exact eigenfunction expansion method is very accurate, but sometimes a simpler result may be convenient. We proceed to seek more concise but approximate method to calculate the neoclassical polarization.

From Fig.(6-2), we see that β_1^2/M_1 dominates the other eigenfunction expansion coefficients. Therefore, it is sometimes convenient to retain only the leading order term in the preceding equation, namely

$$P_1 = 4\sqrt{\pi}\,(1-\varepsilon)\,\frac{\beta_1^2}{M_1}\int_0^\infty \frac{dy y^3 e^{-y}}{\mu_1/\gamma_0 + y^{3/2}}, \tag{6.52}$$

where the coefficients μ_1 and β_1^2/M_1 can be read from Tables I and IV, to find

$$\mu_1 = 1 + 1.46\sqrt{\varepsilon} + 1.48\varepsilon + 0.13\varepsilon^{3/2} \tag{6.53}$$

$$\frac{\beta_1^2}{M_1} = \frac{1}{3\pi} + 0.017\varepsilon - 0.052\varepsilon^{3/2}. \tag{6.54}$$

For a given ε, there are two different approaches to deal with the energy integral in the Eq.(6.52).

(1). **One term numerical approaches.**

For each driving frequency γ_0, we integrate this integral numerically. This approach provides a benchmark to check the other approximate approaches. We denote this method as "*1 Term Exact*".

We may even be less accurate, e.g., ignoring the ε dependence in μ_1.Then Eq.(6.52) becomes

$$P_1 = 4\sqrt{\pi}\,(1-\varepsilon)\,\frac{\beta_1^2}{M_1}\int_0^\infty \frac{dyy^3e^{-y}}{1/\gamma_0 + y^{3/2}}. \tag{6.55}$$

This approximate method is denoted as as "*1 Term Approx*".

(2). **One term approximate analytical approaches.**

There are two approximate methods we have considered. The first method is to apply the observation we found in the preceding chapter by setting $\gamma_0 \to 4\gamma_0$, where $\gamma_0 = p\tau_{ii}$. Thus we obtain

$$P_1 = 3\pi\,(1-\varepsilon)\,\frac{\beta_1^2}{M_1}\frac{4\gamma_0}{\mu_1 + 4\gamma_0}, \tag{6.56}$$

which we denote as "*Approx 1*".

The second method is to use a *Pade*'s approximation. Notice

$$\begin{aligned}\int_0^\infty \frac{dyy^3e^{-y}}{\mu_n/\gamma_0 + y^{3/2}} &= \frac{\gamma_0}{6\mu_n}, \text{ for } \mu_n/\gamma_0 \gg 1,\\ &= \frac{3\sqrt{\pi}}{4}, \text{ for } \mu_n/\gamma_0 \ll 1,\end{aligned}$$

and the *Pade*'s approximation gives

$$\int_0^\infty \frac{dyy^3e^{-y}}{\mu_n/\gamma_0 + y^{3/2}} = \frac{\frac{8}{\sqrt{\pi}}\gamma_0}{\mu_n + \frac{8}{\sqrt{\pi}}\gamma_0}\frac{3\sqrt{\pi}}{4}. \tag{6.57}$$

Then the one term approximation becomes

$$P_1 = 3\pi\,(1-\varepsilon)\,\frac{\beta_1^2}{M_1}\frac{\frac{8}{\sqrt{\pi}}\gamma_0}{\mu_1 + \frac{8}{\sqrt{\pi}}\gamma_0}, \tag{6.58}$$

which is essentially the same as "*Approx 1*" since we take the energy average magnification to be $8/\sqrt{\pi}$; the low frequency energy average magnification. We denote this approximation method as "*Approx 2*".

A comparison of the preceding different methods is shown in Fig.(6-7). For very small ε, $\varepsilon = 0.01$, we can see from Fig.(6-2) that the coefficient β_1^2/M_1 is 100 times larger than the other term. Therefore, we can ignore the higher order terms in the eigenfunction expansion. If the energy integral is computed exactly, the "*1 Term Exact*" curve will be very close to the exact value, as shown by the first plot of Fig.(6-7). We also see, the "*1 Term Approx*" curve is also a quite good approximation for small ε. The small deviation of "*1 Term Approx*" from the exact line is due to the neglect of the higher ε terms in μ_1. For small ε, the curves "*Approx 1*" and "*Approx 2*" are also very accurate in the high frequency and low frequency limits. However, there is almost a 20% error in the middle that comes from the inaccuracy of the energy integral in the middle. This error is a typical feature of a *Pade*'s approximation. The method "*Approx 1*" is only slightly better than "*Approx 2*". The *H-R* low frequency approximation breaks down quickly upon entering the intermediate frequency regime. The *R-H* high frequency approximation is not good for $\varepsilon = 0.01$ because the condition $\gamma \gg 1$ or $\sqrt{\varepsilon p \tau_{ii}} \gg 1$ is easily violated as $\varepsilon \to 0$.

When ε becomes larger the "*1 Term Exact*" curve is still good for most of the frequencies, but becomes less good at very high frequencies, as shown in the second plot of Fig.(6-7). This is because the higher order coefficients β_n^2/M_n become large to within

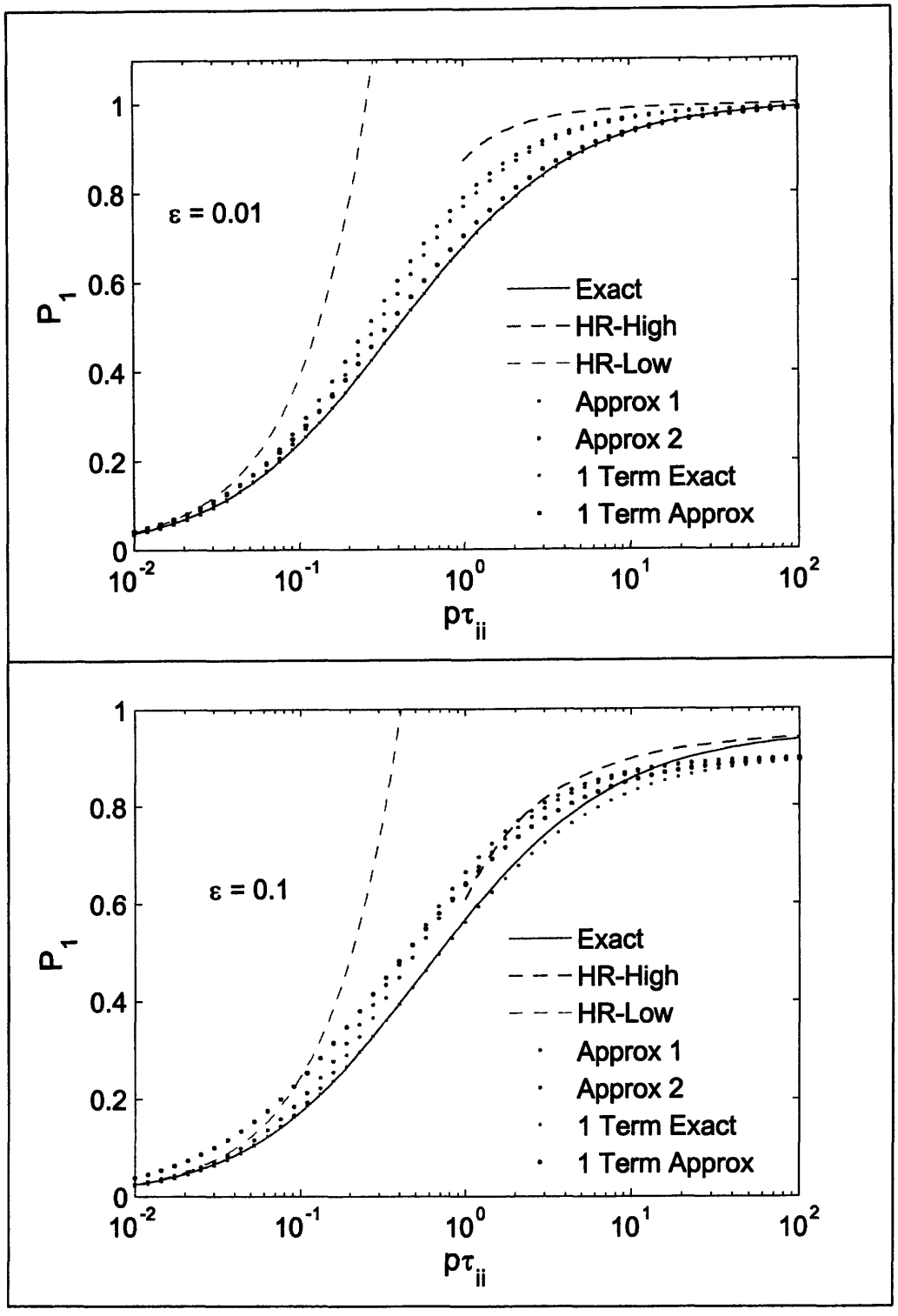

Figure 6-7: A comparison of the frequency dependence of the polarization P_1 from different methods, for $\varepsilon = 0.01$ and 0.1. The "*Exact*" line is calculated by Eq.(6.51) by computing the cofficient μ_n, β_n, and M_n numerically and then adding total 20 terms. "*HR-High*" is the *H-R* high frequency polarization derived from Eq.(5.41), while "*HR-Low*" is the *H-R* high frequency polarization derived from Eq.(5.48).

10% of the β_1^2/M_1, as seen from Fig.(6-2). The higher order contributions will cause the "*1 Term Exact*" curve to have a 10% deviation from the exact line for the high frequency case, as shown in Fig.(6-7). Recall that $\epsilon_{k,nc}^{pol} = \frac{\omega_{pi}^2 q^2}{\omega_{ci}^2 \varepsilon^2}(1 - P_1)$. Therefore, in the high frequency limit, e.g. $p\tau_{ii} \sim 100$, a 10% error in P_1 can cause an order unity error in $\epsilon_{k,nc}^{pol}$. Fortunately, in this limit(relatively large ε and high frequency), the *H-R* high frequency approximation remains valid, even though this is the worst case for the approximate methods discussed so far.

However, we can improve our approximate method to have better performance in the high frequency range. We know from Eq.(3.39) that in the collisionless limit $P_1 = 1 - 1.635\varepsilon^{3/2}$. This limit suggests that a reasonable approximation that satisfies the high frequency asymptotic limit and also has the form of Eq.(6.52) is

$$P_1 = \frac{4}{3\sqrt{\pi}}\left(1 - 1.635\varepsilon^{3/2}\right)\int_0^\infty \frac{dyy^3e^{-y}}{\alpha/\gamma_0 + y^{3/2}}, \tag{6.59}$$

where the quantity α is to be determined by the low frequency asymptotic limit. In the low frequency limit we know from Eq.(5.48) that

$$P_1 = \frac{8}{\sqrt{\pi}}\gamma_0\left(1 - 1.461\sqrt{\varepsilon}\right), \tag{6.60}$$

where $\gamma_0 = p\tau_{ii}$. In this low frequency limit, Eq.(6.59) becomes

$$P_1 = \frac{8\gamma_0}{\alpha\sqrt{\pi}}\left(1 - 1.635\varepsilon^{3/2}\right). \tag{6.61}$$

Setting this equation equal to Eq.(6.60) we find α to be

$$\alpha = 1 + 1.461\sqrt{\varepsilon}, \tag{6.62}$$

to the accuracy of $\mathcal{O}(\sqrt{\varepsilon})$. Therefore the neoclassical polarization can be calculated from Eq.(6.49), (6.59) and (6.62). We denote this approximate method as "*Approx 3*". It is equivalent to what we obtain by setting β_1 and M_1 to their leading values: $\beta_1 = 2/3$ and

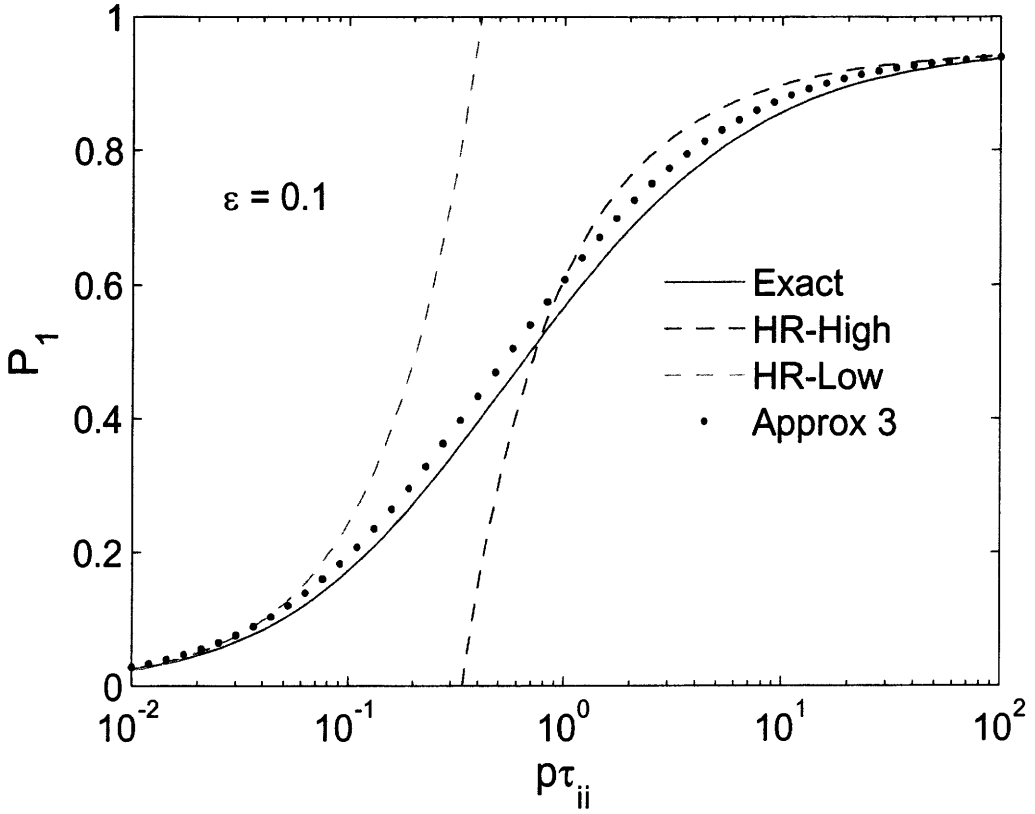

Figure 6-8: A comparison of the frequency dependence of the polarization P_1 from different methods, for $\varepsilon = 0.1$. The exact line is calculated by Eq.(6.51). "*HR-High*" is the *H-R* high frequency polarization derived from Eq.(5.41), while "*HR-Low*" is the *H-R* high frequency polarization derived from Eq.(5.48). The dotted curve "*Approx 3*" is calculated by Eqs.(6.59) and (6.62).

$M_1 = 4\pi/3$, and keeping μ_1 to first order accuracy, $\mu_1 = 1 + 1.461\sqrt{\varepsilon}$ in Eq.(6.52). The comparison between the approximate methods "*1 Term Approx*" and "*1 Term Exact*" in Fig.(6-7) shows that using μ_1 to first order accuracy is good enough for the energy integrals. Therefore, the error in the approximation "*Approx 3*" comes from ignoring the higher order terms of β_n^2/M_n in the eigenfunction expansion. From Fig.(6-2) we expect this error to be about 15%. This estimate is verified by Figs.(6-8) and (6-9) that shows the approximate method "*Approx 3*" is good for almost all collision frequencies and small inverse aspect ratios ε.

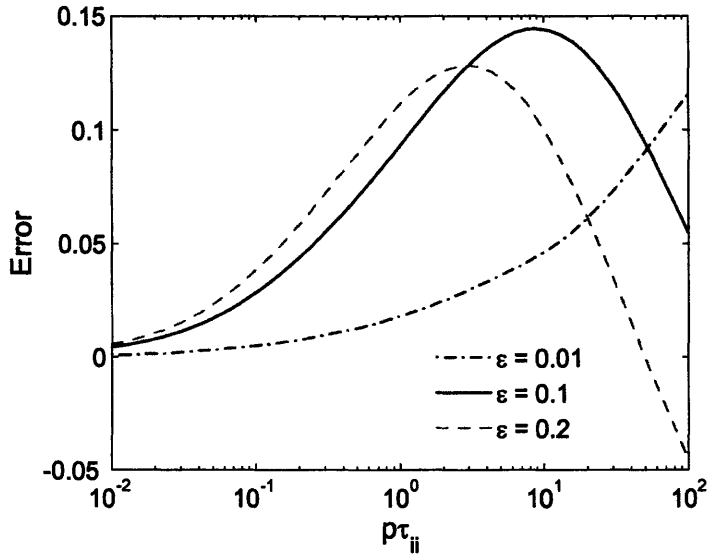

Figure 6-9: The relative error in the calculation of the neoclassical polarization from method "*Approx 3*" of Eqs.(6.59) and (6.62) compared to the exact value, for various $p\tau_{ii}$ and $\varepsilon = 0.01$, 0.1, and 0.2.

Finally, we estimate the upper limit the driving wave frequency can reach in a real tokamak. Taking *ITER* as an example, then $n_i \sim 1.1 \times 10^{14} cm^{-3}$, $T_i \sim 10 kev$ $R_0 \sim 6m$, and $B_0 \sim 5T$. Then, a typical ion-ion collision frequency is $\nu_{ii} \sim 100\,\mathrm{sec}^{-1}$ and the transit frequency is $\omega_t \sim 10^5\,\mathrm{sec}^{-1}$. For the transit average to be valid, we require $p/\omega_t \ll 1$. So $p\tau_{ii} \sim 100$ is about the upper limit that a driving frequency can reach. In Alcator C-Mod, $n_i \sim 2.0 \times 10^{14} cm^{-3}$, $T_i \sim 2kev$ $R_0 \sim 0.64m$, and $B_0 \sim 5T$. Then, a typical ion-ion collision frequency for C-Mod is $\nu_{ii} \sim 1600\,\mathrm{sec}^{-1}$ and the transit frequency is $\omega_t \sim 4.0 \times 10^5\,\mathrm{sec}^{-1}$. Therefore, for C-Mod, $p\tau_{ii} \sim 200$ is the rough upper limit that the driving frequency can reach.

6.5 Collisional Zonal Flow Damping

Having a complete understanding of the role of collisions on neoclassical polarization, we can proceed to investigate the zonal flow damping associated with it. Using Eq.(2.22)

and (2.23), the evolution of the zonal flow potential can be written as

$$\phi_k(t) = \phi_k(t=0)\frac{1}{2\pi i}\int \frac{dpe^{pt}}{p}\frac{\varepsilon^{pol}_{k,cl}}{\varepsilon^{pol}_{k,cl}+\varepsilon^{pol}_{k,nc}(p)}, \tag{6.63}$$

where the classical polarization is $\varepsilon^{pol}_{k,cl} = \frac{\omega^2_{pi}}{\omega^2_{ci}}\frac{q^2}{\varepsilon^2}$ in the long wavelength limit, and the neoclassical polarization can be calculated by Eq.(6.49) and the approximate P_1 of Eq.(6.59). To make the results even simpler, we can apply a *Pade* approximation for the energy integral in Eq.(6.59). Therefore Eq.(6.59) becomes

$$P_1 = \left(1-1.6\varepsilon^{3/2}\right)\frac{\gamma_0}{\gamma_0+\frac{\sqrt{\pi}}{8}\mu_1}, \tag{6.64}$$

where $\gamma_0 = p\tau_{ii}$ and $\mu_1 = 1+1.46\sqrt{\varepsilon}$. Inserting this equation into Eq.(6.49), we find the neoclassical polarization to be

$$\varepsilon^{pol}_{k,nc}(p) = \frac{\omega^2_{pi}}{\omega^2_{ci}}\frac{q^2}{\varepsilon^2}\frac{1.6\varepsilon^{3/2}\gamma_0+\frac{\sqrt{\pi}}{8}\mu_1}{\gamma_0+\frac{\sqrt{\pi}}{8}\mu_1}. \tag{6.65}$$

In the large aspect ratio limit, the neoclassical polarization is much larger than the classical polarization. Therefore, we may ignore the classical polarization in Eq.(6.63). Inserting the neoclassical polarization in Eq.(6.65) into Eq.(6.63), we obtain

$$\phi_k(t) = \phi_k(t=0)\frac{\varepsilon^2}{q^2}\frac{1}{2\pi i}\int \frac{dpe^{pt}}{p}\frac{p\tau_{ii}+\frac{\sqrt{\pi}}{8}\mu_1}{1.6\varepsilon^{3/2}p\tau_{ii}+\frac{\sqrt{\pi}}{8}\mu_1}. \tag{6.66}$$

Inverting the *Laplace* transform we find

$$\phi_k(t) = \phi_k(t=0)\frac{\varepsilon^2}{q^2}\left[1+\left(\frac{1}{1.6\varepsilon^{3/2}}-1\right)e^{-\frac{\mu_1 t}{7.4\varepsilon^{3/2}\tau_{ii}}}\right]. \tag{6.67}$$

From this equation we can see, with collisions the zonal flow damps to a level much smaller than the *R-H* collisionless residual within a decay time of order $\varepsilon^{3/2}\tau_{ii}$. Although the decay time is of order $\varepsilon^{3/2}\tau_{ii}$, it is enhanced by the numerical factor 7.4 to roughly the

magnitude of ion-ion collision time.

Chapter 7

Summary

In the preceding chapters we have extended the original *R-H/H-R* work in many respects. We summarize these extensions as follows.

At the end of Chapter 3 we employed the R-H collisionless distribution to calculate the zonal flow. This calculation revealed that the zonal flow contains not only poloidal rotation, but also a similar size toroidal rotation.

In the first part of Chapter 4, we calculated the neoclassical polarization and *R-H* residual zonal flow level for arbitrary perpendicular wavelengths. First, we extended the *R-H* neoclassical polarization calculation analytically from $k_\perp \rho_p \ll 1$ to $k_\perp \rho_p < 1$ by expanding the calculation to include Q^4 terms. Then we calculated the neoclassical polarization and residual zonal flow level numerically for arbitrary perpendicular wavelengths from $k_\perp \rho_p < 1$ to $k_\perp \rho_i \gg 1$. We find that the effective zonal flow or effective residual caused by a given density perturbation is much weaker for short wavelengths. The weakness of zonal flow is not due to the damping of the zonal flow, but rather due to the weakness of the source potential produced by the initial density perturbation [18]. Notice that this small wavelength result is expected to be valid at the edge of an internal transport barrier (ITB) [46], where the assumption of large parallel mean free path remains valid. Radial wavelengths in the pedestal region of a tokamak are typically comparable to the poloidal ion gyroradius, so small zonal flows are expected there where they are

also reduced by collisions. This result may have some implications for the higher levels of turbulence observed in the pedestal. A complete kinetic treatment of the pedestal must allow arbitrary parallel mean free paths and sharp density and temperature gradients, making the problem still more involved and challenging.

In the second part of Chapter 4, we developed a small inverse aspect ratio expansion method to calculate shaping effects on the *R-H* collisionless residual zonal flow. We find that the elongation is strongly beneficial to the residual zonal flow, while the triangularity is harmful but much weaker. The small ε expansion method employed here is quite general so that it can be applied to more complicated MHD equilibrium that include not only the safety factor, elongation and triangularity effects, but also their shears. In addition, a careful comparison to numerical simulations is desirable and feasible. Another straightforward extension of the present work would be to treat both plasma shape and collisional effects simultaneously.

In Chapter 6 we developed a semi-analytical method, based on an eigenfunction expansion of a *Lorentz* collision operator [30][12], to calculate the collisional neoclassical polarization for the entire driving frequency range and arbitrary collision frequencies below the transit frequency. For high driving frequencies or low collisionalities, the neoclassical polarization is small, so it is sensitive to inverse aspect ratio ε. However, for low driving frequencies or high collisionalities, the neoclassical polarization becomes large and insensitive to ε. In addition to the exact result, we find a fairly good analytical approximation for the neoclassical polarization which is concise and suitable for a large range of driving wave frequencies or collisionalities. We also calculate the collisional zonal flow damping and find that, with collisions the zonal flow damps to a level much smaller than the *R-H* collisionless residual within a decay time of order $\varepsilon^{3/2}\tau_{ii}$. The eigenfunction method employed here is more general than the variational treatment of *H-R* that only considered the weak and strong collisionality limits. This expansion method can be employed to solve even more complicated collisional zonal flow problems.

Appendix A

A Derivation of Nonlinear Drift Kinetic Equation

The electrostatic drift kinetic equation, in $E = v^2/2$ and $\mu = v_\perp^2/2B$ variables, accurate to the first order in gyroradius expansion when the lowest order distribution function is isotropic in velocity space, was shown by Hazeltine[24][23], to be given by,

$$\frac{\partial \overline{f}}{\partial t} + (v_\parallel \mathbf{b} + \mathbf{v}_B + \mathbf{v}_E) \cdot \nabla \overline{f} - C_{ii}\left\{\overline{f}\right\} = \frac{e}{M}(v_\parallel \mathbf{b} + \mathbf{v}_B) \cdot \nabla \phi \frac{\partial \overline{f}}{\partial E}, \qquad \text{(A.1)}$$

where $\mathbf{v}_B$ is the magnetic drift, defined in Eq.(2.2); $\mathbf{v}_E$ is the $\mathbf{E} \times \mathbf{B}$ drift; $\overline{f}$ is the gyroaveraged distribution function, M and e are species mass and charge. Letting

$$\overline{f} = F_0 + f_1,$$

with F_0 a local Maxwellian with $\mathbf{b} \cdot \nabla F_0 = 0$, then $f_1 = \delta f$, an assumed small correction to F_0, satisfies the nonlinear equation

$$\begin{aligned} \frac{\partial f_1}{\partial t} + (v_\parallel \mathbf{b} + \mathbf{v}_B) \cdot \nabla f_1 - C_{ii}\{f_1\} \;=\; & -\frac{e}{T} F_0 (v_\parallel \mathbf{b} + \mathbf{v}_B) \cdot \nabla \phi - (\mathbf{v}_B + \mathbf{v}_E) \cdot \nabla F_0 \\ & -\mathbf{v}_E \cdot \nabla f_1 + e(v_\parallel \mathbf{b} + \mathbf{v}_B) \cdot \nabla \phi \frac{\partial f_1}{\partial E}, \qquad \text{(A.2)} \end{aligned}$$

where we assume $\partial F_0/\partial t \ll \partial f_1/\partial t$.

To further simplify this equation, we estimate the size of the drive terms. We estimate the sizes of term by using $v_E \sim k_\perp \rho \frac{e\phi}{T} v_t$, $\mathbf{v}_B \sim \frac{\rho}{R_0} v_t$. We allow

$$\frac{e v_\parallel \mathbf{b} \cdot \nabla \phi \partial f_1/\partial E}{M \mathbf{v}_E \cdot \nabla f_1} \sim \frac{1}{k_\perp \rho k_\perp q R_0} \leq 1,$$

so that the nonlinear term $v_\parallel \mathbf{b} \cdot \nabla \phi \partial f_1/\partial E$ is not ignored comparing to the $\mathbf{E} \times \mathbf{B}$ nonlinearity $\mathbf{v}_E \cdot \nabla f_1$. However, another nonlinear term $\mathbf{v}_B \cdot \nabla \phi \partial f_1/\partial E$ may be safely ignored since

$$\frac{e \mathbf{v}_B \cdot \nabla \phi \partial f_1/\partial E}{\mathbf{v}_E \cdot \nabla f_1} \sim \frac{1}{k_\perp R_0} \ll 1.$$

For polarization and neoclassical calculations, the distribution F_0 and electrostatic potential ϕ are lowest order flux functions, so there is no contribution from $\mathbf{v}_E \cdot \nabla F_0$. The drive $\mathbf{v}_B \cdot \nabla F_0$ must be retained to evaluate the neoclassical particle and heat flux. As a result, the drift kinetic equation of interest may be written as

$$\begin{aligned} \frac{\partial f_1}{\partial t} + (v_\parallel \mathbf{b} + \mathbf{v}_d) \cdot \nabla f_1 - C_{ii}\{f_1\} &= -\frac{e}{T} F_0 (v_\parallel \mathbf{b} + \mathbf{v}_d) \cdot \nabla \phi - \mathbf{v}_B \cdot \nabla F_0 \\ &\quad - \mathbf{v}_E \cdot \nabla f_1 + \frac{e}{M} v_\parallel \mathbf{b} \cdot \nabla \phi \partial f_1/\partial E. \end{aligned} \quad \text{(A.3)}$$

However, when evaluating the polarization, we might neglect the neoclassical drive $\mathbf{v}_B \cdot \nabla F_0$, because it does not enter the evaluation of the polarization.

Appendix B

Details about Large Q calculation

This appendix presents algebraic details used to evaluate the collisionless neoclassical polarization to $\mathcal{O}(Q^4)$. In particular, we need to evaluate the following integrals:

$$\int d\lambda \oint \frac{d\theta}{\xi}\overline{Q^2},\ \int d\lambda \oint \frac{d\theta}{\xi}\overline{Q^4},\ \int_0^{1-\varepsilon} d\lambda \oint \frac{d\theta}{\xi}\overline{Q}^2,$$
$$\int_0^{1-\varepsilon} d\lambda \oint \frac{d\theta}{\xi}\overline{Q}\ \overline{Q^3},\ \int d\lambda \oint \frac{d\theta}{\xi}\overline{Q^2}^2. \tag{B.1}$$

The first two integrals can be carried out by using the following identities:

$$\int d^3v v_\parallel^2 F_0 = n_0\frac{T_i}{m_i}, \tag{B.2}$$
$$\int d^3v v_\parallel^4 F_0 = 3n_0\left(\frac{T_i}{m_i}\right)^2. \tag{B.3}$$

We first note that we can use the preceding identities to obtain

$$\left\langle \int d^3v F_0 \overline{Q^2} \right\rangle = \left(\frac{IS'}{\Omega_0}\right)^2 \left\langle h^2 \int d^3v v_\parallel^2 F_0 \right\rangle$$
$$= n_0\frac{T_i}{m_i}\left(\frac{IS'}{\Omega_0}\right)^2\left(1+\frac{3}{2}\varepsilon^2\right), \tag{B.4}$$

with $h = 1 + \varepsilon \cos\theta$, and

$$\left\langle \int d^3v F_0 \overline{Q^4} \right\rangle = \left(\frac{IS'}{\Omega_0}\right)^4 \left\langle h^4 \int d^3v v_\parallel^4 F_0 \right\rangle$$
$$= 3n_0 \left(\frac{T_i}{m_i}\right)^2 \left(\frac{IS'}{\Omega_0}\right)^4 \left(1 + 5\varepsilon^2 + \frac{15}{8}\varepsilon^4\right). \tag{B.5}$$

Alternatively, we can write

$$\left\langle \int d^3v F_0 \overline{Q^2} \right\rangle = \frac{3n_0 T_i}{4\pi m_i} \left(\frac{IS'}{\Omega_0}\right)^2 \int d\lambda \oint \frac{d\theta}{\xi} (\xi h)^2 \tag{B.6}$$

and

$$\left\langle \int d^3v F_0 \overline{Q^4} \right\rangle = \frac{15n_0}{4\pi} \left(\frac{T_i}{m_i}\right)^2 \left(\frac{IS'}{\Omega_0}\right)^4 \int d\lambda \oint \frac{d\theta}{\xi} (\xi h)^4. \tag{B.7}$$

Comparing the preceding four equations, we obtain

$$\int d\lambda \oint \frac{d\theta}{\xi} (\xi h)^2 = \frac{4\pi}{3} \left(1 + \frac{3}{2}\varepsilon^2\right) \tag{B.8}$$

and

$$\int d\lambda \oint \frac{d\theta}{\xi} (\xi h)^4 = \frac{4\pi}{5} \left(1 + 5\varepsilon^2 + \frac{15}{8}\varepsilon^4\right). \tag{B.9}$$

Therefore,

$$\int d\lambda \oint \frac{d\theta}{\xi} \overline{Q^2} = \frac{8\pi}{3} \left(1 + \frac{3}{2}\varepsilon^2\right) \frac{m_i E}{T_i} \left(k_\perp \rho_p\right)^2, \tag{B.10}$$

and

$$\int d\lambda \oint \frac{d\theta}{\xi} \overline{Q^4} = \frac{16\pi}{5} \left(1 + 5\varepsilon^2 + \frac{15}{8}\varepsilon^4\right) \left(\frac{m_i E}{T_i}\right)^2 \left(k_\perp \rho_p\right)^4 \tag{B.11}$$

with $k_\perp \rho_p = \frac{IS'}{\Omega_0} \sqrt{\frac{T_i}{m_i}}$, and $E = v^2/2$.

The third and fourth integrals in Eq.(B.1) involve only passing particles. The usual way to deal with them utilizes *elliptic integrals*. Here we employ an alternate method based on an ε expansion to carry out the integrations.

First we look at the integral $\int_0^{1-\varepsilon} d\lambda \oint \frac{d\theta}{\xi}\overline{Q}^2$, where

$$\oint \frac{d\theta}{\xi}\overline{Q}^2 = \left(k_\perp \rho_p\right)^2 \frac{4\pi m_i E}{T_i} \frac{2\pi}{\oint \frac{d\theta}{\xi}}. \tag{B.12}$$

For a large aspect ratio circular tokamak we have

$$\frac{1}{\xi} = \sqrt{\frac{1+\varepsilon\cos\theta}{1-\lambda+\varepsilon\cos\theta}}. \tag{B.13}$$

If we let $x = 1-\lambda$, then $\varepsilon < x < 1$ for passing particles. We may then expand $1/\xi$ to order ε^M,

$$\begin{aligned}\frac{1}{\xi} &= \frac{1}{\sqrt{x}}[1+\frac{1}{2}\left(1-\frac{1}{x}\right)\varepsilon\cos\theta + \\ &\quad + \left(-\frac{1}{8}-\frac{1}{4x}+\frac{3}{8x^2}\right)\varepsilon^2\cos^2\theta + .. + O\left(\varepsilon^{M+1}\right)],\end{aligned} \tag{B.14}$$

where the expansion order M depends on the accuracy desired for the integral $\int_0^{1-\varepsilon} d\lambda \oint \frac{d\theta}{\xi}\overline{Q}^2$. Therefore,

$$\oint \frac{d\theta}{\xi} = \frac{1}{\sqrt{x}} \sum_{n=0}^{M} a_n\left(\frac{1}{x}\right)\varepsilon^n, \tag{B.15}$$

where the coefficient $a_n\left(\frac{1}{x}\right)$ is a nth order polynomial in $1/x$, with $a_0\left(\frac{1}{x}\right) = 2\pi$, and

$$a_2\left(\frac{1}{x}\right) = 2\pi\left(\frac{3}{16x^2}-\frac{1}{8x}-\frac{1}{16}\right), \tag{B.16}$$

for $M = 2$, for example. In fact, only even n terms survive the θ integration since $a_{2m+1}\left(\frac{1}{x}\right) = 0$, for $m = 0, 1, 2....$ Using Eq.(B.15) we find

$$\frac{2\pi}{\oint \frac{d\theta}{\xi}} = \sqrt{x}\sum_{n=0}^{M} b_n\left(\frac{1}{x}\right)\varepsilon^n, \tag{B.17}$$

where $b_0 = 1$,

$$b_2 = -\frac{3}{16x^2}+\frac{1}{8x}+\frac{1}{16}, \tag{B.18}$$

and $b_{2m+1}\left(\frac{1}{x}\right) = 0$, for $m = 0, 1, 2....$ Using Eqs.(B.17) and (B.12) for $M = 2$ we find that

$$\begin{aligned}\int_0^{1-\varepsilon} d\lambda \oint \frac{d\theta}{\xi}\overline{Q}^2 &= \int_\varepsilon^1 dx \oint \frac{d\theta}{\xi}\overline{Q}^2 \\ &= \left(k_\perp \rho_p\right)^2 \frac{4\pi m_i E}{T_i}\left(\frac{2}{3} - \frac{25}{24}\varepsilon^{3/2} + \frac{2}{3}\varepsilon^2\right). \end{aligned} \tag{B.19}$$

We next increase the expansion order M to obtain a more precise result. The coefficient polynomial $b_n\left(\frac{1}{x}\right)$ has the following form

$$b_n\left(\frac{1}{x}\right) = \sum_{k=0}^{n} b_n^{(k)}/x^k, \tag{B.20}$$

where the numerical coefficients $b_n^{(k)}$ can be evaluated using the preceding expansion procedure, e.g.,

$$b_2^{(2)} = -\frac{3}{16},\ b_2^{(1)} = \frac{1}{8},\ b_2^{(0)} = \frac{1}{16} \tag{B.21}$$

in the preceding $M = 2$ case. Once all the numerical coefficients in Eq.(B.20) determined from Eq.(B.14) we obtain

$$\begin{aligned}\int_0^{1-\varepsilon} d\lambda \oint \frac{d\theta}{\xi}\overline{Q}^2 &= \left(k_\perp \rho_p\right)^2 \frac{4\pi m_i E}{T_i}\int_\varepsilon^1 dx\sqrt{x}\sum_{m=0}^{M/2} b_{2m}\left(\frac{1}{x}\right)\varepsilon^{2m} \\ &= \left(k_\perp \rho_p\right)^2 \frac{4\pi m_i E}{T_i}\sum_{m=0}^{M/2}\varepsilon^{2m}\sum_{k=0}^{2m} b_{2m}^{(k)}\int_\varepsilon^1 dx\frac{\sqrt{x}}{x^k}. \end{aligned} \tag{B.22}$$

The preceding integrals can be easily carried out to obtain

$$\int_0^{1-\varepsilon} d\lambda \oint \frac{d\theta}{\xi}\overline{Q}^2 = \left(k_\perp \rho_p\right)^2 \frac{4\pi m_i E}{T_i}\sum_{m=0}^{M/2}\varepsilon^{2m}\sum_{k=0}^{2m}\frac{b_{2m}^{(k)}}{3/2-k}\left(1 - \varepsilon^{3/2-k}\right). \tag{B.23}$$

Now, we look at the term

$$\sum_{m=0}^{M/2} \varepsilon^{2m} \sum_{i=0}^{2m} \frac{b_{2m}^{(i)}}{3/2-i} \left(1-\varepsilon^{3/2-i}\right),$$

when $m=0$, it gives

$$\frac{b_0^{(0)}}{3/2}(1-\varepsilon^{3/2}); \tag{B.24}$$

while for $m=1$ we find

$$\begin{aligned} &\frac{\varepsilon^2 b_2^{(0)}}{3/2}(1-\varepsilon^{3/2}) \\ &+\frac{\varepsilon^2 b_2^{(1)}}{3/2-1}(1-\varepsilon^{3/2-1}) \\ &+\frac{\varepsilon^2 b_2^{(2)}}{3/2-2}(1-\varepsilon^{3/2-2}). \end{aligned} \tag{B.25}$$

If we write

$$\sum_{m=0}^{M/2} \varepsilon^{2m} \sum_{k=0}^{2m} \frac{b_{2m}^{(k)}}{3/2-k} \left(1-\varepsilon^{3/2-k}\right) = \sum_{k=0}^{2M} \Upsilon_{k/2} \varepsilon^{k/2}, \tag{B.26}$$

then

$$\Upsilon_0 = \frac{b_0^{(0)}}{3/2} \to \frac{2}{3}, \tag{B.27}$$

and $\Upsilon_{1/2} = \Upsilon_1 = 0$, and

$$\Upsilon_{3/2} = -\sum_{m=0}^{2M} b_{2m}^{(2m)} \frac{1}{3/2-2m}. \tag{B.28}$$

Although the preceding expression is an infinite series, we find this series converges very rapidly. Just keeping the first several terms we obtain the following precise result

$$\Upsilon_{3/2} \to -1.09. \tag{B.29}$$

Following this procedure, we can also easily obtain

$$\Upsilon_4 = \frac{b_2^{(0)}}{3/2} + \frac{b_2^{(1)}}{3/2-1} + \frac{b_2^{(2)}}{3/2-2} \to \frac{2}{3}. \tag{B.30}$$

Therefore, to order $\mathcal{O}(\varepsilon^2)$ we find

$$\sum_{m=0}^{M/2} \varepsilon^{2m} \sum_{k=0}^{2m} \frac{b_{2m}^{(k)}}{3/2-k} \left(1 - \varepsilon^{3/2-k}\right) \to \frac{2}{3} - 1.09\varepsilon^{3/2} + \frac{2}{3}\varepsilon^2.$$

In general, the integer power coefficients Υ_n in Eq.(B.26) only depend on the coefficients $b_n^{(k)}$, $k = 0, 1, 2, ..., n$, or the polynomial $b_n\left(\frac{1}{x}\right)$. However, the half integer power coefficients $\Upsilon_{(2n+1)/2}$ in Eq.(B.26) require an infinite series to approach the exact value. Fortunately this series usually converges very rapidly. The expansion procedure we described here is different from the conventional approach that uses *elliptic integrals*. We expand the integrand from the beginning to avoid the *elliptic integrals* since we know the final result will be a *Taylor* series in inverse aspect ratio ε. This approach is algebraically less involved and makes some complicated integrals easier to handle. Using this expansion procedure, we obtain

$$\begin{aligned} \int_0^{1-\varepsilon} d\lambda \oint \frac{d\theta}{\xi} \overline{Q}^2 &= \left(k_\perp \rho_p\right)^2 \frac{m_i E}{T_i} \frac{8\pi}{3} (1 - 1.635\varepsilon^{3/2} \\ &\quad + \varepsilon^2 - 0.36\varepsilon^{5/2} - 0.0285\varepsilon^{7/2} + \frac{1}{10}\varepsilon^4), \end{aligned} \tag{B.31}$$

which is accurate to $\mathcal{O}(\varepsilon^4)$.

Next we evaluate the integral $\int_0^{1-\varepsilon} d\lambda \oint \frac{d\theta}{\xi} \overline{Q}\ \overline{Q^3}$ in Eq.(B.1):

$$\int_0^{1-\varepsilon} d\lambda \oint \frac{d\theta}{\xi} \overline{Q}\ \overline{Q^3} = \left(k_\perp \rho_p\right)^4 \left(\frac{2m_i E}{T_i}\right)^2 \frac{\oint d\theta h \oint d\theta \xi^2 h^3}{\oint \frac{d\theta}{\xi}}, \tag{B.32}$$

where

$$\oint d\theta \xi^2 h^3 = \oint d\theta \, (1 - \lambda h) \, h^3$$
$$= 2\pi \left(1 + \frac{3}{2}\varepsilon^2 - \lambda \left(1 + 3\varepsilon^2 + \frac{3}{8}\varepsilon^4\right)\right). \quad \text{(B.33)}$$

Therefore,

$$\oint \frac{d\theta}{\xi} \overline{Q} \, \overline{Q^3} = (k_\perp \rho_p)^4 \left(\frac{2m_i E}{T_i}\right)^2 \frac{2\pi}{\oint \frac{d\theta}{\xi}} (1 + \frac{3}{2}\varepsilon^2$$
$$-\lambda \left(1 + 3\varepsilon^2 + \frac{3}{8}\varepsilon^4\right)). \quad \text{(B.34)}$$

We can apply the same technique as we did to evaluate $\int_0^{1-\varepsilon} d\lambda \oint \frac{d\theta}{\xi} \overline{Q}^2$ to obtain

$$\int_0^{1-\varepsilon} d\lambda \oint \frac{d\theta}{\xi} \overline{Q} \, \overline{Q^3} = (k_\perp \rho_p)^4 \left(\frac{m_i E}{T_i}\right)^2 \frac{16\pi}{5} (1 - \frac{1}{6}\varepsilon^2 \quad \text{(B.35)}$$
$$-0.23\varepsilon^{5/2} + 3.9\varepsilon^{7/2} - \frac{55}{12}\varepsilon^4). \quad \text{(B.36)}$$

The final integral in Eq.(B.1), $\int d\lambda \oint \frac{d\theta}{\xi} \overline{Q^2}^2$, contains both passing and trapped particle contributions. For the passing particle contribution we follow the same procedure as we did to evaluate $\int_0^{1-\varepsilon} d\lambda \oint \frac{d\theta}{\xi} \overline{Q}^2$ to obtain

$$\int_0^{1-\varepsilon} d\lambda \oint \frac{d\theta}{\xi} \overline{Q^2}^2 = (k_\perp \rho_p)^4 \left(\frac{2m_i E}{T_i}\right)^2 \int_0^{1-\varepsilon} d\lambda \frac{\left(\oint d\theta \xi h^2\right)^2}{\oint \frac{d\theta}{\xi}}$$
$$= (k_\perp \rho_p)^4 \left(\frac{2m_i E}{T_i}\right)^2 (\frac{4\pi}{5} + \frac{4\pi}{15}\varepsilon^2$$
$$+0.99\varepsilon^{5/2} - 5.4\varepsilon^{7/2} + \frac{7\pi}{5}\varepsilon^4). \quad \text{(B.37)}$$

The trapped particle contribution is more complicated.

$$\int_{1-\varepsilon}^{1+\varepsilon} d\lambda \oint \frac{d\theta}{\xi} \overline{Q^2}^2 = (k_\perp \rho_p)^4 \left(\frac{2m_i E}{T_i}\right)^2 \int_{1-\varepsilon}^{1+\varepsilon} d\lambda \frac{\left(\oint d\theta \xi h^2\right)^2}{\oint \frac{d\theta}{\xi}}, \quad \text{(B.38)}$$

where we need to evaluate both $\oint d\theta \xi h^2$ and $\oint \frac{d\theta}{\xi}$ for the trapped particles. First we have

$$\oint d\theta \xi h^2 = 2\int_0^{\theta_b} d\theta \sqrt{1-\lambda+\varepsilon\cos\theta}\,(1+\varepsilon\cos\theta)^{3/2}, \tag{B.39}$$

where the turning angle θ_b is defined by $\theta_b = \arccos\left(\frac{1-\lambda}{\varepsilon}\right)$. We may define $x \equiv \frac{1-\lambda+\varepsilon}{2\varepsilon} = \sin^2(\theta_b/2)$, and $\sin y \equiv \sin(\theta/2)/\sin(\theta_b/2)$, then

$$d\theta = \frac{2\sin\frac{\theta_b}{2}\cos y}{\sqrt{1-x\sin^2 y}}dy. \tag{B.40}$$

Hence, Eq.(B.39) can be evaluated as

$$\begin{aligned}
\oint d\theta \xi h^2 &\cong 2\sqrt{2\varepsilon}\int_0^{\theta_b} d\theta \sqrt{x-\sin^2\frac{\theta}{2}}\left(1+\frac{3}{2}\varepsilon\cos\theta\right) \\
&= 4\sqrt{2\varepsilon}x\int_0^{\pi/2} dy \frac{1-\sin^2 y}{\sqrt{1-x\sin^2 y}}\left[1+\frac{3}{2}\varepsilon\left(1-2x\sin^2 y\right)\right] \\
&= 2\sqrt{2\varepsilon}\left\{\left[2+\varepsilon(2x-1)\right]E(x)+(x-1)(2-\varepsilon)K(x)\right\},
\end{aligned} \tag{B.41}$$

where $K(x)$ and $E(x)$ are complete *Elliptic Integrals* of the first and second kind, respectively. Similarly, we obtain the bounce time for the trapped particles

$$\oint \frac{d\theta}{\xi} = \frac{4}{\sqrt{2\varepsilon}}\left[\left(1-\frac{1}{2}\varepsilon\right)K(x)+\varepsilon E(x)\right]. \tag{B.42}$$

Using the preceding two equations, the integral in Eq.(B.37) can be written as

$$\begin{aligned}
\int_0^{1-\varepsilon} d\lambda \oint \frac{d\theta}{\xi}\overline{Q^2}^2 &= (k_\perp\rho_p)^4\left(\frac{2m_iE}{T_i}\right)^2(2\varepsilon)^{3/2}\int_0^1 dx \\
&\quad \frac{\left\{\left[2+\varepsilon(2x-1)\right]E(x)+(x-1)(2-\varepsilon)K(x)\right\}^2}{\left(1-\frac{1}{2}\varepsilon\right)K(x)+\varepsilon E(x)}.
\end{aligned} \tag{B.43}$$

This integral can be expanded in ε and then evaluated numerically to obtain

$$\int_0^{1-\varepsilon} d\lambda \oint \frac{d\theta}{\xi}\overline{Q^2}^2 = (k_\perp\rho_p)^4\left(\frac{2m_iE}{T_i}\right)^2\left[2.68\varepsilon^{5/2}+4.4\varepsilon^{7/2}+\mathcal{O}\left(\varepsilon^{9/2}\right)\right]. \tag{B.44}$$

From this expression we see that the trapped particle contribution only contains half integer powers of ε.

Appendix C

The Neoclassical Polarization Calculation for Shaped Plasma

Some of the detailed algebra needed to evaluate the shaped plasma polarization is presented in this appendix.

When we calculate the neoclassical polarization in Eq.(4.87), we use the small ε expansion for the second term with $x = 1 - \lambda$ to obtain

$$\begin{aligned}\frac{1}{\sqrt{B_0/B - \lambda}} &= \frac{1}{\sqrt{x}}\{1 - \frac{\varepsilon\cos\theta}{2x} + \frac{\varepsilon^2}{2x}[\left(\widetilde{A} + \frac{\kappa^2}{2q^2}\right)\cos^2\theta + \\ &\left(\widetilde{B} + \frac{1}{2q^2}\right)\sin^2\theta] + \frac{3}{8}\frac{\varepsilon^2}{x^2}\cos^2\theta + ... + \mathcal{O}\left(\varepsilon^{M+1}\right)\}, \qquad \text{(C.1)}\end{aligned}$$

and

$$\begin{aligned}\frac{dl_p}{B_p}\sqrt{B/B_0} \;\rightarrow\; & d\theta\{1 + \varepsilon\left(\frac{1}{2} - 2\widetilde{A}\right)\cos\theta + [(-\frac{1}{8} + \frac{3}{2}\widetilde{A} \\ & + \frac{\kappa^2}{4q^2})\cos^2\theta + (-\frac{1}{2}\widetilde{B} + \frac{1}{4q^2})\sin^2\theta]\varepsilon^2\}. \qquad \text{(C.2)}\end{aligned}$$

Since $\frac{dl_p}{B_p}\sqrt{B/B_0}$ is expanded only to $\mathcal{O}(\varepsilon^2)$, all the high order terms, $\mathcal{O}(\varepsilon^3)$, are ignored in this calculation and our calculation is only valid to $\mathcal{O}\left(\varepsilon^{5/2}\right)$. Using the pre-

ceding two equations along with $\xi = \sqrt{1-\lambda B/B_0}$, we may integrate over θ to obtain the form

$$\oint \frac{dl_p}{B_p}\frac{B}{B_0\xi} \rightarrow \frac{1}{\sqrt{x}}\sum_{n=0}^{M} a_n\left(\frac{1}{x}\right)\varepsilon^n, \tag{C.3}$$

where the coefficient $a_n\left(\frac{1}{x}\right)$ is a nth order polynomial in $1/x$, with $a_0\left(\frac{1}{x}\right) = 2\pi$, and

$$\begin{aligned} a_2\left(\frac{1}{x}\right) &= \frac{3\pi}{8x^2} + \frac{\pi}{8q^2x}\left[2\left(1+\kappa^2\right) + \left(-2+12\widetilde{A}+4\widetilde{B}\right)q^2\right] \\ &\quad -\frac{\pi}{8q^2}\left[-2\left(1+\kappa^2\right) + \left(1+12\widetilde{A}+4\widetilde{B}\right)q^2\right]. \end{aligned} \tag{C.4}$$

In fact, only even n terms survive the θ integration so $a_{2m+1}\left(\frac{1}{x}\right) = 0$, for $m = 0, 1, 2...$, since the power index of ε is the same power as $\cos\theta\sin\theta$ in each term of the expansion of $\frac{dl_p}{B_p}\frac{B}{B_0\xi}$. The coefficient $a_n\left(\frac{1}{x}\right)$ is a nth order polynomial in $1/x$ since the index of ε is the same or greater than that of $1/x$ in Eq.(C.1). In addition, the coefficient $1/x^n$ in the polynomial coefficient $a_n\left(\frac{1}{x}\right)$ must be a number independent of the shaping effects, because it comes from the $\varepsilon\cos\theta/x$ term of Eq.(C.1). Therefore, the inverse of Eq.(C.3) can be expanded in ε as

$$\frac{1}{\oint \frac{dl_p}{B_p}\frac{B}{B_0\xi}} \rightarrow \sqrt{x}\sum_{n=0}^{M} b_n\left(\frac{1}{x}\right)\varepsilon^n, \tag{C.5}$$

where $b_0 = 1/2\pi$, and

$$\begin{aligned} b_2\left(\frac{1}{x}\right) &= -\frac{3}{32\pi x^2} - \frac{1+\kappa^2+\left(6\widetilde{A}+2\widetilde{B}-1\right)q^2}{16\pi q^2 x} \\ &\quad + \frac{-2-2\kappa^2+\left(12\widetilde{A}+4\widetilde{B}+1\right)q^2}{32\pi q^2}, \end{aligned} \tag{C.6}$$

and the polynomial coefficients $b_n\left(\frac{1}{x}\right)$ vanish for odd n and have the same features as $a_n\left(\frac{1}{x}\right)$. Then, Eq.(4.97) can be rewritten as

$$\int_0^{\lambda_c} d\lambda \frac{1}{\oint \frac{dl_p}{B_p}\frac{B}{B_0\xi}} \rightarrow \sum_{n=0}^{M}\int_{\varepsilon(1+\alpha\varepsilon)}^{1} dx\sqrt{x}b_n\left(\frac{1}{x}\right)\varepsilon^n, \tag{C.7}$$

where $\alpha \equiv \widetilde{A}+\kappa^2/2q^2$. We evaluate the preceding expression term by term. For a general term, $n = 2m$,

$$\int_{\varepsilon(1+\alpha\varepsilon)}^{1} dx\sqrt{x}b_{2m}\left(\frac{1}{x}\right)\varepsilon^{2m} = \sum_{k=0}^{2m} b_{2m}^{(k)}\varepsilon^{2m}\int_{\varepsilon(1+\alpha\varepsilon)}^{1} dx\frac{\sqrt{x}}{x^k}, \tag{C.8}$$

where we assume $b_{2m}\left(\frac{1}{x}\right) = \sum_{k=0}^{2m} b_{2m}^{(k)}/x^k$, and $b_{2m}^{(k)}$ are functions of shaping effects and $b_{2m}^{(2m)}$ is a number. The preceding integration is straight forward,

$$\int_{\varepsilon(1+\alpha\varepsilon)}^{1} dx\sqrt{x}b_{2m}\left(\frac{1}{x}\right)\varepsilon^{2m} = \sum_{k=0}^{2m} b_{2m}^{(k)}\frac{\varepsilon^{2m}}{3/2-k}\left[1-\varepsilon^{3/2-k}\left(1+\alpha\varepsilon\right)^{3/2-k}\right]. \tag{C.9}$$

When $m = 0$ we get

$$\int_{\varepsilon(1+\alpha\varepsilon)}^{1} dx\sqrt{x}b_{2m}\left(\frac{1}{x}\right)\varepsilon^{2m} \to b_0\frac{1}{3/2}\left[1-\varepsilon^{3/2}\left(1+\alpha\varepsilon\right)^{3/2}\right], \tag{C.10}$$

while for $m = 1$ we find

$$\begin{aligned}\int_{\varepsilon(1+\alpha\varepsilon)}^{1} dx\sqrt{x}b_{2m}\left(\frac{1}{x}\right)\varepsilon^{2m} \;\to\; & b_2^{(0)}\frac{\varepsilon^2}{3/2}\left[1-\varepsilon^{3/2}\left(1+\alpha\varepsilon\right)^{3/2}\right] \\ & + b_2^{(1)}\frac{\varepsilon^2}{1/2}\left[1-\varepsilon^{1/2}\left(1+\alpha\varepsilon\right)^{1/2}\right] \\ & + b_2^{(2)}\frac{\varepsilon^2}{-1/2}\left[1-\varepsilon^{-1/2}\left(1+\alpha\varepsilon\right)^{-1/2}\right].\end{aligned} \tag{C.11}$$

Finally for $m = 2$ we obtain

$$\begin{aligned}\int_{\varepsilon(1+\alpha\varepsilon)}^{1} dx\sqrt{x}b_{2m}\left(\frac{1}{x}\right)\varepsilon^{2m} \;\rightarrow\; & b_4^{(0)}\frac{\varepsilon^4}{3/2}\left[1-\varepsilon^{3/2}\left(1+\alpha\varepsilon\right)^{3/2}\right] \\ & +b_4^{(1)}\frac{\varepsilon^4}{1/2}\left[1-\varepsilon^{1/2}\left(1+\alpha\varepsilon\right)^{1/2}\right] \\ & +b_4^{(2)}\frac{\varepsilon^4}{-1/2}\left[1-\varepsilon^{-1/2}\left(1+\alpha\varepsilon\right)^{-1/2}\right] \\ & +b_4^{(3)}\frac{\varepsilon^4}{-3/2}\left[1-\varepsilon^{-3/2}\left(1+\alpha\varepsilon\right)^{-3/2}\right] \\ & +b_4^{(4)}\frac{\varepsilon^4}{-5/2}\left[1-\varepsilon^{-5/2}\left(1+\alpha\varepsilon\right)^{-5/2}\right] \qquad \text{(C.12)}\end{aligned}$$

After calculating the value of $b_{2m}^{(k)}$, the integral in Eq.(C.7) can be expressed in terms of an ε expansion

$$\int_0^{\lambda_c} d\lambda \frac{1}{\oint \frac{dl_p}{B_p}\frac{B}{B_0\xi}} \rightarrow \sum_{i=0}^{\infty} \Upsilon_{k/2}\varepsilon^{k/2}, \qquad \text{(C.13)}$$

where the coefficients $\Upsilon_{k/2}$ are

$$\Upsilon_0 = b_0\frac{1}{3/2} = \frac{1}{3\pi}, \qquad \text{(C.14)}$$

and $\Upsilon_{1/2} = \Upsilon_1 = 0$, and

$$\Upsilon_{3/2} = -\sum_{m=0}^{\infty} b_{2m}^{(2m)}\frac{1}{3/2-2m}. \qquad \text{(C.15)}$$

Notice that $b_{2m}^{(2m)}$ is a number, so the coefficient $\Upsilon_{3/2}$ is independent of shaping effects. This series converges very rapidly. Within an error of 2%, we only need the first two terms to obtain $\Upsilon_{3/2} \rightarrow -\frac{25}{48\pi}$, but the exact coefficient is

$$\Upsilon_{3/2} \rightarrow -0.173. \qquad \text{(C.16)}$$

The next coefficient in this ϵ expansion series is

$$\Upsilon_2 = \sum_{k=0}^{2} b_2^{(k)} \frac{1}{3/2-k} \tag{C.17}$$

$$\rightarrow -\frac{1+\kappa^2+\left(-2+3\widetilde{A}+\widetilde{B}\right)q^2}{6\pi q^2}. \tag{C.18}$$

The last interesting coefficient is

$$\Upsilon_{5/2} = -\alpha \sum_{m=0}^{\infty} b_{2m}^{(2m)} - \sum_{m=0}^{\infty} b_{2m}^{(2m-1)} \frac{1}{3/2-(2m-1)} \tag{C.19}$$

$$\rightarrow -0.0383 + 0.0797\widetilde{A} + 0.0765\widetilde{B} + \frac{0.0383}{q^2} - \frac{0.0367\kappa^2}{q^2}, \tag{C.20}$$

where keeping up to ten terms in the preceding series gives the result to an error of 1%.

Appendix D

The Fitting Procedure

This appendix gives the details of the fitting procedure employed in Chapter 6 for calculating the eigenfunction expansion coefficients $\mu_n(\varepsilon)$, $\beta_n(\varepsilon)$ and $M_n(\varepsilon)$.

For each mode number n, we can compute $\mu_n(\varepsilon)$, $\beta_n(\varepsilon)$ and $M_n(\varepsilon)$ for various ε values, and then fit the numerical curves for the first few coefficients $u(n,k)$, $B(n,k)$ and $M(n,k)$, which are defined in Eqs.(6.29), (6.30), and (6.31). When $\varepsilon \to 0$, the coefficients $\mu_n(\varepsilon)$, $\beta_n(\varepsilon)$ and $M_n(\varepsilon)$ should approach their lowest order values, $\mu_n(0) = 2n^2 - n$, $\beta_n(0) = 2\delta_{n1}/3$, and $M_n(0) = 3\pi/(4n-1)$, which can be found in Eqs.(6.37), (6.38) and (6.39). This is shown in Fig.(D-1) for μ_n and M_n. Usually the first order coefficients $u(n,1)$, $B(n,1)$, and $M(n,1)$ will be the most accurate, the second order coefficients $u(n,1)$, $B(n,1)$ and $M(n,1)$ less accurate, and so on. To get better fitting results, we employ additional information about the properties of these coefficients.

First, we know the coefficient $u(n,1)$ from Ref.([30])

$$u(n,1) = 1.461\frac{4n-1}{3}\left[\frac{(2n-1)!!}{(2n-2)!!}\right]^2 \tag{D.1}$$

Therefore, to accuracy of $\mathcal{O}(\sqrt{\varepsilon})$

$$\mu_n(\varepsilon) = 2n^2 - n + 1.461\sqrt{\varepsilon}\frac{4n-1}{3}\left[\frac{(2n-1)!!}{(2n-2)!!}\right]^2. \tag{D.2}$$

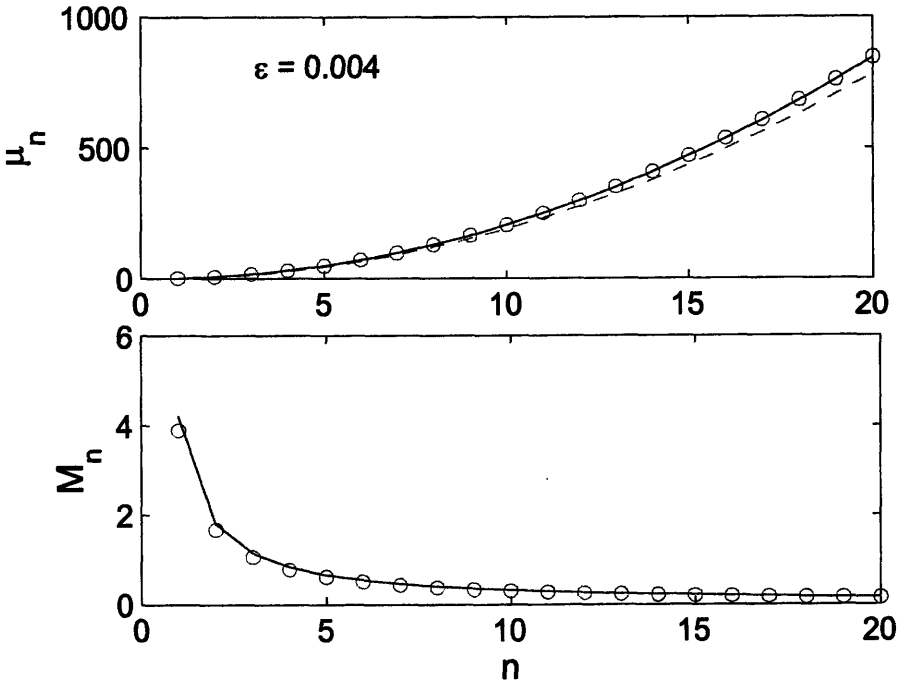

Figure D-1: The eigenfunction expansion coefficients varies with modenumber n for small ε, $\varepsilon = 0.004$. The red circles are the exact numerical value for $\varepsilon = 0.004$. In the first plot of μ_n, the dashed green line is lowest order contribution, $\mu_n = 2n^2 - n$, and the solid blue line contains the first order correction from Eq.(D.2). In the third plot of M_n, the solid blue line contains only the lowest order contribution $M_n = 3\pi/(4n-1)$. We do not plot β_n since to lowest order it is simply $\beta_n = 2\delta_{n1}/3$.

This result is verified in the first plot of Fig.(D-1).

When we fit the coefficients $u(n,k)$, $B(n,k)$, and $M(n,k)$, there exist some constraints between them which improve the fitting accuracy, since we know the exact neoclassical polarization in the collisionless high frequency and the collisional low frequency limits.

In the collisionless high frequency limit, we know from Eq.(3.39) that $P_1 = 1 - 1.635\varepsilon^{3/2}$. On the other hand, we know from Eq.(6.50) that

$$P_1 = 3\pi(1-\varepsilon)\sum_{n=1}^{\infty}\frac{\beta_n^2}{M_n}. \tag{D.3}$$

Therefore

$$\sum_{n=1}^{\infty}\frac{\beta_n^2}{M_n} \cong \frac{1}{3\pi}\left(1+\varepsilon-1.635\varepsilon^{3/2}\right). \tag{D.4}$$

Inserting Eqs.(6.37), (6.38), and (6.39) into $\sum_{n=1}^{\infty}\frac{\beta_n^2}{M_n}$, and expanding in ε, we find

$$\begin{aligned}\sum_{n=1}^{\infty}\frac{\beta_n^2}{M_n} &= \frac{1}{3\pi}+\left[\frac{B(1,1)}{\pi}-\frac{M(1,1)}{4\pi^2}\right]\sqrt{\varepsilon} \\ &+[\sum_{n=1}^{\infty}\frac{4n-1}{4\pi}B(n,1)^2+\frac{B(1,2)}{\pi}+\frac{3}{16\pi^3}M(1,1)^2 \\ &-\frac{3}{4\pi^2}B(1,1)M(1,1)-\frac{1}{4\pi^2}M(1,2)]\varepsilon+\mathcal{O}\left(\varepsilon^{3/2}\right)\end{aligned} \tag{D.5}$$

Comparing this equation to Eq.(D.4), gives

$$M(1,1) = 4\pi B(1,1), \tag{D.6}$$

and

$$\begin{aligned}M(1,2) &= -\frac{4\pi}{3}+\pi\sum_{n=1}^{\infty}\frac{4n-1}{4\pi}B(n,1)^2+4\pi B(1,2) \\ &-3B(1,1)M(1,1)+\frac{3}{4\pi}M(1,1)^2.\end{aligned} \tag{D.7}$$

We can also proceed to next order by comparing the $\varepsilon^{3/2}$ coefficients in Eq.(D.5) and (D.4), which will give an expression for $M(1,3)$ in terms of the constant 1.635 and other coefficients.

In the low frequency collisional limit, from Eq.(5.48) we know

$$P_1 = \frac{8}{\sqrt{\pi}} p\tau_{ii} \left(1 - 1.461\sqrt{\varepsilon}\right). \tag{D.8}$$

In this limit we know from Eq.(6.47) and Eq.(6.48) that

$$P_1 = 24\sqrt{\pi}\,(1-\varepsilon) \sum_{n=1}^{\infty} \frac{\beta_n^2}{M_n \mu_n}. \tag{D.9}$$

Again, comparing the ε expansion coefficients of Eq.(D.9) and Eq.(D.8), we obtain

$$u(1,1) = 1.461 \tag{D.10}$$

and $u(1,2)$ and $u(1,3)$, etc. Interestingly, in Ref.([30]) the coefficient $u(1,1)$ is calculated by a variational method, while here we obtain it by a different approach.

The general fitting procedure proceeds as follows:

(1) Fit the coefficients $B(n,k)$, especially $B(n,1)$ and $B(n,2)$ accurately.

(2) Calculate $M(1,1)$ and $M(1,2)$ from $B(n,k)$ by using Eqs.(D.6) and (D.7), etc.

(3) Calculate $u(n,1)$ from Eq.(D.1).

(4) Fix the above known coefficients and numerically fit the remaining coefficients.

Bibliography

[1] T.M. Antonsen, B. Lane. *Phys. Fluids*, 23:1205, 1980.

[2] M.A. Beer. *Ph.D. dissertation*, 1995.

[3] I.B. Bernstein, K. Molvig. *Phys. Fluids*, 26:1488, 1983.

[4] J. Candy, R.E. Waltz. *Phys. Rev. Lett.*, 91:045001, 2003.

[5] P.J. Catto. *Plasma Phys.*, 20:719, 1978.

[6] P.J. Catto, M.N. Rosenbluth, K.T. Tsang. *Phys. Fluids*, 22:1284, 1979.

[7] P.J. Catto, W.M. Tang, D.E. Baldwin. *Plasma Phys.*, 23:639, 1981.

[8] P.J. Catto, K.T. Tsang. *Phys. Fluids*, 21:1381, 1978.

[9] L. Chen, Z. Lin, R. White. *Phys. Plasmas*, 7:3129, 2000.

[10] B. Coppi, G. Rewoldt. *Phys. Rev. Lett.*, 33:1329, 1974.

[11] B. Coppi, M.N. Rosenbluth, R.Z. Sagdeev. *Phys. Fluids.*, 10:582, 1967.

[12] J.G. Cordey. *Nucl. Fusion*, 16:499, 1976.

[13] P.H. Diamond, S.I. Itoh, K. Itoh, T.S. Hahm. *Plasma Phys. and Contro. Fusion*, 47:R35, 2005.

[14] A.M. Dimits, G. Bateman, et al. *Phys. Plasmas*, 7:969, 2000.

[15] A.M. Dimits, T.J. Williams, J.A. Byers, B.I. Cohen. *Phys. Rev. Lett.*, 77:71, 1996.

[16] R.R. Dominguez, M.N. Rosenbluth. *Nucl. Fusion*, 29:844, 1989.

[17] W. Dorland, G.W. Hammett. *Phys. Fluids B*, 5:812, 1993.

[18] W. Dorland, F. Jenko, M. Kotschenruther, B.N. Rogers. *Phys. Rev. Lett.*, 85:5579, 2000.

[19] D. Ernst. *Phys. Plasmas*, 11:2637, 2004.

[20] D. Ernst. *Private Communication*, 2006.

[21] E.A. Frieman, L. Chen. *Phys. Fluids*, 25:502, 1982.

[22] G. Hammett. *Private Communication*, 2006.

[23] R. D. Hazeltine. *Plasma Phys*, 15:77, 1973.

[24] R. D. Hazeltine. *Plasma Confinement.* Addison-Wesley Pub. Com., Redwood City, CA, 1991.

[25] P. Helander, D.J. Sigmar. *Neoclassical Transport Theory.* Wiley, New York, 2001.

[26] F.L. Hinton, R.D. Hazeltine. Theory of plasma transport in toroidal confinement systems. *Rev. Mod. Phys.*, 48:239, 1976.

[27] F.L. Hinton, M.N. Rosenbluth. *Plasma Phys. Control. Fusion*, 41:A653, 1999.

[28] S.P. Hirshman, D.J. Sigmar. Neoclassical transport of impurities in tokamak plasmas. *Nucl. Fusion*, 21:1079, 1981.

[29] W. Horton. Drift waves and transport. *Rev. Mod. Phys.*, 71:735, 1999.

[30] C.T. Hsu, P.J. Catto, D.J. Sigmar. *Phys. Fluids B*, 2:280, 1990.

[31] F. Jenko, W. Dorland, M. Kotschenreuther, B.N.Rogers. *Phys. Plasma*, 7:1904, 2000.

[32] B.B. Kadomtsev, O.P. Pogutse. *Sov. Phys.-JETP*, 24:1172, 1971.

[33] Y.B. Kim, P.H. Diamond, H. Biglari, J.D. Callen. *Phys. Fluids B*, 3:384, 1991.

[34] M. Kotschenreuther, G. Rewoldt, W.M. Tang. *Comput. Phys. Commun*, 88:128, 1991.

[35] M. Kotschenruther, W. Dorland, M.A. Beer, G.W. Hammett. *Phys. Plasmas*, 85:5579, 1995.

[36] Z. Lin, T.S. Hahm, W.W. Lee, W.M. Tang, R.B. White. *Science*, 281:1835, 1998.

[37] C.S. Liu, M.N. Rosenbluth, W.M. Tang. *Phys. Fluids*, 19:1040, 1976.

[38] R.L. Miller, M.S. Chu, J.M. Greene, Y.R. Lin-Liu, R.E. Waltz. *Phys. Plasmas*, 5:973, 1998.

[39] K. Molvig, S.P. Hirshman, J.C. Whitson. *Phys. Rev. Lett*, 43:582, 1979.

[40] C.L. Rettig, T.L. Rhodes, J.N. Leboeuf, et al. *Phys. plasmas*, 8(5):2232, 2001.

[41] M. N. Rosenbluth, R. D. Hazeltine, F. L. Hinton. Plasma transport in toroidal confinement systems. *Phys. Fluids*, 15(1):116, 1972.

[42] M. N. Rosenbluth, D.W. Ross, D.P. Kostomarov. *Nucl. Fusion*, 12:2, 1972.

[43] M. N. Rosenbluth, M.L. Sloan. *Phys. Fluids*, 14(8):1725, 1971.

[44] M.N. Rosenbluth, F.L. Hinton. *Phys. Rev. Lett.*, 80:724, 1998.

[45] S.D. Scott, et. al. *Phys. Rev. Lett.*, 64:531, 1990.

[46] B.W. Stallard, C.M. Greenfield, G.M. Staebler. *Phys. Plasmas*, 6:1978, 1999.

[47] P.W. Terry. Suppression of turbulence and transport by sheared flow. *Rev. Mod. Phys.*, 72:109, 2000.